Promoted Direct Air Capture of Carbon Dioxide by Synergistic Water Harvesting

Yongqiang Wang

ORCID: 0000-0001-9565-4944

Submitted in total fulfilment of the requirements of the degree of Doctor of Philosophy

October 2023

Department of Chemical Engineering

The University of Melbourne

Abstract

Adsorption-based direct air capture (DAC) of carbon dioxide has been widely recognized as a necessary measure to contain atmospheric CO_2 concentrations. Chemisorbents like solid amines are effective in capturing ppm level CO_2. However, because of the large heat of adsorption, the regeneration of solid amines requires high energy consumption and a significant driving force, compromising the economic viability and productivity of DAC.

A vapor-promoted desorption (VPD) process was developed to recover the CO_2 adsorbed on solid amines by *in situ* vapor purge using water harvested from the atmosphere synergistically. A double-layered adsorption configuration, sequentially packed with solid amines and water adsorbents, was used to perform direct air capture based on the VPD process. The desorption of CO_2 was substantially enhanced in the presence of concentrated water vapors at around 100 °C, resulting in the concurrent production of 97.7% purity CO_2 and fresh water at ambient pressure. CO_2 working capacities of 1.0 mmol/g could be achieved using a commercial amine-grafted resin. Furthermore, a solar-heating DAC prototype was demonstrated to power the regeneration, recovering over 98% of the adsorbed CO_2 while consuming 10.4 MJ/kgCO_2 thermal energy.

PEI-impregnated sorbents have been extensively studied for DAC due to their high atmospheric CO_2 adsorption capacities. However, efficient recovery of the adsorbed CO_2 from PEI has received limited attention. The developed VPD process was employed to effectively regenerate PEI-impregnated sorbents, producing fresh water and 98% pure CO_2 with a remarkable working capacity of 1.61 mmol/g at 105 °C. The high CO_2 working capacity was realized through a reduction in CO_2 partial pressure inside the column caused by the increase of water vapor pressure. The *in situ* vapor purge allowed for the recovery of more than 95% of the CO_2 adsorbed on PEI, with an energy consumption of only 8.9 MJ/kgCO_2 for sorbent regeneration.

While the VPD process has demonstrated excellent performance in regenerating PEI-impregnated sorbents, a significant concern arises from amine deactivation at high regeneration temperatures. To address this issue, a vapor-promoted temperature vacuum swing adsorption (VPTVSA) process was developed, reducing the temperature required for the *in situ* vapor purge. This VPTVSA process regenerated PEI-impregnated sorbents at temperatures as low as 60 °C, producing 99% purity CO_2 with a stable working capacity of

1.10-1.13 mmol/g over 45 cycles. The minimum work required for adsorbent regeneration was only 1.62 MJ/kgCO_2, over 37% lower than temperature-vacuum swing desorption. This low-temperature regeneration process not only reduces the exergy demand but also has the potential to extend the lifespan of numerous low-cost PEI-impregnated sorbents, contributing to a reduction in the overall cost of DAC.

Declaration

This is to certify that:

1) the thesis comprises only my original work towards the PhD except where indicated in the Preface,

2) due acknowledgement has been made in the text to all other material used,

3) the thesis is fewer than 100,000 words in length, exclusive of tables, maps, bibliographies and appendices

Yongqiang Wang

October 2023

Preface

(i) The publication status of all chapters:

Chapter 1: Unpublished material not submitted for publication.

Chapter 2: Unpublished material not submitted for publication.

Chapter 3: Submitted for publication to Joule on August 22, 2023.

Chapter 4: Unpublished material not submitted for publication.

Chapter 5: Unpublished material not submitted for publication.

Chapter 6: Unpublished material not submitted for publication.

(ii) Sources of funding:

This work is sponsored by the Australia Research Council DP190101336 and DP210103888.

Acknowledgements

I would like to express my gratitude to the following individuals for their invaluable support and guidance throughout my studies as a PhD student:

First, I would like to thank my Principal Supervisor, Associate Professor Gang Li, for his continuous and kind support. His ability to provide innovative ideas and suggestions has been crucial in enhancing the quality of my research. His constructive guidance on academic writing has also been extremely helpful. I would also like to acknowledge the assistance provided to me to attend the 14th International Conference on the Fundamentals of Adsorption (FOA14) in the USA.

I am also grateful to my Co-Supervisor, Professor Paul Webley, for providing me with the opportunity to pursue my doctoral studies at the University of Melbourne. His guidance and mentorship, especially during the early stages of my research as a young PhD student, introduced me to a new and promising research field.

I would like to thank Professor Peter Scales, my Committee Chair, for his valuable insights and advice during our annual meetings.

I must thank Associate Professor Hui Ding at Tianjin University for hosting me in his research laboratory during the tough period when I was stranded in China for two and a half years due to the COVID-19 pandemic.

My appreciation goes to Dr. Penny Xiao and Dr. Ranjeet Singh for their dedication to managing daily laboratory affairs and the maintenance of experimental equipment in our lab.

I express my gratitude to Professor Guoping Hu at the Chinese Academy of Sciences and Dr. Longbing Qu for their suggestions that have contributed to my research work.

I extend my gratitude to the collaborative community at the Clean Energy Lab, including Dr. Mandy Men, Dr. Lefu Tao, Dr. Yalou Guo, Jining Guo, Chao Wu, Dingqi Wang, Zhi Yu, Dr. Qiuran Yang, and all other lab members.

I am also grateful to my parents and sister for their encouragement, belief, and financial support in my research pursuits.

Finally, I would like to express my appreciation to my wife, Dan Zhao, for her unwavering

support throughout this challenging journey and for her assistance as a laboratory manager at Tianjin University, both in administration and research work.

Table of Contents

Abstract I

Acknowledgements VII

Table of Contents IX

List of Tables XIII

List of Figures XV

1 Introduction 1

1.1 Climate change and global warming 1

1.2 Carbon capture and storage 1

1.3 Negative emissions and carbon removal technologies 2

1.4 Direct air capture processes 3

1.5 Thesis outline 5

1.6 References 6

2 Literature review 9

2.1 Overview 9

2.2 Sorbent materials 9

2.2.1 Supported alkali sorbents 9

2.2.2 Solid amine sorbents 10

2.2.3 Metal-organic frameworks 20

2.2.4 Zeolites 22

2.3 Adsorption processes for direct air capture 23

2.3.1 Temperature swing adsorption (TSA) 23

2.3.2 Temperature-vacuum swing adsorption (TVSA) 24

2.3.3 Other processes 27

2.4 References 29

3 Development of a vapor-promoted desorption process for direct air capture 37

3.1 Introduction 37
3.2 Experimental 38
3.2.1 Vapor-promoted desorption process 38
3.2.2 Materials and characterizations 39
3.2.3 Experimental setups for direct air capture 40
3.2.4 Energy consumption analysis 43
3.3 Results and discussion 44
3.3.1 Regeneration efficiency 44
3.3.2 Adsorption properties 46
3.3.3 Cyclic performance of vapor-promoted DAC 51
3.3.4 Performance estimation for VPD 54
3.3.5 Solar-powered DAC prototype 57
3.4 Conclusions 61
3.5 References 62
4 Vapor-promoted regeneration of amine-impregnated sorbents 65
4.1 Introduction 65
4.2 Experimental 66
4.2.1 Materials 66
4.2.2 Preparation of amine-impregnated sorbents 66
4.2.3 Characterizations 66
4.2.4 Vapor-promoted desorption for the regeneration of AIS 67
4.2.5 Energy consumption analysis 68
4.3 Results and discussion 70
4.3.1 Thermodynamic analysis of AIS regeneration 70
4.3.2 Adsorption properties and thermal stability 72
4.3.3 Performance of the VPD process for regenerating AIS 75
4.3.4 Energy consumption of VPD 80

4.4 Conclusions 81
4.5 References 82
5 Enhancing CO_2 desorption by synergistic generation of low-temperature vapors 85
5.1 Introduction 85
5.2 Experimental 86
5.2.1 Materials and synthesis 86
5.2.2 Characterizations 86
5.2.3 Experimental setup 87
5.2.4 Desorption kinetics model 88
5.2.5 Analysis of energy consumption and exergy demand 89
5.3 Results and discussion 90
5.3.1 Working principle of vapor-promoted TVSA 90
5.3.2 Adsorption properties 91
5.3.3 VPTVSA cycles for direct air capture 96
5.3.4 VPTVSA with different adsorbent volume fractions 102
5.4 Conclusions 107
5.5 References 108
6 Summary and future work 111
6.1 Summary 111
6.2 Future work 113

List of Tables

Table 2.1 Brief overview of PEI-impregnated adsorbents designed for DAC. 14

Table 2.2 Performance of reported adsorption-based DAC processes. 27

Table 3.1 Dual-site Langmuir model parameters of CO_2 adsorption on Lewatit resin..... 39

Table 4.1 Parameters used for evaluating energy consumption in vapor-promoted regeneration. 69

Table 4.2 Dual-site Langmuir model parameters of CO_2 adsorption on PEI/HP20 and PEI/HP2MGL. 71

Table 5.1 Dual-site Langmuir model parameters of CO_2 adsorption on 33PEI/HP20 and 50PEI/HP20. 93

Table 5.2 Parameters used for evaluating energy consumption and exergy demand of VPTVSA process. 105

List of Figures

Figure 1.1 Schematic diagram illustrating carbon capture and storage [7]. 2

Figure 1.2 The role of carbon dioxide removal in climate change mitigation [10]. 3

Figure 1.3 An absorption process for DAC based on the Kraft process [23]. 4

Figure 1.4 Schematic illustration of a DAC process based on adsorption (phase 1) and desorption (phase 2) cycles [29]. 5

Figure 2.1 Mechanism for the reaction of CO_2 with (a) primary amines and (b) tertiary amines in DAC. 11

Figure 2.2 Three main classes of solid amine sorbents [1]. 12

Figure 2.3 Chemical structures of amines commonly used for impregnation [16]. 13

Figure 2.4 Scheme of linkage configurations for 3-aminopropyltriethoxysilane (APTS) grafting over a silica surface [29]. 15

Figure 2.5 The agglomeration of amine molecules (TEPA) within pores and on the surface of silica [44]. 19

Figure 2.6 Synthesis of oxidation-stable PEI-impregnated sorbent [49]. 20

Figure 2.7 The structure of an alkylamine-appended metal-organic framework for direct air capture [55]. 22

Figure 2.8 Four-step temperature-vacuum swing adsorption cycle [71]. 25

Figure 2.9 Sorbent-coated carbon fibers and electrically driven TVSA modules [77]. 26

Figure 2.10 Mechanism of moisture swing adsorption based on ion exchange resins [41]. ... 28

Figure 2.11 A pH swing adsorption process designed for DAC [81]. 29

Figure 3.1 Working principle of vapor-promoted desorption for DAC. 38

Figure 3.2 Scheme of the setup for breakthrough experiments. 41

Figure 3.3 Scheme of the setup for testing the cyclic performance of vapor-promoted DAC. 41

Figure 3.4 Adsorption columns for electrical heating (Top) and solar heating (Bottom). 42

Figure 3.5 Solar-powered DAC prototype for high purity CO_2 and water production from the

air. 43
Figure 3.6 Regeneration efficiency and CO_2 working capacities of TVSA and vapor-promoted desorption processes. 45
Figure 3.7 Adsorption properties of VP OC 1065 resin and silica gel. 46
Figure 3.8 Fourier transform infrared spectroscopy spectra of VP OC 1065 pretreated using 25 °C air with 30% relative humidity (RH). 47
Figure 3.9 *In situ* Fourier transform infrared spectroscopy spectra of VP OC 1065 after 0, 5, 10, 15, 20, 25 and 30 min treatment in flowing N_2 atmosphere at 100 °C. The sample was pretreated with 25 °C and 30% RH air for 12 hours. 48
Figure 3.10 Cyclic CO_2 adsorption capacity of VP OC 1065 regenerated under (A) 70 °C and (B) 110 °C air flows. CO_2 adsorption was performed using 30 °C dry air with 400 ppm CO_2. The CO_2 uptake of the first adsorption cycle was denoted as q_0. 49
Figure 3.11 Cyclic CO_2 adsorption capacity of VP OC 1065 regenerated under (A) 120 °C and (B) 150 °C CO_2 flows. CO_2 adsorption was performed using CO_2 at 30 °C and 1 bar. The CO_2 uptake of the first adsorption cycle was denoted as q_0. 49
Figure 3.12 CO_2-induced deactivation mechanism analysis. (A) *In situ* FTIR spectra for VP OC 1065 after 0, 1, 2, 3, and 4 hours (bottom to top) treatment using CO_2 stream at 150 °C. (B-C) Proposed mechanism for (B) open-chain ureas formation and (C) cyclic ureas formation. 50
Figure 3.13 Performance of cyclic vapor-promoted DAC in comparison to desorption without *in situ* vapor purge. 51
Figure 3.14 Six vapor-promoted DAC cycles using 320 mL VP OC resin and 80 mL silica gel. (A) CO_2 loading and (B) desorption temperature profiles. 53
Figure 3.15 ^1H NMR spectra for the (A) deionized water and (B) water products. DMSO with 12 ppm concentration was employed as the reference. 53
Figure 3.16 Investigation on the impact of feed air humidity and co-adsorbed water in VPD. 54
Figure 3.17 To achieve regeneration efficiency *R* ranging from 0.70 to 0.93, the

corresponding desorption temperature as a function of the molar ratio of equilibrium loading of adsorbed water to CO_2 (n_{water}/n_{CO2} at the end of the adsorption step). 55
Figure 3.18 Predicting regeneration efficiency *R* of VPD under desorption pressures of (A) 100 kPa and (B) 50 kPa, at given volume fraction of resin, desorption temperature, and relative humidity of feed air. 56
Figure 3.19 Solar heating performance of the photothermal DAC prototype. 58
Figure 3.20 Performance of solar-powered DAC prototype with 320 mL resin and 80 mL silica gel (case 1). 59
Figure 3.21 Performance of solar-powered DAC prototype with different volume fractions of resin (case 2 and case 3). 59
Figure 3.22 Temperature profiles of the resin in the columns with and without silica gel during the cooling process after solar-powered regeneration. 60
Figure 3.23 Energy consumption and regeneration efficiency *R* of VPD process, compared with reported TVSA and steam-assisted TVSA (STVSA) processes using the same CO_2 adsorbent [19]. 61
Figure 4.1 Experimental setup for performing breakthrough experiments and DAC cycles. . 68
Figure 4.2 CO_2 adsorption isotherms of AIS. 70
Figure 4.3 Equilibrium adsorption capacities of PEI/HP2MGL, PEI/HP20, and PEI/FS for (a) 400 ppm and (b) 5% CO_2 at different adsorption temperatures, obtained through thermogravimetric analysis. 71
Figure 4.4 Regeneration efficiency (*R*) calculations for PEI/HP2MGL at various desorption temperatures and pressures, with fixed adsorption conditions of 25 °C and 400 ppm CO_2. ... 72
Figure 4.5 CO_2 adsorption properties of PEI/HP20, PEI/HP2MGL, and PEI/FS. 73
Figure 4.6 Porosity and thermal stability analyses for PEI/HP20, PEI/HP2MGL, and PEI/FS.74
Figure 4.7 Performance of *in situ* vapor purge for the regeneration of AIS. 76
Figure 4.8 Effects of *in situ* vapor for the regeneration of PEI/FS. 78
Figure 4.9 Products of cyclic DAC based on vapor-promoted desorption. 79

Figure 4.10 The temperature profiles of PEI/FS during the cooling process of various DAC cycles. Fresh air at 25 °C and 60% RH was used as the feed stream, with 320 mL PEI/FS and 80 mL silica gel as adsorbents. 80
Figure 4.11 Energy consumption for the regeneration of PEI/FS. 81
Figure 5.1 Experimental setup for performing breakthrough experiments and DAC cycles. . 87
Figure 5.2 Working principle of vapor-promoted temperature-vacuum swing adsorption (VPTVSA) process for DAC. 91
Figure 5.3 Physical appearance of a synthesized PEI-impregnated resin (33PEI/HP20)..... 92
Figure 5.4 Experimental CO_2 adsorption isotherms of (a) 33PEI/HP20 and (b) 50PEI/HP20 at 25, 40 and 55 °C, fitted to the Dual-site Langmuir model. 92
Figure 5.5 Thermodynamic assessment of amine-impregnated sorbent regeneration..... 93
Figure 5.6 Adsorption properties and pore structures of 33PEI/HP20 and 50PEI/HP20. 94
Figure 5.7 CO_2 adsorption capacities of PEI-impregnated resins under different feed air relative humidities at 25 °C and 330 ppm. 95
Figure 5.8 Adsorption-desorption profiles of 33PEI/HP20 and 50PEI/HP20 during 12 consecutive temperature swing cycles. Adsorption: 100% CO_2 at 30 °C; Desorption: dry air at (a) 70 °C, (b) 90 °C and (c) 110 °C. 96
Figure 5.9 Performance of cyclic DAC based on vapor-promoted TVSA. 97
Figure 5.10 Cyclic CO_2 and water working capacities during 45 DAC cycles. 98
Figure 5.11 The influence of feed air relative humidity on the VPTVSA process. 99
Figure 5.12 (a) CO_2 loading profiles, (b) regeneration temperature profiles and (c) CO_2 working capacity of 33PEI/HP20 during regeneration under different desorption pressures.100
Figure 5.13 (a) CO_2 loading profiles, (b) regeneration temperature profiles and (c) CO_2 working capacity of 50PEI/HP20 during regeneration under different desorption pressures.101
Figure 5.14 CO_2 desorption kinetics analysis for PEI-impregnated resins with different PEI loadings. 102
Figure 5.15 Schematic diagram illustrating different adsorbent volume fractions applied in

VPTVSA. 103
Figure 5.16 Performance of the VPTVSA process with different silica gel volume fractions.104
Figure 5.17 The breakdown of energy consumption for providing sensible heat (Q_s), latent heat (Q_l), and evacuation (W_v) in the desorption stage of the VPTVSA process. The process without silica gel is equivalent to the conventional TVSA. 106
Figure 5.18 Analysis of minimum work requirements for regenerating 33PEI/HP20 in the VPTVSA process. 107

1 Introduction

1.1 Climate change and global warming

Greenhouse gases such as carbon dioxide (CO_2), methane (CH_4), and water vapor (H_2O) possess the capacity to absorb longwave radiation emitted from the Earth's surface. This phenomenon constitutes the greenhouse effect, a vital mechanism for maintaining a habitable climate. However, human activities, primarily the burning of fossil fuels and industrial processes, have significantly increased the concentration of these gases in the atmosphere, especially carbon dioxide. Specifically, atmospheric CO_2 concentrations, which remained stable at around 250 ppm throughout human evolution, have increased by 160% to approximately 420 ppm [1, 2]. Due to the dramatic increase in atmospheric CO_2 concentrations, the Earth's average surface temperature has risen by 1.1 °C compared to the late 19th century up to the present day [3]. This has also resulted in severe environmental issues, including climate change, extreme weather events, and rising sea levels. In the face of the greenhouse effect and its associated global warming, reducing human-induced greenhouse gas emissions has become one of the most critical challenges in this century.

The Paris Agreement has established an international objective to curb global warming to well below 2 °C and make efforts to limit it to 1.5 °C compared to pre-industrial temperatures [4]. Various strategies have been employed to address global warming, such as the utilization of renewable energy sources, the enhancement of energy efficiency in industries, and the implementation of carbon capture and storage (CCS) [5, 6].

1.2 Carbon capture and storage

Carbon Capture and Storage is a technology designed to reduce greenhouse gas emissions, primarily CO_2, from industrial processes and power generation (Figure 1.1). This technology involves capturing CO_2 from large point sources, compressing the CO_2, and securely storing it underground to prevent its release into the atmosphere [7]. One of the key advantages of CCS is that it doesn't need costly replacements or shifts to entirely new technologies, making it widely acknowledged as one of the most crucial methods for mitigating climate change [6]. With the development of CO_2 utilization technologies, the captured CO_2 can also be converted to various chemicals and fuels [8], which makes carbon capture even more important and promising.

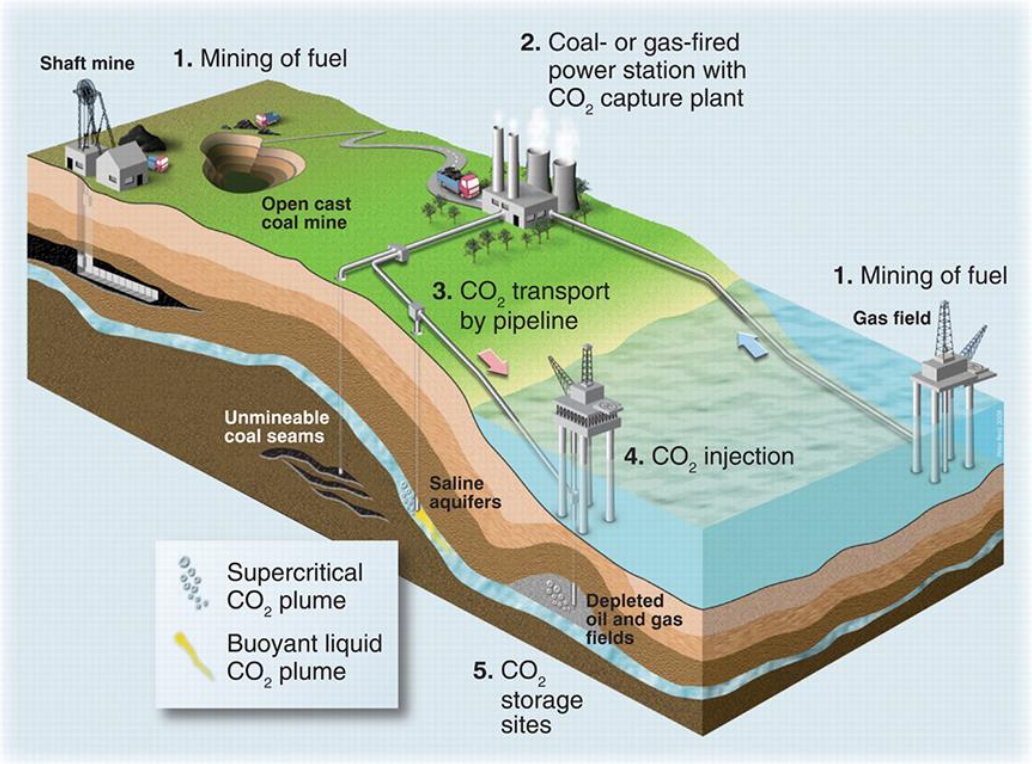

Figure 1.1 Schematic diagram illustrating carbon capture and storage [7].

1.3 Negative emissions and carbon removal technologies

Various climate change mitigation scenarios have been proposed based on the development and implementation of carbon capture technologies [9, 10]. And most of these scenarios suggest that relying solely on conventional carbon capture technology to reduce emissions may not be sufficient in addressing climate change [11]. To prevent a greater than 1.5 °C rise in temperature, zero net CO_2 emissions must be achieved by 2050, as estimated by the Intergovernmental Panel on Climate Change (IPCC) [12]. For the 2 °C target, achieving gross negative CO_2 emissions of approximately 10 Gt per year by mid-century is still required, as shown in Figure 1.2. However, recent estimates indicate that in 2022, greenhouse gas emissions represented 13% to 36% of the remaining carbon budget needed to restrict global warming to 1.5 °C, suggesting that the allowable emissions could be depleted within the next 2 to 7 years [13]. Therefore, there is a growing urgency to attain zero net CO_2 emissions ahead of schedule, leading to an urgent demand for carbon removal technologies (CRTs) or negative emission technologies.

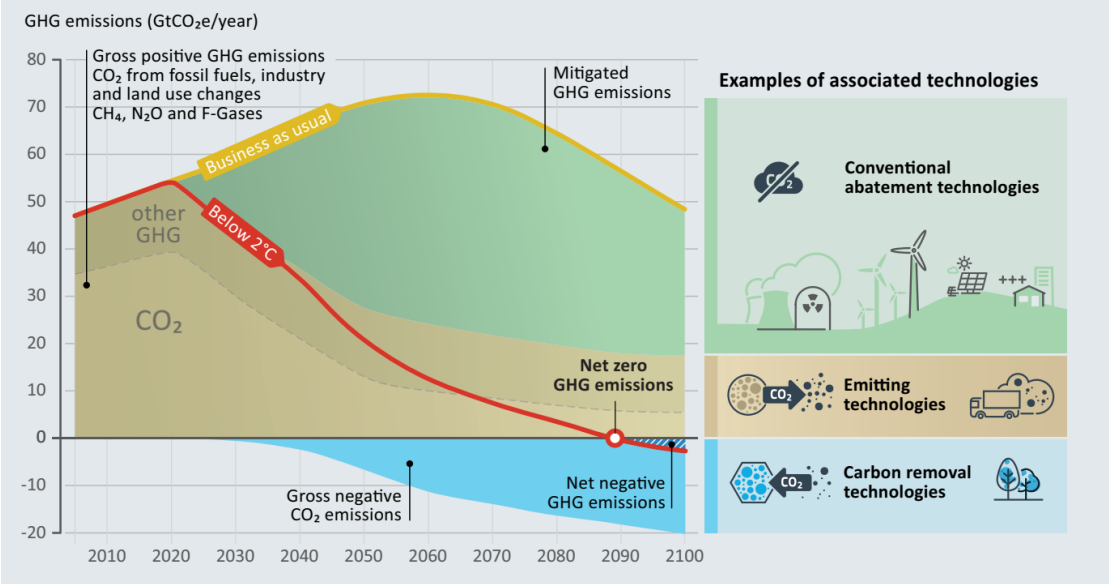

Figure 1.2 The role of carbon dioxide removal in climate change mitigation [10].

CRTs are designed to capture and remove CO_2 from the atmosphere [14], addressing the excess greenhouse gases that have accumulated over decades of industrial activity. Presently, there are more than 10 CRTs that have been developed, such as afforestation [15], soil carbon sequestration [16], enhanced weathering [17], bioenergy with carbon capture and storage [18], and direct air capture [19], among others. Direct air capture (DAC), involving the direct extraction of CO_2 from the atmosphere, has gained significant attention as one of the most crucial approaches for achieving negative emissions.

1.4 Direct air capture processes

DAC and CCS share fundamental principles related to the capture of carbon dioxide from various sources. Therefore, the development of DAC benefits from the knowledge and experiences gained in the field of conventional carbon capture technologies. Conventional CCS usually focuses on concentrated streams, such as flue gas (15% CO_2), natural gas (5-20% CO_2), or refinery off-gas (> 80% CO_2) [20]. Different processes, including absorption into liquid solution systems, adsorption onto solids, cryogenic separation, and permeation through membranes, have been employed to capture CO_2 from these large point sources [6]. However, due to the extremely low atmospheric CO_2 concentration (420 ppm), significant modifications to existing processes are necessary before they can be effectively adapted for DAC applications. For instance, cryogenic separation is nearly impossible to apply in DAC due to the low CO_2 partial pressure in the atmosphere. Currently, adsorption and absorption

technologies have been widely applied in DAC.

Absorption using base solutions with strong CO_2-binding affinities has been widely investigated for carbon capture from dilute sources [21] and is suitable for direct air capture [22]. At present, absorption is the most mature method for direct air capture, and an industrial plant has been constructed by Carbon Engineering using a process akin to the traditional Kraft process employed in the paper industry [23]. The mechanism of the process is described in Figure 1.3. Initially, CO_2 in the atmosphere is captured using an aqueous KOH/K_2CO_3 solution. Subsequently, the obtained solution undergoes precipitation through the reaction between K_2CO_3 and $Ca(OH)_2$ to regenerate KOH. Finally, solid $CaCO_3$ is collected and subjected to calcination to release CO_2, while the resulting CaO is hydrated to form $Ca(OH)_2$. In addition to KOH, NaOH, and $Ca(OH)_2$ solutions have also been employed for direct air capture using similar processes [24, 25]. Amino acid solutions were also developed to capture atmospheric CO_2, with a guanidine compound used to react with the CO_2-loaded solution and regenerate the amino acids [26].

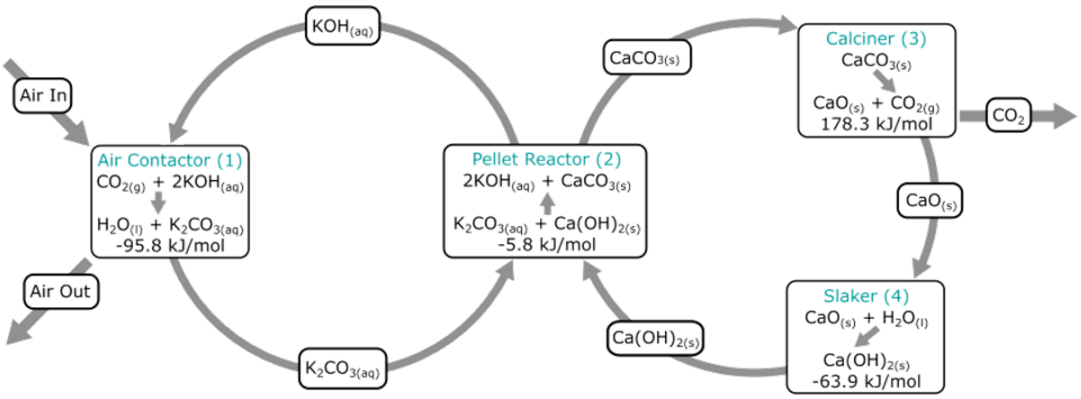

Figure 1.3 An absorption process for DAC based on the Kraft process [23].

In terms of the financial costs associated with capturing CO_2 from the air using the absorption method, the estimated costs were \$147-\$264 per ton of CO_2 for natural gas-fueled systems and \$140-\$254 per ton of CO_2 for coal-fueled systems [27]. According to a recent academic report published by Carbon Engineering, the cost of their direct air capture process ranged from \$94 to \$232 per ton of CO_2 captured [23].

While Keith et al. have made optimizations to the absorption process to reduce operational and capital costs, it remains expensive primarily due to the high capital costs and the elevated temperature (900 °C) necessary for the regeneration process [23]. While absorption technology for DAC is relatively mature, adsorption, which is an emerging technology in this

field, has the potential to lower overall costs due to its relatively low regeneration temperature of around 100 °C [28].

Compared to absorption in the liquid phase, adsorption involves the adhesion of atmospheric CO_2 to the surface of a solid sorbent at ambient temperatures [29]. Desorption or regeneration is the reverse process of adsorption, involving the release or detachment of adsorbed CO_2 from the sorbent surface, typically triggered by changes in environmental conditions such as pressure and temperature (Figure 1.4).

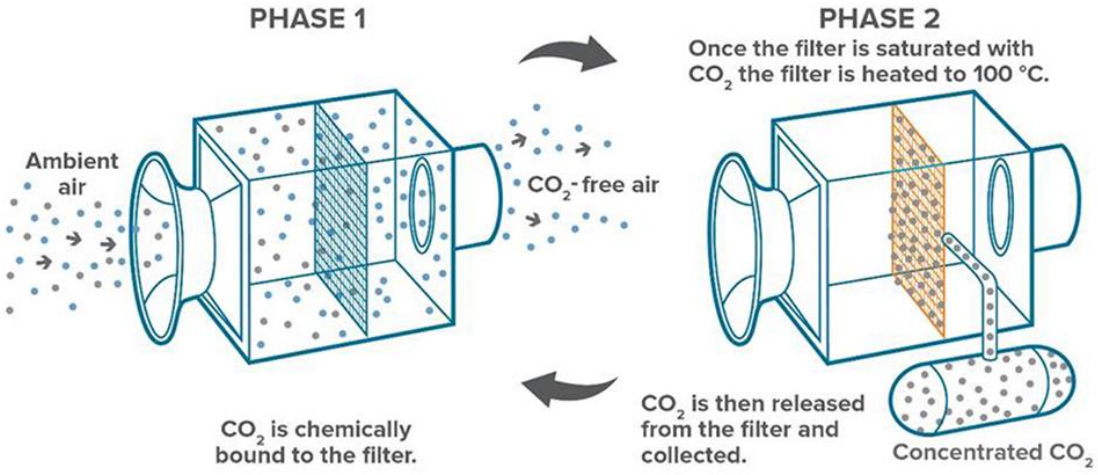

Figure 1.4 Schematic illustration of a DAC process based on adsorption (phase 1) and desorption (phase 2) cycles [29].

Based on reported techno-economic analyses, the cost of adsorption-based DAC varies between $86 and $221 per ton of CO_2 captured, with the sorbent capital cost being the primary contributor to these expenses [30, 31]. Consequently, there are two key areas to address for further reducing the cost of DAC:

1. Sorbent: The creation of cost-effective sorbents with high CO_2 adsorption capacity and excellent stability.

2. Regeneration process: The development of an efficient regeneration method that can operate under moderate conditions to effectively recover the adsorbed CO_2 and prevent sorbent deactivation.

1.5 Thesis outline

Adsorption-based direct air capture is an important method for achieving our climate targets. Previous studies have predominantly focused on material design to enhance the CO_2

adsorption capacity of sorbents for DAC, while research on the regeneration process has not received sufficient attention. The objective of this thesis is to develop efficient regeneration processes for sorbents used in DAC, enabling the recovery or release of adsorbed CO_2 under moderate conditions.

The work in this thesis is organized as follows: Chapter 2 presents a literature review that surveys existing research within this field. In Chapter 3 presents a vapor-promoted desorption technology that enhances the regeneration of chemisorbents through *in situ* vapor purge using water synergistically harvested from the air. Chapter 4 presents the application of vapor-promoted desorption in the regeneration of polyethylenimine-impregnated sorbents. In Chapter 5, the required temperatures for regenerating polyethylenimine-impregnated sorbents are further reduced using a vapor-promoted temperature-vacuum swing adsorption process. Chapter 6, the final chapter, presents key conclusions and outlines future research needs within this field.

1.6 References

[1] B. Hönisch, N.G. Hemming, D. Archer, M. Siddall, J.F. McManus, Atmospheric carbon dioxide concentration across the mid-pleistocene transition, Science 324 (2009) 1551-1554.

[2] W. Cheng, L. Dan, X. Deng, J. Feng, Y. Wang, J. Peng, J. Tian, W. Qi, Z. Liu, X. Zheng, D. Zhou, S. Jiang, H. Zhao, X. Wang, Global monthly gridded atmospheric carbon dioxide concentrations under the historical and future scenarios, Scientific Data 9 (2022) 1-13.

[3] K. Haustein, M.R. Allen, P.M. Forster, F.E.L. Otto, D.M. Mitchell, H.D. Matthews, D.J. Frame, A real-time global warming index, Sci. Rep.-UK 7 (2017) 1-6.

[4] C. Schleussner, J. Rogelj, M. Schaeffer, T. Lissner, R. Licker, E.M. Fischer, R. Knutti, A. Levermann, K. Frieler, W. Hare, Science and policy characteristics of the Paris Agreement temperature goal, Nat. Clim. Change 6 (2016) 827-835.

[5] A.M. Omer, Focus on low carbon technologies: The positive solution, Renewable and Sustainable Energy Reviews 12 (2008) 2331-2357.

[6] M. Bui, C.S. Adjiman, A. Bardow, E.J. Anthony, A. Boston, S. Brown, P.S. Fennell, S. Fuss, A. Galindo, L.A. Hackett, J.P. Hallett, H.J. Herzog, G. Jackson, J. Kemper, S. Krevor, G.C. Maitland, M. Matuszewski, I.S. Metcalfe, C. Petit, G. Puxty, J. Reimer, D.M. Reiner, E.S. Rubin, S.A. Scott, N. Shah, B. Smit, J.P.M. Trusler, P. Webley, J. Wilcox, N. Mac Dowell, Carbon capture and storage (CCS): the way forward, Energ. Environ. Sci. 11 (2018) 1062-1176.

[7] R.S. Haszeldine, Carbon capture and storage: How green can black be? Science 325 (2009) 1647-1652.

[8] B.M. Tackett, E. Gomez, J.G. Chen, Net reduction of CO_2 via its thermocatalytic and electrocatalytic transformation reactions in standard and hybrid processes, Nature Catalysis 2 (2019) 381-386.

[9] J. Rogelj, A. Popp, K.V. Calvin, G. Luderer, J. Emmerling, D. Gernaat, S. Fujimori, J. Strefler, T. Hasegawa, G. Marangoni, V. Krey, E. Kriegler, K. Riahi, D.P. van Vuuren, J. Doelman, L. Drouet, J. Edmonds, O. Fricko, M. Harmsen, P. Havlík, F. Humpenöder, E. Stehfest, M. Tavoni, Scenarios towards limiting global mean temperature increase below 1.5 °C, Nat. Clim. Change 8 (2018) 325-332.

[10] The Emissions Gap Report 2017, United Nations Environment Programme (UNEP).

[11] S.E. Tanzer, A. Ramírez, When are negative emissions negative emissions? Energ. Environ. Sci. 12 (2019) 1210-1218.

[12] Global Warming of 1.5 ºC, Intergovernmental Panel on Climate Change (IPCC).

[13] Z. Liu, Z. Deng, S. Davis, P. Ciais, Monitoring global carbon emissions in 2022, Nature Reviews Earth & Environment 4 (2023) 205-206.

[14] T. Terlouw, C. Bauer, L. Rosa, M. Mazzotti, Life cycle assessment of carbon dioxide removal technologies: a critical review, Energ. Environ. Sci. 14 (2021) 1701-1721.

[15] J.C. Doelman, E. Stehfest, D.P. van Vuuren, A. Tabeau, A.F. Hof, M.C. Braakhekke, D.E.H.J. Gernaat, M. van den Berg, W.J. van Zeist, V. Daioglou, H. van Meijl, P.L. Lucas, Afforestation for climate change mitigation: Potentials, risks and trade-offs, Global Change Biol. 26 (2020) 1576-1591.

[16] P. Smith, Soil carbon sequestration and biochar as negative emission technologies, Global Change Biol. 22 (2016) 1315-1324.

[17] J. Hartmann, A.J. West, P. Renforth, P. Köhler, C.L. De La Rocha, D.A. Wolf-Gladrow, H.H. Dürr, J. Scheffran, Enhanced chemical weathering as a geoengineering strategy to reduce atmospheric carbon dioxide, supply nutrients, and mitigate ocean acidification, Rev. Geophys. 51 (2013) 113-149.

[18] D.L. Sanchez, N. Johnson, S.T. McCoy, P.A. Turner, K.J. Mach, Near-term deployment of carbon capture and sequestration from biorefineries in the United States, Proceedings of the National Academy of Sciences 115 (2018) 4875-4880.

[19] E.S. Sanz-Pérez, C.R. Murdock, S.A. Didas, C.W. Jones, Direct capture of CO_2 from ambient air, Chem. Rev. 116 (2016) 11840-11876.

[20] M.E. Boot-Handford, J.C. Abanades, E.J. Anthony, M.J. Blunt, S. Brandani, N. Mac Dowell, J.R. Fernández, M. Ferrari, R. Gross, J.P. Hallett, R.S. Haszeldine, P. Heptonstall, A. Lyngfelt, Z. Makuch, E. Mangano, R.T.J. Porter, M. Pourkashanian, G.T. Rochelle, N. Shah, J.G. Yao, P.S. Fennell, Carbon capture and storage update, Energ. Environ. Sci. 7 (2014) 130-189.

[21] B.A. Oyenekan, G.T. Rochelle, Alternative stripper configurations for CO_2 capture by aqueous amines, AIChE J. 53 (2007) 3144-3154.

[22] J.K. Stolaroff, D.W. Keith, G.V. Lowry, Carbon dioxide capture from atmospheric air using sodium hydroxide spray, Environ. Sci. Technol. 42 (2008) 2728-2735.

[23] D.W. Keith, G. Holmes, D. St. Angelo, K. Heidel, A process for capturing CO_2 from the

atmosphere, Joule 2 (2018) 1573-1594.

[24] V. Nikulshina, D. Hirsch, M. Mazzotti, A. Steinfeld, CO_2 capture from air and co-production of H_2 via the $Ca(OH)_2$-$CaCO_3$ cycle using concentrated solar power-Thermodynamic analysis, Energy 31 (2006) 1715-1725.

[25] V. Nikulshina, N. Ayesa, M.E. Gálvez, A. Steinfeld, Feasibility of Na-based thermochemical cycles for the capture of CO_2 from air-Thermodynamic and thermogravimetric analyses, Chem. Eng. J. 140 (2008) 62-70.

[26] F.M. Brethomé, N.J. Williams, C.A. Seipp, M.K. Kidder, R. Custelcean, Direct air capture of CO_2 via aqueous-phase absorption and crystalline-phase release using concentrated solar power, Nature Energy 3 (2018) 553-559.

[27] National Academies of Sciences, Engineering, and Medicine, Negative emissions technologies and reliable sequestration: a research agenda, (2019).

[28] X. Zhu, W. Xie, J. Wu, Y. Miao, C. Xiang, C. Chen, B. Ge, Z. Gan, F. Yang, M. Zhang, D. O'Hare, J. Li, T. Ge, R. Wang, Recent advances in direct air capture by adsorption, Chem. Soc. Rev. 51 (2022) 6574-6651.

[29] C. Beuttler, L. Charles, J. Wurzbacher, The role of direct air capture in mitigation of anthropogenic greenhouse gas emissions, Frontiers in Climate 1 (2019) 1-7.

[30] A. Sinha, M.J. Realff, A parametric study of the techno-economics of direct CO_2 air capture systems using solid adsorbents, AIChE J. 65 (2019) 1-8.

[31] H. Azarabadi, K.S. Lackner, A sorbent-focused techno-economic analysis of direct air capture, Appl. Energ. 250 (2019) 959-975.

2 Literature review

2.1 Overview

In this chapter, the existing literature is reviewed to investigate sorption materials used in adsorption-based direct air capture, along with an in-depth analysis of prevailing adsorption processes. The initial section of this review focuses on providing a comprehensive overview of various sorbent types, with particular emphasis on solid amine sorbents. The subsequent section delves into the core principles and concepts governing cycle design for DAC processes, while also offering insights into performance data from previously reported studies.

2.2 Sorbent materials

Given the low atmospheric carbon dioxide concentrations, the adsorption driving force for DAC is exceptionally weak. As a result, the development of sorbents with a strong affinity for CO_2 is one of the most prominent research areas in the field of DAC. Sorbents employed in direct air capture must exhibit a high adsorption capacity at low CO_2 partial pressures and demonstrate excellent selectivity over N_2 and O_2. Several solid materials have been recently developed or tested for direct air capture [1]. And the sorbents can be categorized into four types: supported alkali sorbents [2, 3], solid amine sorbents [4, 5], metal-organic frameworks (MOFs), and zeolites [6].

2.2.1 Supported alkali sorbents

Inorganic bases, particularly K_2CO_3 and Na_2CO_3, have been investigated and used for the adsorption of CO_2 from the atmosphere. The reaction pathway depends on various factors, including adsorption temperature and humidity. Typically, $NaHCO_3$ or $KHCO_3$ is formed during the adsorption process and subsequently heated to release CO_2 during the desorption or regeneration process [3, 7].

To enhance the surface area and reaction kinetics of these bases, porous supports such as alumina and carbon are commonly employed to support the active species. Veselovskaya et al. synthesized a composite sorbent K_2CO_3/Al_2O_3 and applied it in direct air capture, achieving an adsorption capacity of 0.91-1.11 mmol/g. Despite the relatively high regeneration temperature

of 300 °C, the sorbent exhibited remarkable stability, enduring over 80 cycles [7]. In a separate study, Okunev et al. proposed the use of K_2CO_3/Y_2O_3 as a sorbent for DAC. This sorbent demonstrated a CO_2 adsorption capacity of 0.64 mmol/g for temperature swing adsorption (TSA) cycles at a regeneration temperature of 250 °C. However, it showed reduced stability when regeneration was conducted at 300 °C, with a decrease in capacity from 0.64 to 0.23 mmol/g [2].

In the context of supported alkali sorbents, the challenge lies in the high regeneration temperatures, often exceeding 200 °C, which demand substantial energy input. To address this issue, Rafael et al. prepared a sorbent by supporting Na_2CO_3 on activated carbon honeycombs for CO_2 enrichment in greenhouses [3]. Notably, they employed a humidity swing process to lower the regeneration temperature, desorbing CO_2 with a flush of humid air (water pressure 75 mbar) at 65 °C. The same research group also investigated K_2CO_3 supported on activated carbon honeycombs as a sorbent for DAC [8]. Their findings revealed that K_2CO_3 showed more promise than Na_2CO_3 due to its higher adsorption capacity. Specifically, the K_2CO_3-based sorbent could adsorb 0.1 mmol CO_2/g under regeneration conditions of 50 °C and a water pressure of 90 mbar.

Supported alkali sorbents are typically prepared from cheap raw materials, holding the potential to reduce sorbent capital costs. However, research on supported alkali sorbents in DAC also encounters significant challenges, including their limited CO_2 adsorption capacity, energy-intensive regeneration process, and the need for improved selectivity. Achieving long-term stability and increasing adsorption capacities under varying humidity conditions are critical areas that require further investigation to enhance their viability in DAC applications.

2.2.2 Solid amine sorbents

Solid amine sorbents, which involve amines impregnated or grafted onto porous solids, represent a crucial class of sorbents extensively used in practical DAC demonstrations. Their exceptional adsorption performance at low CO_2 concentrations arises from the chemical reactions between the supported amine groups and CO_2 [1]. The mechanism for the reaction of CO_2 with primary and tertiary amines is illustrated in Figure 2.1. In the absence of water, only primary and secondary amine groups can combine with CO_2 to form ammonium carbamates. Theoretically, 1 mol of amine group can react with 0.5 mol of CO_2 without water, resulting in a maximum CO_2/amine ratio of 0.5 [9]. Under humid conditions, amine groups can adsorb both CO_2 and water to form bicarbonates, increasing the maximum CO_2/amine ratio to 1 in

this situation. Thus, solid amine sorbents have the advantage of not experiencing a reduction in their adsorption capacity with the presence of moisture. In fact, their adsorption performance remains stable or may even improve in the presence of moisture [9]. This property makes solid amine sorbents particularly effective for capturing carbon dioxide from moist air. As the most widely explored class of sorbents for DAC, extensive research has been conducted to identify suitable candidates with exceptional adsorption performance.

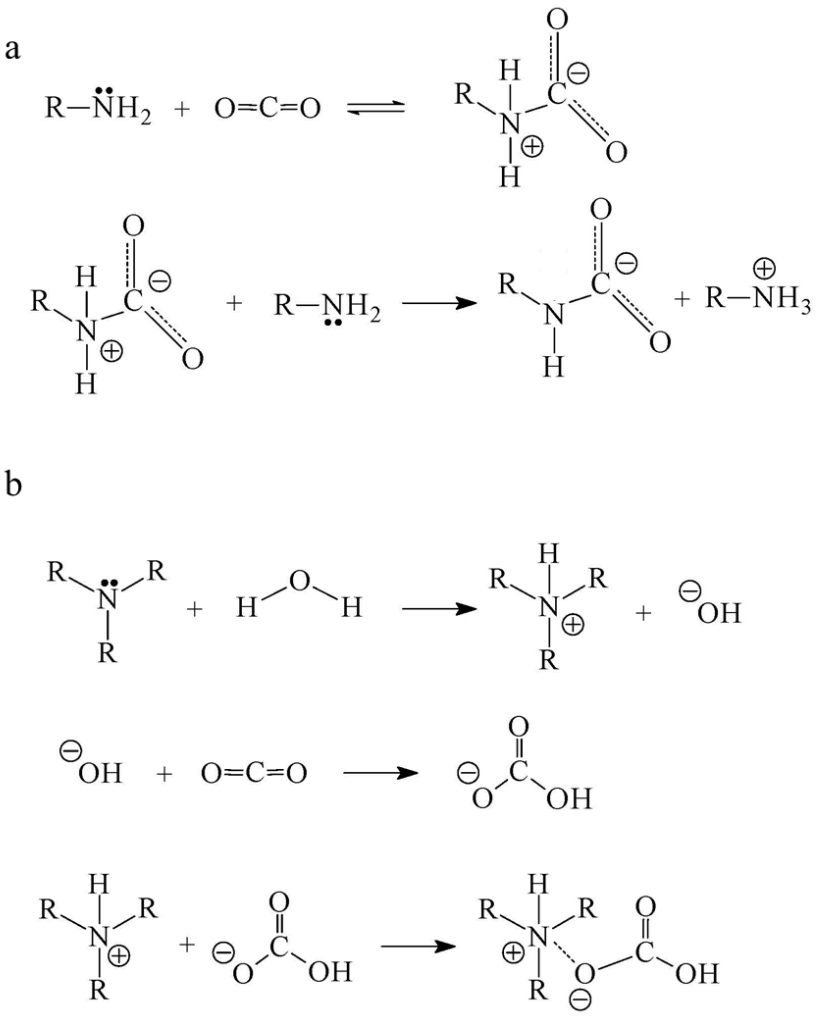

Figure 2.1 Mechanism for the reaction of CO_2 with (a) primary amines and (b) tertiary amines in DAC.

Solid amine sorbents can generally be categorized into three classes [10], as depicted in Figure 2.2. The first-class sorbents, amine-impregnated sorbents, involve the physical impregnation of amine molecules into porous supports. In the case of second-class sorbents, amine molecules are chemically grafted to porous supports through covalent bonds. The third-class sorbents are typically prepared through *in situ* polymerization of monomers containing amine groups.

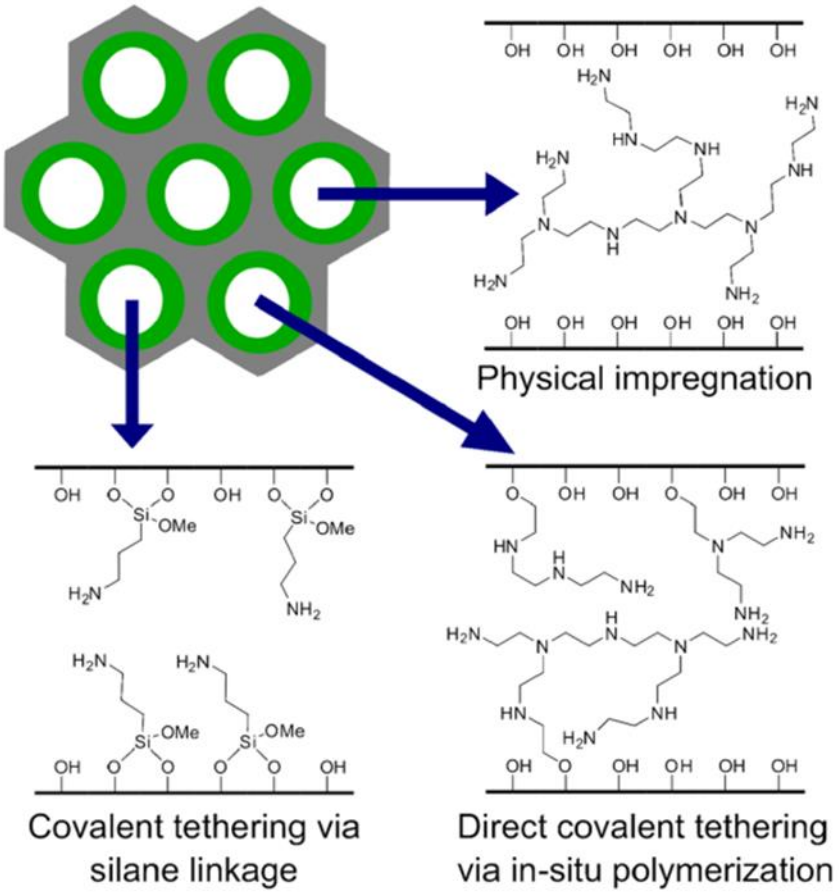

Figure 2.2 Three main classes of solid amine sorbents [1].

2.2.2.1 Amine-impregnated sorbents

Extensive research efforts have been dedicated to the development of class 1 materials, known as amine-impregnated sorbents (AIS), due to the advantage of easy preparation, low cost, and high amine content [11-13]. Through the deposition of amines such as polyethylenimine (PEI), tetraethylenepentamine (TEPA), and polyallylamine (PAA) onto various solid supports, these sorbents have demonstrated outstanding capability for atmospheric CO_2 capture [6, 14, 15] (Figure 2.3). Table 2.1 lists the CO_2 uptake of reported PEI-impregnated sorbents across different support materials.

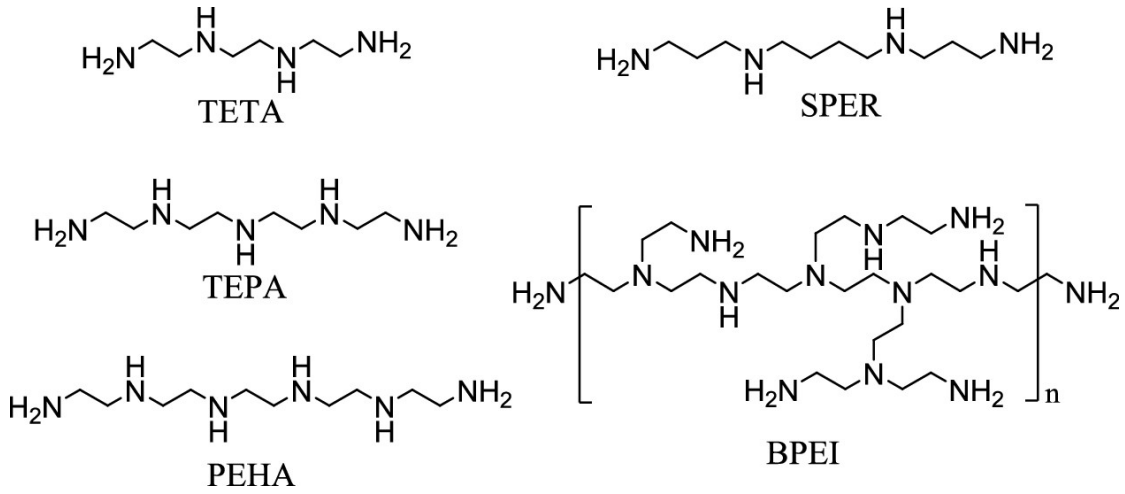

Figure 2.3 Chemical structures of amines commonly used for impregnation [16].

In the early stages of DAC sorbent development, around the year 2010, silica with mesoporous or macroporous structures was commonly chosen for impregnating PEI, displaying good atmospheric CO_2 adsorption capacities. For instance, Olah et al. found that a PEI-supported fumed silica sorbent had an impressive capacity of 1.7 mmol/g for capturing atmospheric CO_2 [11]. Their study also explored the impact of water on the adsorption process, revealing that the presence of water was beneficial when the PEI loading was 33 wt%. The group also investigated the impact of parameters including PEI loading, adsorption and desorption temperature, particle size, and PEI molecular weight on the adsorption behavior [17]. Similarly, Jones et al. conducted tests using a class 1 sorbent, PEI-impregnated silica, for atmospheric CO_2 capture [18]. While the prepared sorbent achieved an impressive adsorption capacity of 2.36 mmol/g, the material displayed limited thermal stability. To address this limitation, the authors modified the sorbents with 3-aminopropyltrimethoxysilane or tetraethyl orthotitanate, significantly enhancing the thermal stability of the sorbents. The results demonstrated that the modified sorbents could be reused more than four times without significant capacity loss.

Besides 3-amino-propyltrimethoxysilane and tetraethyl orthotitanate, other additives were used to improve the performance of class 1 sorbents. For instance, Jones et.al employed $AlCl_3 \cdot 6H_2O$ and $ZrOCl_2 \cdot 8H_2O$ to modify PEI-supported SBA-15, and the amine efficiency significantly improved [19, 20]. The group proved that the improved performance was the result of the modified pore structure of SBA-15 with microporosity. The results highlighted the importance of the microstructure of support materials. The same group also employed PEG200 as an additive to increase the thermodynamic performance of PEI-supported SBA-15 and alumina [21]. Sayari et.al supported PEI on the extra-large-pore silica (pore-expanded

MCM-41) which was modified by cetyltrimethylammonium bromide (CTMABr) [22]. The authors supposed that the additive played a key role in modifying the distribution of PEI supported on pore-expanded MCM-41. Under humid conditions, the amine efficiency could reach 7.31 mmol/gPEI which is the highest efficiency among the PEI-based sorbents for DAC.

Table 2.1 Brief overview of PEI-impregnated adsorbents designed for DAC.

Amine	Support	Loading[a]	RH	Uptake (mmol/g)[b]	Ref.
PEI (Mw=25 000)	Fumed silica	33wt%	0%	1.18	[11]
PEI (Mw=25 000)	Fumed silica	33wt%	67%	1.77	[11]
PEI (Mw=25 000)	Fumed silica	50wt%	0%	1.7	[11]
PEI (Mw=25 000)	Fumed silica	50wt%	67%	1.41	[11]
PEI (Mw=800)	Silica	45.1wt%	0%	2.36	[18]
PEI (Mw=800)	Zr7-SBA-15	34.7wt%	0%	0.85	[19]
PEI (Mw=800)	Pore-expanded MCM-41	40wt%	80%	2.92	[22]
PEI (Mn=600)	HP20	50wt%	0%	2.26	[23]
PEI (Mw=600)	Mesoporous carbon[c]	55wt%	80%	2.58	[24]
PEI (Mw=600)	Mesoporous carbon[c]	55wt%	0%	2.25	[24]
PEI solution[d]	Nanofibrillated cellulose	44wt%	80%	2.22	[25]

[a] PEI loading of CO_2 adsorbents.

[b] CO_2 uptakes at 25 °C and 400 ppm.

[c] Span 80 was used as a diffusion additive.

[d] Mr=600000-1000000.

Based on the above research works, the selection of the support for class 1 sorbents is one of the most crucial tasks. Yu et.al employed spherical resin HP20 with adjustable pores to support PEI for direct air capture [23]. And the adsorption capacity was 2.26 mmol/g from 400 ppm CO_2 at 25 °C. Compared with typical supports such as mesoporous silica, the HP20 is mechanically stable and easy to handle. Mesoporous carbon was employed by Long et.al to support PEI for DAC [24]. The advantage of the used mesoporous carbon was that the pore volume was larger than 3 cm^3/g. The as-prepared sorbent exhibited an adsorption capacity of 2.25 mmol/g for 400 ppm CO_2. Steinfeld et.al developed PEI-supported nanofibrillated cellulose prepared by freeze-drying process [25]. The sorbent exhibited an extremely fast adsorption rate, and the adsorption half time was only 10.6 min while the adsorption capacity was 2.22 mmol/g. Since the structured support is suitable for DAC because of the low pressure

drop, Jones et.al employed a monolithic alumina honeycomb as the support for PEI [26]. A volumetric capacity of 350 mol $CO_2/m^3_{monolith}$ could be obtained, and the equilibration time for adsorption was 350 min.

Although PEI is the most frequently used active specie for CO_2 capture, some other amine molecules have been investigated for direct air capture as well. Jones et.al used poly(propylenimine) (PPI) to prepare several PPI-based class 1 sorbents [27]. Triethylenetetramine, TPTA, EI-den, and PI-den were used in the study and compared with PEI. The authors found that PPI-based sorbents had better adsorption performance and stability than PEI-based sorbents.

2.2.2.2 Covalently supported amine sorbents

For class 2 sorbents, amine groups are supported on solid materials through covalent bonds (Figure 2.4). Generally, the amine loading is limited by the number of surface functional groups such as -OH, thus the adsorption capacity is also limited. Since the amine groups are covalently supported, the stability of the sorbents is generally better than that of class 1 sorbents [28].

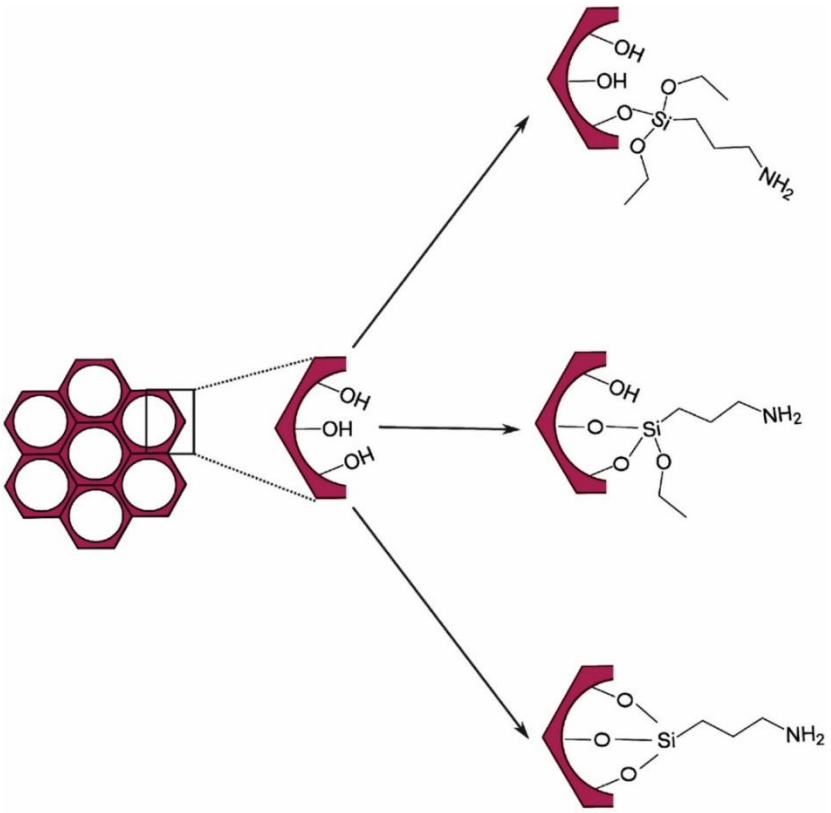

Figure 2.4 Scheme of linkage configurations for 3-aminopropyltriethoxysilane (APTS)

grafting over a silica surface [29].

Steinfeld et.al prepared diamine-functionalized silica gel from commercial silica gel beads and [N-(2-aminoethyl)-3-aminopropyl] trimethoxysilane (AEATPMS) for DAC [5]. The sorbent had a cyclic adsorption amount of 0.2 mmol/g and could be cycled more than 40 times. A temperature-vacuum swing adsorption (TVSA) process was established to obtain CO_2 with a purity of 97%. The same group prepared an amine-grafted sorbent by freeze-drying an aqueous suspension of nanofibrillated cellulose and N-(2-aminoethyl)-3-aminopropylmethyldimethoxy silane (AEAPDMS). Under conditions of a CO_2 concentration of 506 ppm in air and a relative humidity of 40% at 25 °C, the adsorption capacity reached 1.39 mmol/g [30]. They also evaluated the stability of AEAPDMS supported cellulose as a sorbent for DAC [31]. The results proved that O_2 played the most important role in the degradation process. And the contact between amine groups and O_2 led to loss of amine groups and the formation of amide/imide species.

Yang et.al used 3-aminopropyltrimethoxysilane (APTS) and SBA-15 to prepare a class 2 sorbent, and compared the prepared sorbent with zeolites [4]. The results illustrated that the prepared amine-grafted silica was the only sorbent that had the ability to capture CO_2 from humid gases, although the amine supported material had a relatively slow uptake rate. The author also found that the uptake rate was as important as the equilibrium adsorption capacity in cyclic studies. Shen et.al used the same amine molecule which was supported on silica aerogel with high pore volume (1-2.5 cm^3/g) [32]. And the adsorption capacities were 1.80 and 2.57 mmol/g in dry and humid conditions, respectively.

While many amine molecules can be used to prepare amine-grafted materials, Jones et.al evaluated the performance of different types of amines [33]. Silanes with primary amine, secondary amine and tertiary amine were used to prepare different class 2 sorbents. According to the results, the sorbent with primary amines had the best adsorption performance, and tertiary amine groups had negligible CO_2 adsorption capacity. The group also suggested that secondary amines are less efficient than primary amines for CO_2 adsorption, due to unfavorable entropic factors associated with the organization of the second alkyl chain in secondary amines [34]. The choice of solvents also plays an important role in preparing amine-grafted materials, and the use of a nonpolar solvent was suggested by Feitosa et al [29]. They tested different solvents for grafting amines, and cyclohexane yielded the sorbent with the highest nitrogen loading (5.21%) and CO_2 adsorption capacity.

For commercial-available sorbent for DAC, a benchmark amine-grafted resin, Lewatit VP OC 1065, has been widely investigated for adsorbing atmospheric CO_2 [35]. The sorbent is a divinylbenzene crosslinked polymer with primary amine groups, exhibiting adsorption capacities higher than 1 mmol/g under DAC conditions. The material can be fully regenerated at around 100 °C and also has excellent stability, which makes the resin a good candidate for a DAC process.

2.2.2.3 Sorbents prepared by in situ polymerization of amines

Class 3 sorbents are generally prepared by polymerization of amine monomers, and the properties and structures are relatively flexible. Jones et al. synthesized a poly(L-lysine) brush-mesoporous silica hybrid sorbent through *in situ* ring-opening polymerization in SBA-15, achieving a CO_2 adsorption capacity of 0.6 mmol/g at 400 ppm and 25 °C [36]. Subsequently, the same research group synthesized a hyperbranched aminosilica through *in situ* ring-opening polymerization of aziridine in SBA-15 [37]. They achieved a high amine loading of 10 mmol N/g using this preparation method, resulting in an adsorption capacity of 1.5 mmol/g. This sorbent exhibited excellent reusability and was comparable to the class 2 sorbent AEATPMS-SBA-15. Liu et al. also used *in situ* polymerization of L-alanine to create an amine-functionalized three-dimensional interconnected macroporous silica sorbent [38]. This sorbent had a high amine loading (over 10.98 mmol N/g), and achieved a remarkable CO_2 adsorption capacity of 2.65 mmol/g in simulated ambient air.

3-aminopropyl triethoxysilane and vinyl triethoxysilane were used by Abhilash et.al to prepare a class 3 sorbent which had a CO_2 adsorption capacity of 1.68 mmol/g from atmospheric air [39]. The desorption of the sorbent was easier than other sorbents, while the complete desorption occurred at 80 °C. Therefore, the sorbent did not have to be heated to a high temperature and could be used for more than 100 cycles. Zhou et.al developed an amine-grafted porous polymer network, PPN-6-CH_2DETA with a loading capacity of 1.04 mmol/g [40]. However, the desorption temperature was high and a temperature of 120 °C was required.

An important part of class 3 sorbents is the materials that can reversibly capture CO_2 from ambient air by humidity swing. Wang et.al reported an amine-based anion exchange resin with quaternary ammonium cations for DAC [41]. The sorbent adsorbed CO_2 in dry conditions and released CO_2 in humid conditions. Thus, a moisture swing process was developed to regenerate the sorbent. Chen et.al also developed quaternized chitosan (QCS)/poly(vinyl

alcohol) hybrid aerogels for moisture swing adsorption [42]. The cyclic CO_2 adsorption capacity from 400 ppm was 0.18 mmol/g, while the adsorption half time (about 10 min) was shorter than most of the sorbents developed for DAC.

2.2.2.4 Stability of amines in DAC

Based on the tests reported above, Class 1 sorbents generally exhibit higher adsorption capacity due to their higher amine loading, whereas Class 2 and 3 sorbents demonstrate limited adsorption capacity because of their lower amine density. However, amine loss due to leaching and evaporation often occurs in impregnated materials, primarily because of the weak interactions between amines and the support [43]. In comparison to bonded amines, impregnated amines tend to exhibit a more significant loss in adsorption capacity after cyclic experiments. The primary deactivation mechanisms involved in DAC sorbents include O_2-induced deactivation, CO_2-induced deactivation, and steam-induced deactivation.

It has been widely reported that oxygen environments can deactivate amines at temperatures exceeding 70 °C, primarily due to the oxidation of the amine groups [43]. Yogo et al. investigated the impact of oxidation duration time, treatment temperature, oxygen concentration, and TEPA loading on amine-impregnated sorbents [44]. They found that under oxidative treatment conditions at 80 °C for 18 hours, the stability of the samples improved as the TEPA loading increased from 30% to 60%. This improvement in stability was attributed to the decrease in the O_2 diffusion rate, which occurred due to the agglomeration of amine molecules within the pores of the mesoporous silica (Figure 2.5). Li et al. also explored the impact of oxygen on amine-impregnated sorbents during CO_2 adsorption and their oxidative stability during desorption [45]. They discovered that precise control of the operating temperature enhances both selectivity and resistance to oxidation. An optimal regeneration temperature of 80 °C was suggested to achieve the oxidative stability of amine-impregnated sorbents. In addition, because of the weak interaction between amine groups and the support material, amine-impregnated sorbents are prone to amine leaching when exposed to a steam stripping regeneration process. Jones et al. conducted stability testing on PEI-impregnated mesoporous γ-alumina under continuous steam exposure at 115 °C [46]. After 24 hours of treatment, the CO_2 sorption capacity decreased from 1.7 mmol/g to 0.66 mmol/g, and the amine loading dropped from 7.81 mmol N/g to 2.34 mmol N/g.

Class 2 sorbents, such as the commercial amine-grafted sorbent Lewatit VP OC 1065, were found to possess thermal and hydrothermal stability at high temperatures, but underwent

oxidative degradation at moderate temperatures (above 70 °C) [47]. Higher temperatures (above 120 °C) caused degradation in concentrated dry CO_2, whereas adding moisture improved CO_2-induced stability [48]. Therefore, to prevent oxygen-induced deactivation, it is advisable to choose a regeneration temperature of no more than 80 °C. Additionally, it is essential to keep the temperature below 120 °C to avoid CO_2-induced deactivation.

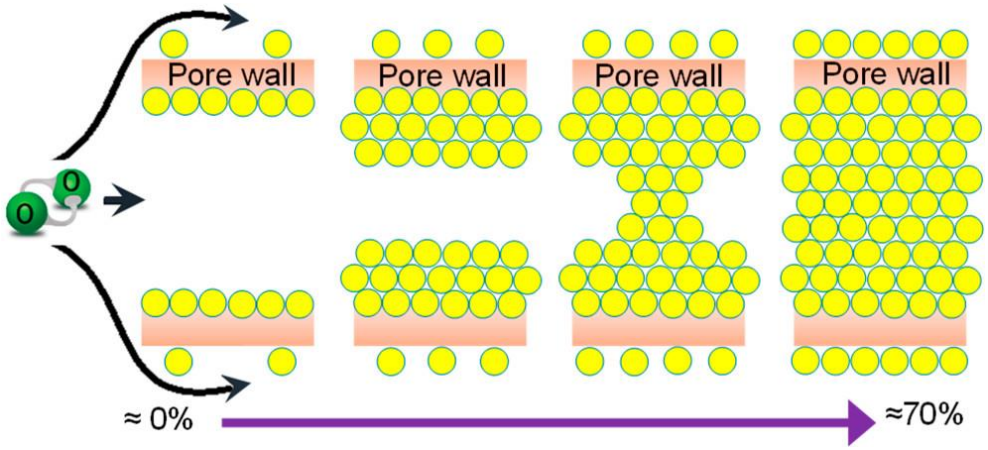

Figure 2.5 The agglomeration of amine molecules (TEPA) within pores and on the surface of silica [44].

To address stability concerns associated with impregnated amines, Choi et al. developed a highly stable sorbent [49]. During the preparation process, PEI underwent a reaction with 1,2-epoxybutane for stabilization, and small quantities of chelators were pre-loaded onto a silica support to prevent deactivation caused by metal impurities (Figure 2.6). The prepared stable sorbent only lost 8.5% of its CO_2 working capacity even after 30 days of treatment in an O_2-containing flue gas at 110 °C. Goeppert et al. employed a similar method to stabilize other amines, such as TEPA, by reacting them with propylene oxide [50]. This treatment prevented the leaching of impregnated amines and improved the adsorption kinetics. However, such modification reactions compromise the CO_2 sorption capacity.

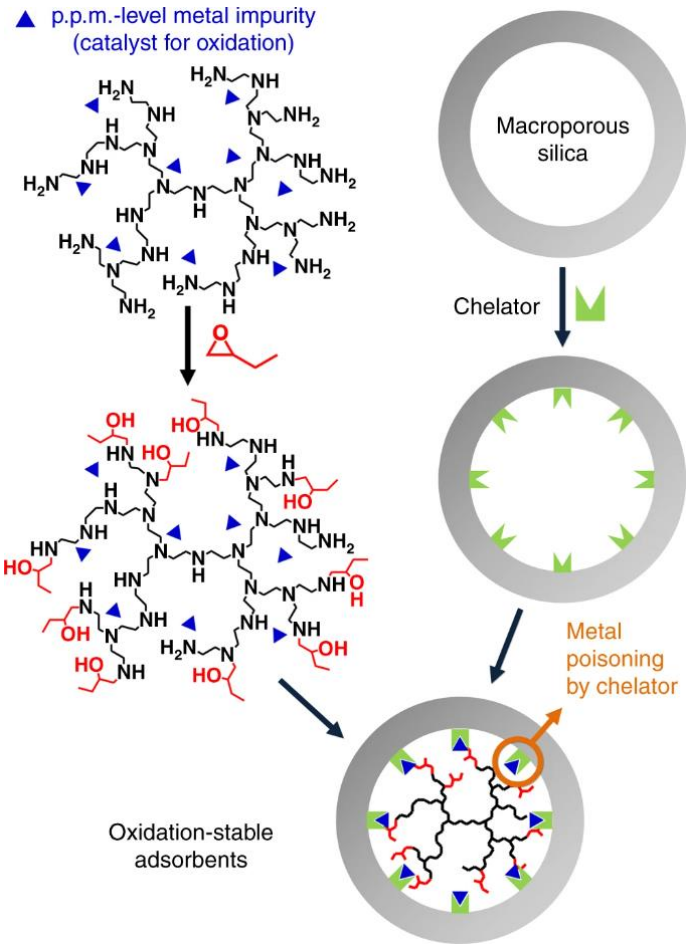

Figure 2.6 Synthesis of oxidation-stable PEI-impregnated sorbent [49].

2.2.3 Metal-organic frameworks

Metal-organic frameworks (MOFs) represent an emerging class of novel adsorbents that have garnered significant attention for carbon capture applications. These materials typically consist of various metal-based clusters and organic linkers, allowing for versatile material designs suited for various applications [51]. While only a limited number of MOFs have been developed and proven to be suitable for direct air capture, the potential of these materials remains promising, driven by the rapid advancement of MOF research.

Zaworotko et al. conducted tests to assess the adsorption capacity of various MOFs for capturing CO_2 from the atmosphere [6]. They examined HKUST-1, Mg-MOF-74, and SIFSIX-3-Ni using temperature programmed desorption analysis. However, similar to 13X zeolite, these metal-organic frameworks could efficiently capture CO_2 only under dry conditions.

Some MOFs have been developed to address the issue of competitive adsorption with water.

Eddaoudi et al. reported a fluorinated metal-organic framework known as NbOFFIVE-1-Ni, designed for trace CO_2 removal. NbOFFIVE-1-Ni demonstrated a CO_2 uptake of 1.3 mmol/g at a CO_2 concentration of 400 ppm [52]. Interestingly, despite having a high water uptake of 13.8 wt%, the presence of adsorbed water did not significantly impact the CO_2 adsorption capacity of this adsorbent. In 2014, Shekhah et al. introduced a hybrid ultramicroporous material called SIFSIX-3-Cu, designed for the removal of trace carbon dioxide from humid environments [53]. This material demonstrated a substantial adsorption capacity of 1.24 mmol/g at a CO_2 concentration of 400 ppm. Notably, the adsorption capacity of SIFSIX-3-Cu remained unaffected by the presence of water, distinguishing it from other physisorbent materials. However, prolonged exposure to humid conditions had a detrimental effect on its adsorption performance. Additionally, Yoon et al. synthesized a microporous copper silicate material characterized by distinct H_2O-specific and CO_2-specific adsorption sites. Impressively, this material maintained its CO_2 adsorption capacity even in the presence of atmospheric moisture and exhibited exceptional stability under wet conditions [54].

Although some physisorbent MOFs with hydrolytic stability have been developed, their CO_2 uptakes have generally remained below 1.5 mmol/g. To further enhance the performance of MOFs, Hong et al. created an alkylamine-appended metal-organic framework, mmen-Mg_2(dobpdc), using both solvothermal and microwave methods (Figure 2.7) [55]. This amine-grafted MOF exhibited outstanding CO_2 adsorption capacity at low pressures, capturing 2.0 mmol/g at 390 ppm and 25°C. Additionally, Hong et al. developed a diamine-functionalized metal-organic framework with high CO_2 capacities of 2.83 mmol/g under DAC conditions, and this material remained stable even after exposure to humidity [56]. Yaghi et al. modified IRMOF-74-III with two primary alkylamines [57]. And while the general mechanism of CO_2 adsorption by amine groups involves the generation of ammonium carbamates, the authors demonstrated that the chemisorption product for this material was carbamic acid based on solid-state NMR results.

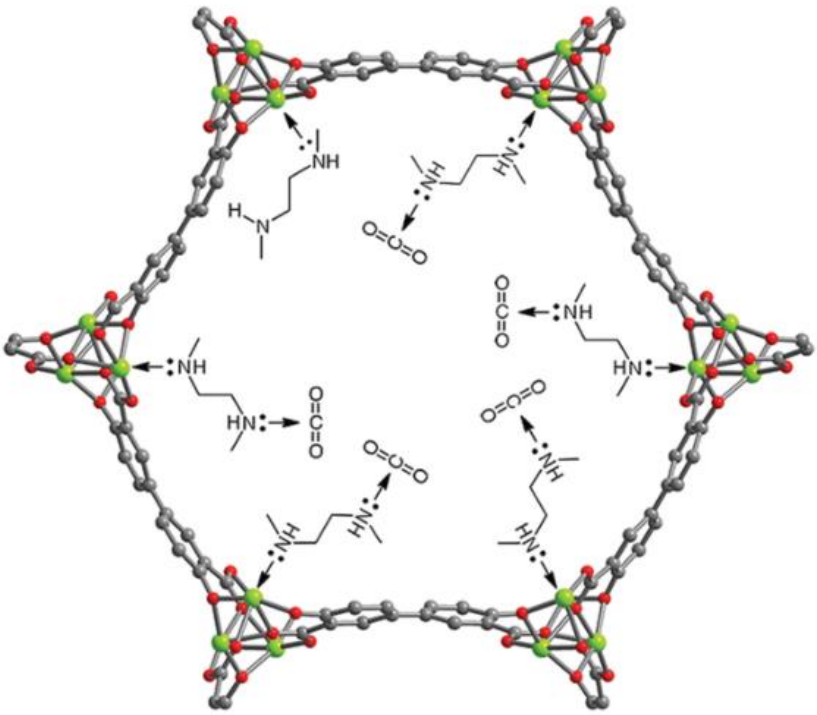

Figure 2.7 The structure of an alkylamine-appended metal-organic framework for direct air capture [55].

Green, red, and gray spheres represent Mg, O, and C atoms respectively.

Certain MOFs, such as UiO-66, have exhibited mesopores suitable for amine impregnation, leading to the development and application of amine-impregnated MOFs for atmospheric carbon capture [58]. Jones et al. prepared PEI-supported MIL-101(Cr), achieving a high CO_2 adsorption capacity of 1.35 mmol/g [12]. However, at high PEI loadings, although CO_2 uptake was high, adsorption kinetics were limited due to pore blockage.

While MOFs show promise as adsorbents for DAC, their high cost remains a significant obstacle to practical application in DAC. Further research is needed to address the challenges associated with large-scale, cost-effective MOF production for DAC purposes.

2.2.4 Zeolites

Physisorbents such as zeolite 13X can also be employed for direct air capture, but the competitive adsorption of atmospheric water significantly limits their applicability in DAC processes [6]. Yang et al. synthesized two microporous materials, Li-LSX and K-LSX, and conducted breakthrough experiments to assess their performance in direct air capture [4]. The results showed that Li-LSX and K-LSX exhibited atmospheric CO_2 adsorption capacities of

0.82 and 0.25 mmol/g under dry conditions. However, these uptakes dropped significantly to below 0.03 mmol/g in the presence of moisture. Using physisorbents for DAC in cold environments with low water content can potentially mitigate the impact of moisture on CO_2 adsorption performance by reducing competitive water adsorption. Jones et al. investigated the CO_2 sorption characteristics of low silica zeolites, including 3A, 4A, 5A, and 13X, for direct air capture (DAC) at -20 °C [59]. However, zeolite 5A demonstrated a significant 39% reduction in CO_2 adsorption capacity compared with experiments under dry conditions. To address the issue of competitive adsorption, a two-stage, two-bed process was developed to remove the water through a desiccant bed before adsorbing atmospheric CO_2. By using silica gel as a desiccant to remove atmospheric water, zeolite 13X showed potential feasibility for cold-temperature DAC, with an estimated energy requirement of 4359 MJ/tCO_2.

2.3 Adsorption processes for direct air capture

While most studies in the field of DAC have primarily focused on designing and synthesizing novel materials to enhance CO_2 adsorption performance, the efficient regeneration of adsorbents has been largely overlooked. DAC requires a strong affinity between CO_2 and sorbents, making the recovery of adsorbed CO_2 more challenging than in conventional carbon capture processes. Methods such as pressure swing adsorption (PSA) are widely used for carbon capture from large point sources [60-62]. However, applying these methods to DAC is energy-intensive, as pressurizing a significant amount of feed air is required. Furthermore, it is not feasible to reduce the desorption pressure below the feed CO_2 partial pressure (40 Pa) for vacuum swing adsorption (VSA). Typically, increasing the sorbent temperature is necessary to provide the driving force for CO_2 desorption. Therefore, temperature swing adsorption and temperature-vacuum swing adsorption have been developed and employed for DAC [63]. Table 2.2 presents the adsorption processes developed for DAC alongside their corresponding performance metrics.

2.3.1 Temperature swing adsorption (TSA)

Temperature swing adsorption, also known as temperature concentration swing adsorption in DAC, involves purging the sorbent at elevated temperatures (50-150 °C) using an inert gas stream such as N_2. This regeneration approach has been extensively studied in conjunction with investigations of DAC sorbents [11, 17, 19, 64]. But only a few works have been conducted to analyze the performance of TSA in practical DAC cycles. Elfving et al.

performed TSA cycles to investigate the desorption behavior of an amine-grafted resin, employing N_2 as a purge gas during the desorption step [65]. More than 85% of the adsorbed CO_2 was released at 60 °C. Liu et al. designed a bubbling fluidized bed reactor filled with PEI-impregnated silica [66]. Sorbent regeneration was achieved using N_2 as the stripping gas at 130 °C, resulting in a product stream with a CO_2 purity of approximately 6%. Olah et al. used dry air to regenerate PEI-impregnated silica at 85 °C [11]. And the CO_2 purity of the product was no more than 4.3%. In large-scale DAC applications, the requirement for high-purity CO_2 products (around 95%) for utilization or storage can compromise the use of TSA processes [67].

To address the issue of low product purity caused by inert gas purge, steam stripping was employed for regenerating sorbents. Since steam can be easily condensed and separated from CO_2 products, steam stripping is a potential process for producing high-purity CO_2 from the air. However, steam stripping can deactivate amines at high temperatures and reduce sorption capacity. For instance, the CO_2 adsorption capacity of PEI-impregnated alumina and PEI-impregnated silica decreased by 25.2% and 81.3%, respectively, after being treated at 105 °C for 24 hours [68].

2.3.2 Temperature-vacuum swing adsorption (TVSA)

TVSA is another prevalent process employed in practical DAC demonstrations using solid amines as CO_2 sorbents [69]. In contrast to temperature swing adsorption, TVSA uses a vacuum pump to reduce the CO_2 partial pressure during the regeneration process, providing the driving force for sorbent regeneration, as shown in Figure 2.8. Typically, regeneration in TVSA is conducted at a desorption pressure ranging from 5-20 kPa at 80-120 °C [5, 70].

Based on the adsorption behavior of developed sorbents like Lewatit VP OC 1065 and PEI-impregnated MOFs, the performance of TVSA processes in DAC has been extensively modelled and simulated [72-74]. Gazzani et al. conducted a comparative study of an aqueous scrubbing process and the TVSA process for DAC [74]. The results showed that TVSA outperformed the aqueous scrubbing process due to its lower exergy demand, which ranged from 1.4-3.7 MJ/kgCO_2. Both technologies have the potential to achieve DAC at a cost below \$200 per ton of captured CO_2.

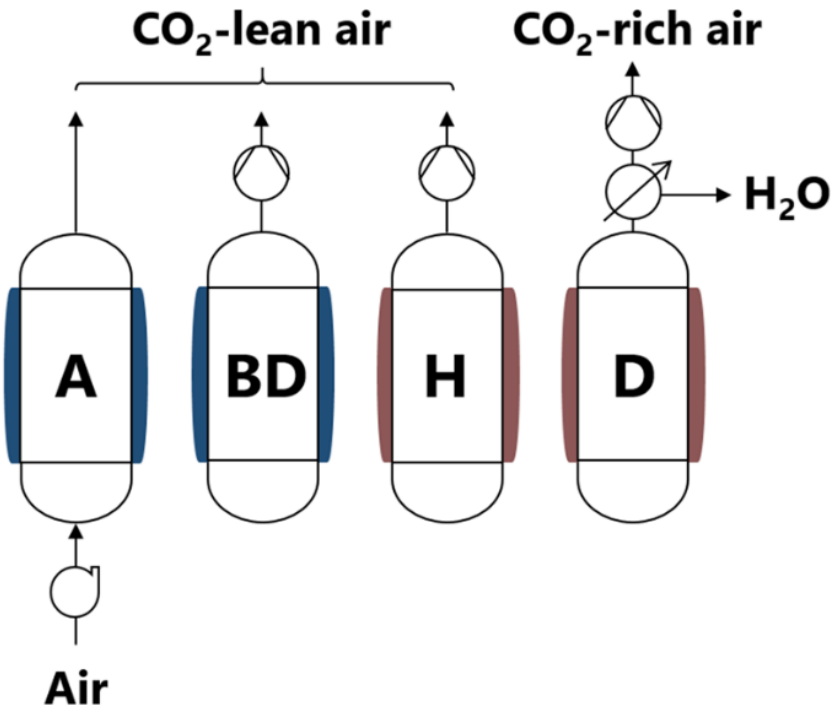

Figure 2.8 Four-step temperature-vacuum swing adsorption cycle [71].

A: adsorption step, BD: blow-down step, H: heating step, D: desorption step

Steinfeld et al. performed experimental works to investigate the TVSA process for DAC using a diamine-functionalized silica gel sorbent [5]. In dry conditions, desorption was challenging, with a CO_2 working capacity of only 0.03 mmol/g at 10 kPa. Conducting adsorption in a humid environment increased the working capacity to over 0.2 mmol/g. Elfving et al. investigated regeneration methods, particularly TVSA, for DAC using amine-based adsorbents [65]. Despite using a low desorption pressure of 2.5 kPa at 100 °C, the CO_2 working capacity reached only 0.39 mmol/g due to the strong interaction between CO_2 and amines.

Regarding pilot-scale demonstrations, the Thornton group developed a DAC module using a MOF-based sorbent [75]. Regeneration occurred at 80 °C and 3.7 kPa, with low electrical energy consumption (2.28 kWh/kgCO_2) and high CO_2 purity (70-80%). Besides, Bajamundi et al. designed a bench-scale DAC device comprising eight beds filled with amine-functionalized adsorbent [76]. Desorption was performed by heating the bed to approximately 80 °C under vacuum conditions, resulting in products with a purity range of 95-100%. The DAC system achieved a CO_2 working capacity of 0.36 mmol/g, with a specific energy requirement of 13 kWh/kgCO_2. To enhance the desorption driving force and recover more adsorbed CO_2, Lee et al. developed an electrically driven TVSA (ETVSA) module

(Figure 2.9) [77]. This module used sorbent-coated carbon fibers that exhibited Joule heating when a potential was applied, resulting in significantly accelerated CO_2 desorption through directly applied electric potential. A pilot-scale analysis estimated a cost of approximately \$160 per ton of captured CO_2.

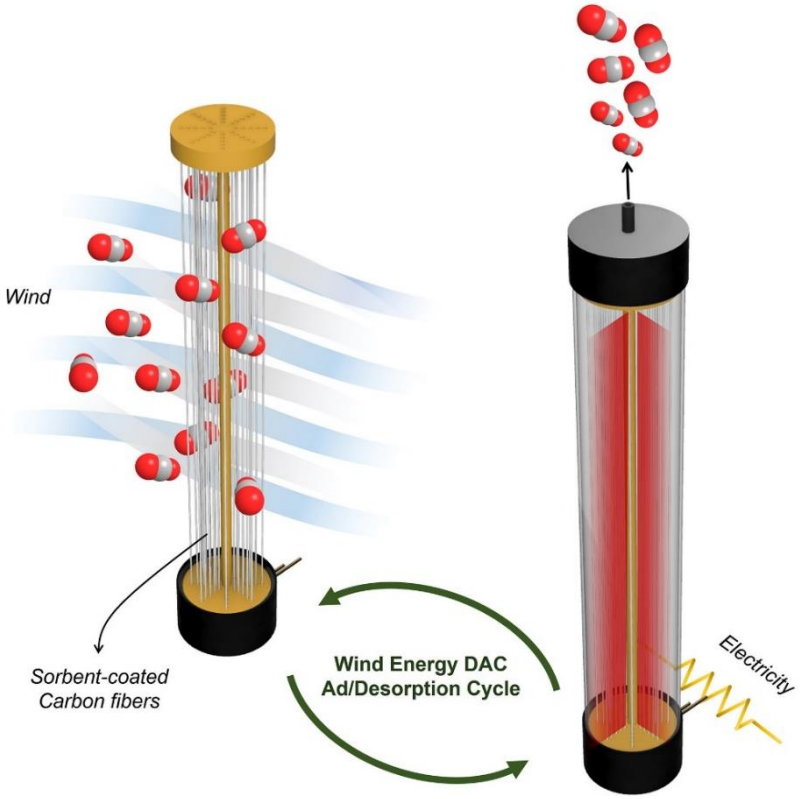

Figure 2.9 Sorbent-coated carbon fibers and electrically driven TVSA modules [77].

Steam stripping can also be coupled with TVSA to provide an additional driving force for sorbent regeneration. Chaffe et al. employed the steam-assisted TVSA process to fully regenerate a polyethylenimine-impregnated silica sorbent at 12 kPa and 100 °C [78]. In humid conditions, the presence of co-adsorbed water slowed CO_2 desorption due to additional energy requirements. Importantly, the sorbent demonstrated excellent stability, retaining 92% of its capacity after 50 cycles (>1500 hours). Mazzotti et al. designed a steam-assisted TVSA process for direct air capture and analyzed the performance through simulations [71]. The results indicated that using a steam purge in the TVSA regeneration process enhances CO_2 desorption kinetics and allows for greater CO_2 production at lower evacuation pressures. Through steam stripping, the desorption rate increased by more than 16 times compared to conventional TVSA processes. However, energy consumption for sorbent regeneration increased due to the additional thermal energy required to generate steam, as confirmed by Brilman et al [79].

2.3.3 Other processes

In addition to TSA and TVSA, there are also a few other processes used to conduct adsorption-based DAC. For example, Gary et al. discovered that the regeneration of PEI-impregnated sorbents could be enhanced by applying microwave irradiation [80]. The CO_2 desorption rate increased with the microwave output due to microwave-induced rotational-vibrational coupling transitions. Under microwave irradiation at near room temperature, a CO_2 working capacity of 0.6-1.4 mmol/g could be achieved.

Table 2.2 Performance of reported adsorption-based DAC processes.

Process	Adsorbent	W_c[a] (mmol/g)	T_{de} (°C)	P_{de} (bar)	E (MJ/kg_{CO2})	X_{CO2}	Ref.
TSA	Amine-based adsorbent	0.42	60	1	4.5	1.3%	[65]
TSA	PEI-silica	1.14	130	1	6.6	<7%	[66]
TSA	PEI-silica	1.70	85	1	-	4.3%	[11]
TVSA	SI-AEATPMS	0.21	90	0.15	10	97%	[5]
TVSA	Amine-based adsorbent	0.39	100	0.025	7.5	-	[65]
TVSA	MOF	0.30	80	0.037	8.2	75%	[75]
TVSA	Amine-based polymer	0.36	80	0.075	46.8	95%	[76]
ETVSA	Sorbent-coated fibers	0.54	110	0.3	7.2	82%	[77]
STVSA	PEI-silica	1.69	100	0.12	-	-	[78]
STVSA	VP OC 1065	0.77	116	0.5	15.04	-	[79]
MSA	Na_2CO_3-carbon	0.10	65	1	-	-	[3]
pH swing	Anion exchange resin	1.17	25	1	12.2	95%	[81]

[a] W_c: working capacity; T_{de}: desorption temperature; P_{de}: desorption pressure; E: energy consumption; X_{CO2}: product purity.

Moisture swing adsorption (MSA) is also an emerging process for DAC. Wang et al. developed an amine-based anion exchange resin with the ability to adsorb CO_2 under dry conditions and release it by wetting the resin (Figure 2.10) [41]. This moisture swing process is realized based on the transition between carbonate and bicarbonate ions under different moisture content. Using this mechanism, carbonate-supported carbon materials also exhibited moisture swing adsorption behaviors [3]. Sorbent regeneration was tested at a mild temperature of 65 °C through moisture swing to provide low-concentration CO_2 for greenhouses. However, the working capacity was only 0.1 mmol/g.

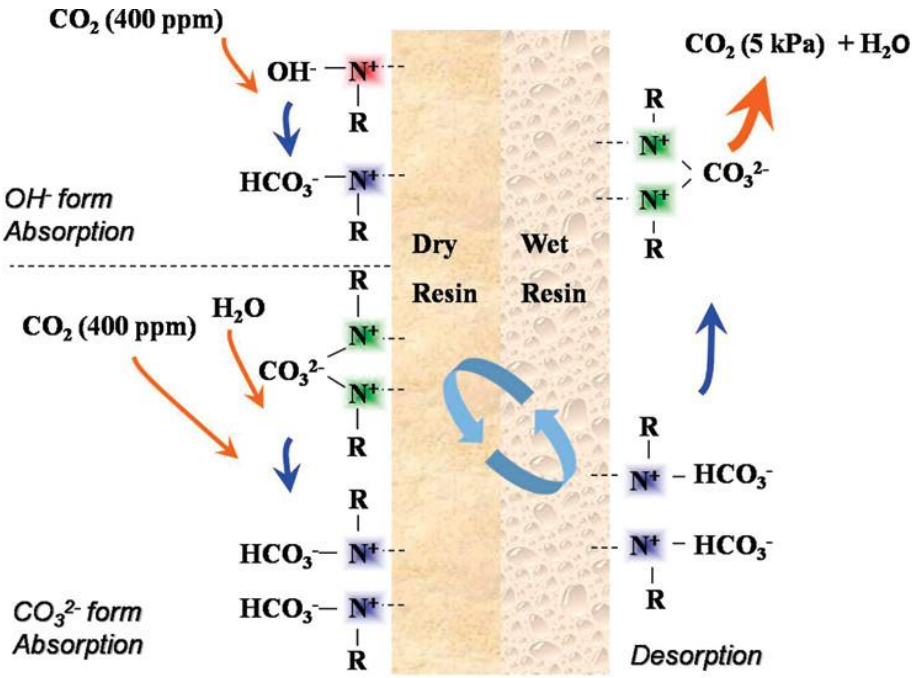

Figure 2.10 Mechanism of moisture swing adsorption based on ion exchange resins [41].

Another recently developed process was pH swing adsorption (Figure 2.11) powered by electrical energy [81]. In this process, after adsorbing atmospheric CO_2 using an amine-functionalized anion exchange resin, a NaOH solution was passed over the resin to recover the alkaline adsorption sites. The spent regeneration solution was then utilized to produce NaOH again in an electrochemical cell. While a high CO_2 working capacity of 1.76 mmol/g could be achieved at room temperature, it's worth noting that the energy consumption of the electrochemical cell could be as high as 537 kJ/mol. Although these new adsorption processes show unique potential, they are still in the experimental stage and require pilot-scale testing to confirm their feasibility in practical DAC systems.

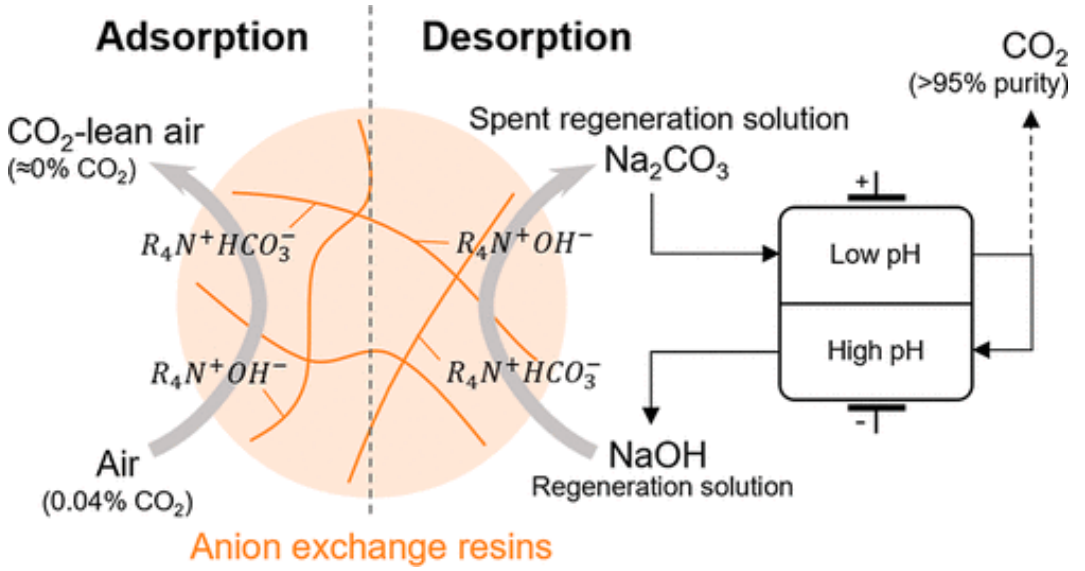

Figure 2.11 A pH swing adsorption process designed for DAC [81].

2.4 References

[1] E.S. Sanz-Pérez, C.R. Murdock, S.A. Didas, C.W. Jones, Direct capture of CO_2 from ambient air, Chem. Rev. 116 (2016) 11840-11876.

[2] V.S. Derevschikov, J.V. Veselovskaya, T.Y. Kardash, D.A. Trubitsyn, A.G. Okunev, Direct CO_2 capture from ambient air using K_2CO_3/Y_2O_3 composite sorbent, Fuel 127 (2014) 212-218.

[3] R. Rodríguez-Mosqueda, E.A. Bramer, G. Brem, CO_2 capture from ambient air using hydrated Na_2CO_3 supported on activated carbon honeycombs with application to CO_2 enrichment in greenhouses, Chem. Eng. Sci. 189 (2018) 114-122.

[4] N.R. Stuckert, R.T. Yang, CO_2 capture from the atmosphere and simultaneous concentration using zeolites and amine-grafted SBA-15, Environ. Sci. Technol. 45 (2011) 10257-10264.

[5] J.A. Wurzbacher, C. Gebald, A. Steinfeld, Separation of CO_2 from the air by temperature-vacuum swing adsorption using diamine-functionalized silica gel, Energ. Environ. Sci. 4 (2011) 3584.

[6] A. Kumar, D.G. Madden, M. Lusi, K.J. Chen, E.A. Daniels, T. Curtin, J.J. Perry, M.J. Zaworotko, Direct air capture of CO_2 by physisorbent materials, Angewandte Chemie International Edition 54 (2015) 14372-14377.

[7] J.V. Veselovskaya, V.S. Derevschikov, T.Y. Kardash, O.A. Stonkus, T.A. Trubitsina, A.G. Okunev, Direct CO_2 capture from ambient air using K_2CO_3/Al_2O_3 composite sorbent, Int. J. Greenh. Gas Con. 17 (2013) 332-340.

[8] R. Rodríguez-Mosqueda, J. Rutgers, E.A. Bramer, G. Brem, Low temperature water vapor pressure swing for the regeneration of adsorbents for CO_2 enrichment in greenhouses via direct air capture, Journal of CO_2 Utilization 29 (2019) 65-73.

[9] J. Young, E. García-Díez, S. Garcia, M. van der Spek, The impact of binary water-CO_2

isotherm models on the optimal performance of sorbent-based direct air capture processes, Energ. Environ. Sci. 14 (2021) 5377-5394.

[10] A. Goeppert, M. Czaun, G.K. Surya Prakash, G.A. Olah, Air as the renewable carbon source of the future: an overview of CO_2 capture from the atmosphere, Energ. Environ. Sci. 5 (2012) 7833.

[11] A. Goeppert, M. Czaun, R.B. May, G.K.S. Prakash, G.A. Olah, S.R. Narayanan, Carbon dioxide capture from the air using a polyamine based regenerable solid adsorbent, J. Am. Chem. Soc. 133 (2011) 20164-20167.

[12] L.A. Darunte, A.D. Oetomo, K.S. Walton, D.S. Sholl, C.W. Jones, Direct air capture of CO_2 using amine functionalized MIL-101(Cr), ACS Sustain. Chem. Eng. 4 (2016) 5761-5768.

[13] A. Goeppert, S. Meth, G.K.S. Prakash, G.A. Olah, Nanostructured silica as a support for regenerable high-capacity organoamine-based CO_2 sorbents, Energ. Environ. Sci. 3 (2010) 1949.

[14] H.T. Kwon, M.A. Sakwa-Novak, S.H. Pang, A.R. Sujan, E.W. Ping, C.W. Jones, Aminopolymer-impregnated hierarchical silica structures: unexpected equivalent CO_2 uptake under simulated air capture and flue gas capture conditions, Chem. Mater. 31 (2019) 5229-5237.

[15] W. Chaikittisilp, R. Khunsupat, T.T. Chen, C.W. Jones, Poly(allylamine)-mesoporous silica composite materials for CO_2 capture from simulated flue gas or ambient air, Ind. Eng. Chem. Res. 50 (2011) 14203-14210.

[16] Q.T. Vu, H. Yamada, K. Yogo, Effects of amine structures on oxidative degradation of amine-functionalized adsorbents for CO_2 capture, Ind. Eng. Chem. Res. 60 (2021) 4942-4950.

[17] A. Goeppert, H. Zhang, M. Czaun, R.B. May, G.K.S. Prakash, G.A. Olah, S.R. Narayanan, Easily regenerable solid adsorbents based on polyamines for carbon dioxide capture from the air, ChemSusChem 7 (2014) 1386-1397.

[18] S. Choi, M.L. Gray, C.W. Jones, Amine-tethered solid adsorbents coupling high adsorption capacity and regenerability for CO_2 capture from ambient air, ChemSusChem 4 (2011) 628-635.

[19] Y. Kuwahara, D. Kang, J.R. Copeland, N.A. Brunelli, S.A. Didas, P. Bollini, C. Sievers, T. Kamegawa, H. Yamashita, C.W. Jones, Dramatic enhancement of CO_2 uptake by poly(ethyleneimine) using zirconosilicate supports, J. Am. Chem. Soc. 134 (2012) 10757-10760.

[20] M.A. Sakwa-Novak, A. Holewinski, C.B. Hoyt, C. Yoo, S. Chai, S. Dai, C.W. Jones, Probing the role of Zr addition versus textural properties in enhancement of CO_2 adsorption performance in Silica/PEI composite sorbents, Langmuir 31 (2015) 9356-9365.

[21] M.A. Sakwa-Novak, S. Tan, C.W. Jones, Role of additives in composite PEI/Oxide CO_2 adsorbents: Enhancement in the amine efficiency of supported PEI by PEG in CO_2 capture from simulated ambient air, ACS Appl. Mater. Inter. 7 (2015) 24748-24759.

[22] A. Sayari, Q. Liu, P. Mishra, Enhanced adsorption efficiency through materials design for

direct air capture over supported polyethylenimine, ChemSusChem 9 (2016) 2796-2803.

[23] Z. Chen, S. Deng, H. Wei, B. Wang, J. Huang, G. Yu, Polyethylenimine-impregnated resin for high CO_2 adsorption: An efficient adsorbent for CO_2 capture from simulated flue gas and ambient air, ACS Appl. Mater. Inter. 5 (2013) 6937-6945.

[24] J. Wang, H. Huang, M. Wang, L. Yao, W. Qiao, D. Long, L. Ling, Direct capture of low-concentration CO_2 on mesoporous carbon-supported solid amine adsorbents at ambient temperature, Ind. Eng. Chem. Res. 54 (2015) 5319-5327.

[25] H. Sehaqui, M.E. Gálvez, V. Becatinni, Y. Cheng Ng, A. Steinfeld, T. Zimmermann, P. Tingaut, Fast and reversible direct CO_2 capture from air onto all-polymer nanofibrillated cellulose-polyethylenimine foams, Environ. Sci. Technol. 49 (2015) 3167-3174.

[26] M.A. Sakwa-Novak, C. Yoo, S. Tan, F. Rashidi, C.W. Jones, Poly(ethylenimine)-functionalized monolithic alumina honeycomb adsorbents for CO_2 capture from air, ChemSusChem 9 (2016) 1859-1868.

[27] S.H. Pang, L. Lee, M.A. Sakwa-Novak, R.P. Lively, C.W. Jones, Design of aminopolymer structure to enhance performance and stability of CO_2 sorbents: poly(propylenimine) vs poly(ethylenimine), J. Am. Chem. Soc. 139 (2017) 3627-3630.

[28] C.W. Jones, CO_2 capture from dilute gases as a component of modern global carbon management, Annu. Rev. Chem. Biomol. 2 (2011) 31-52.

[29] L.F. Feitosa, B.B. Pozes, A.S. Silva, L.F. Castro, L.S.C. Júnior, C.B. Quitete, M.A. Fraga, Surface molecular design of organic-inorganic mesoporous hybrid materials for CO_2 capture, Journal of Environmental Chemical Engineering 9 (2021) 104951.

[30] C. Gebald, J.A. Wurzbacher, P. Tingaut, T. Zimmermann, A. Steinfeld, Amine-based nanofibrillated cellulose as adsorbent for CO_2 capture from air, Environ. Sci. Technol. 45 (2011) 9101-9108.

[31] C. Gebald, J.A. Wurzbacher, P. Tingaut, A. Steinfeld, Stability of amine-functionalized cellulose during temperature-vacuum-swing cycling for CO_2 capture from air, Environ. Sci. Technol. 47 (2013) 10063-10070.

[32] Y. Kong, X. Shen, S. Cui, M. Fan, Facile synthesis of an amine hybrid aerogel with high adsorption efficiency and regenerability for air capture via a solvothermal-assisted sol-gel process and supercritical drying, Green Chem. 17 (2015) 3436-3445.

[33] S.A. Didas, A.R. Kulkarni, D.S. Sholl, C.W. Jones, Role of amine structure on carbon dioxide adsorption from ultradilute gas streams such as ambient air, ChemSusChem 5 (2012) 2058-2064.

[34] M.A. Alkhabbaz, P. Bollini, G.S. Foo, C. Sievers, C.W. Jones, Important roles of enthalpic and entropic contributions to CO_2 capture from simulated flue gas and ambient air using mesoporous silica grafted amines, J. Am. Chem. Soc. 136 (2014) 13170-13173.

[35] W. Buijs, S. de Flart, Direct air capture of CO_2 with an amine resin: A molecular modeling study of the CO_2 capturing process, Ind. Eng. Chem. Res. 56 (2017) 12297-12304.

[36] W. Chaikittisilp, J.D. Lunn, D.F. Shantz, C.W. Jones, Poly(L-lysine) brush-mesoporous silica hybrid material as a biomolecule‐based adsorbent for CO_2 capture from simulated

flue gas and air, Chem.-Eur. J. 17 (2011) 10556-10561.

[37] S. Choi, J.H. Drese, P.M. Eisenberger, C.W. Jones, Application of amine-tethered solid sorbents for direct CO_2 capture from the ambient air, Environ. Sci. Technol. 45 (2011) 2420-2427.

[38] F. Liu, L. Wang, Z. Huang, C. Li, W. Li, R. Li, W. Li, Amine-tethered adsorbents based on three-dimensional macroporous silica for CO_2 capture from simulated flue gas and air, ACS Appl. Mater. Inter. 6 (2014) 4371-4381.

[39] K.A.S. Abhilash, T. Deepthi, R.A. Sadhana, K.G. Benny, Functionalized polysilsesquioxane-based hybrid silica solid amine sorbents for the regenerative removal of CO_2 from air, ACS Appl. Mater. Inter. 7 (2015) 17969-17976.

[40] W. Lu, J.P. Sculley, D. Yuan, R. Krishna, H. Zhou, Carbon dioxide capture from air using amine-grafted porous polymer networks, The Journal of Physical Chemistry C 117 (2013) 4057-4061.

[41] T. Wang, K.S. Lackner, A. Wright, Moisture swing sorbent for carbon dioxide capture from ambient air, Environ. Sci. Technol. 45 (2011) 6670-6675.

[42] J. Song, J. Liu, W. Zhao, Y. Chen, H. Xiao, X. Shi, Y. Liu, X. Chen, Quaternized chitosan/PVA aerogels for reversible CO_2 capture from ambient air, Ind. Eng. Chem. Res. 57 (2018) 4941-4948.

[43] M. Jahandar Lashaki, S. Khiavi, A. Sayari, Stability of amine-functionalized CO_2 adsorbents: a multifaceted puzzle, Chem. Soc. Rev. 48 (2019) 3320-3405.

[44] Q.T. Vu, H. Yamada, K. Yogo, Oxidative degradation of tetraethylenepentamine-impregnated silica sorbents for CO_2 capture, Energ. Fuel. 33 (2019) 3370-3379.

[45] Y. Miao, Y. Wang, X. Zhu, W. Chen, Z. He, L. Yu, J. Li, Minimizing the effect of oxygen on supported polyamine for direct air capture, Sep. Purif. Technol. 298 (2022) 121583.

[46] M.A. Sakwa-Novak, C.W. Jones, Steam induced structural changes of a poly(ethylenimine) impregnated γ-Alumina sorbent for CO_2 extraction from ambient air, ACS Appl. Mater. Inter. 6 (2014) 9245-9255.

[47] Q. Yu, J.D.L.P. Delgado, R. Veneman, D.W.F. Brilman, Stability of a benzyl amine based CO_2 capture adsorbent in view of regeneration strategies, Ind. Eng. Chem. Res. 56 (2017) 3259-3269.

[48] A. Sayari, A. Heydari-Gorji, Y. Yang, CO_2-induced degradation of amine-containing adsorbents: Reaction products and pathways, J. Am. Chem. Soc. 134 (2012) 13834-13842.

[49] K. Min, W. Choi, C. Kim, M. Choi, Oxidation-stable amine-containing adsorbents for carbon dioxide capture, Nat. Commun. 9 (2018) 1-7.

[50] A. Goeppert, H. Zhang, R. Sen, H. Dang, G.K.S. Prakash, Oxidation-resistant, cost-effective epoxide-modified polyamine adsorbents for CO_2 capture from various sources including air, ChemSusChem 12 (2019) 1712-1723.

[51] N. Stock, S. Biswas, Synthesis of metal-organic frameworks (MOFs): Routes to various MOF topologies, morphologies, and composites, Chem. Rev. 112 (2012) 933-969.

[52] P.M. Bhatt, Y. Belmabkhout, A. Cadiau, K. Adil, O. Shekhah, A. Shkurenko, L.J. Barbour, M. Eddaoudi, A fine-tuned fluorinated MOF addresses the needs for trace CO_2 removal and air capture using physisorption, J. Am. Chem. Soc. 138 (2016) 9301-9307.

[53] O. Shekhah, Y. Belmabkhout, Z. Chen, V. Guillerm, A. Cairns, K. Adil, M. Eddaoudi, Made-to-order metal-organic frameworks for trace carbon dioxide removal and air capture, Nat. Commun. 5 (2014) 1-7.

[54] S.J. Datta, C. Khumnoon, Z.H. Lee, W.K. Moon, S. Docao, T.H. Nguyen, I.C. Hwang, D. Moon, P. Oleynikov, O. Terasaki, K.B. Yoon, CO_2 capture from humid flue gases and humid atmosphere using a microporous coppersilicate, Science 350 (2015) 302-306.

[55] T.M. McDonald, W.R. Lee, J.A. Mason, B.M. Wiers, C.S. Hong, J.R. Long, Capture of carbon dioxide from air and flue gas in the alkylamine-appended metal-oganic framework mmen-Mg_2(dobpdc), J. Am. Chem. Soc. 134 (2012) 7056-7065.

[56] W.R. Lee, S.Y. Hwang, D.W. Ryu, K.S. Lim, S.S. Han, D. Moon, J. Choi, C.S. Hong, Diamine-functionalized metal-organic framework: exceptionally high CO_2 capacities from ambient air and flue gas, ultrafast CO_2 uptake rate, and adsorption mechanism, Energ. Environ. Sci. 7 (2014) 744-751.

[57] R.W. Flaig, T.M. Osborn Popp, A.M. Fracaroli, E.A. Kapustin, M.J. Kalmutzki, R.M. Altamimi, F. Fathieh, J.A. Reimer, O.M. Yaghi, The chemistry of CO_2 capture in an amine-functionalized metal-organic framework under dry and humid conditions, J. Am. Chem. Soc. 139 (2017) 12125-12128.

[58] Z. Li, H. Chen, C. Chen, Q. Guo, X. Li, Y. He, H. Wang, N. Feng, H. Wan, G. Guan, High dispersion of polyethyleneimine within mesoporous UiO-66s through pore size engineering for selective CO_2 capture, Chem. Eng. J. 375 (2019) 121962.

[59] M. Song, G. Rim, F. Kong, P. Priyadarshini, C. Rosu, R.P. Lively, C.W. Jones, Cold-temperature capture of carbon dioxide with water coproduction from air using commercial zeolites, Ind. Eng. Chem. Res. 61 (2022) 13624-13634.

[60] J.M. Simmons, H. Wu, W. Zhou, T. Yildirim, Carbon capture in metal-organic frameworks-a comparative study, Energ. Environ. Sci. 4 (2011) 2177.

[61] M. Khurana, S. Farooq, Integrated adsorbent-process optimization for carbon capture and concentration using vacuum swing adsorption cycles, AIChE J. 63 (2017) 2987-2995.

[62] Y.R. Tao, H.J. Xu, A critical review on potential applications of Metal-Organic Frameworks (MOFs) in adsorptive carbon capture technologies, Appl. Therm. Eng. 236 (2024) 121504.

[63] X. Zhu, W. Xie, J. Wu, Y. Miao, C. Xiang, C. Chen, B. Ge, Z. Gan, F. Yang, M. Zhang, D. O'Hare, J. Li, T. Ge, R. Wang, Recent advances in direct air capture by adsorption, Chem. Soc. Rev. 51 (2022) 6574-6651.

[64] L. Wang, M. Al-Aufi, C.N. Pacheco, L. Xie, R.M. Rioux, Polyethylene glycol (PEG) addition to polyethylenimine (PEI)-impregnated silica increases amine accessibility during CO_2 sorption, ACS Sustain. Chem. Eng. 7 (2019) 14785-14795.

[65] J. Elfving, J. Kauppinen, M. Jegoroff, V. Ruuskanen, L. Järvinen, T. Sainio, Experimental comparison of regeneration methods for CO_2 concentration from air using amine-based adsorbent, Chem. Eng. J. 404 (2021) 126337.

[66] W. Zhang, H. Liu, C. Sun, T.C. Drage, C.E. Snape, Capturing CO_2 from ambient air using a polyethyleneimine-silica adsorbent in fluidized beds, Chem. Eng. Sci. 116 (2014) 306-316.

[67] M. Erans, E.S. Sanz-Pérez, D.P. Hanak, Z. Clulow, D.M. Reiner, G.A. Mutch, Direct air capture: process technology, techno-economic and socio-political challenges, Energ. Environ. Sci. 15 (2022) 1360-1405.

[68] W. Chaikittisilp, H. Kim, C.W. Jones, Mesoporous alumina-supported amines as potential steam-stable adsorbents for capturing CO_2 from simulated flue gas and ambient air, Energ. Fuel. 25 (2011) 5528-5537.

[69] S. Deutz, A. Bardow, Life-cycle assessment of an industrial direct air capture process based on temperature-vacuum swing adsorption, Nature Energy 6 (2021) 203-213.

[70] J.A. Wurzbacher, C. Gebald, N. Piatkowski, A. Steinfeld, Concurrent separation of CO_2 and H_2O from air by a temperature-vacuum swing adsorption/desorption cycle, Environ. Sci. Technol. 46 (2012) 9191-9198.

[71] V. Stampi-Bombelli, M. van der Spek, M. Mazzotti, Analysis of direct capture of CO_2 from ambient air via steam-assisted temperature-vacuum swing adsorption, Adsorption 26 (2020) 1183-1197.

[72] J.A. Wurzbacher, C. Gebald, S. Brunner, A. Steinfeld, Heat and mass transfer of temperature-vacuum swing desorption for CO_2 capture from air, Chem. Eng. J. 283 (2016) 1329-1338.

[73] T. Deschamps, M. Kanniche, L. Grandjean, O. Authier, Modeling of vacuum temperature swing adsorption for direct air capture using aspen adsorption, Clean Technologies 4 (2022) 258-275.

[74] F. Sabatino, A. Grimm, F. Gallucci, M. van Sint Annaland, G.J. Kramer, M. Gazzani, A comparative energy and costs assessment and optimization for direct air capture technologies, Joule 5 (2021) 2047-2076.

[75] M.M. Sadiq, M.P. Batten, X. Mulet, C. Freeman, K. Konstas, J.I. Mardel, J. Tanner, D. Ng, X. Wang, S. Howard, M.R. Hill, A.W. Thornton, A pilot-scale demonstration of mobile direct air capture using metal-organic frameworks, Advanced Sustainable Systems 4 (2020) 1-8.

[76] C.J. E. Bajamundi, J. Koponen, V. Ruuskanen, J. Elfving, A. Kosonen, J. Kauppinen, J. Ahola, Capturing CO_2 from air: Technical performance and process control improvement, Journal of CO_2 Utilization 30 (2019) 232-239.

[77] W.H. Lee, X. Zhang, S. Banerjee, C.W. Jones, M.J. Realff, R.P. Lively, Sorbent-coated carbon fibers for direct air capture using electrically driven temperature swing adsorption, Joule 7 (2023) 1241-1259.

[78] R.P. Wijesiri, G.P. Knowles, H. Yeasmin, A.F.A. Hoadley, A.L. Chaffee, Desorption process for capturing CO_2 from air with supported amine sorbent, Ind. Eng. Chem. Res. 58 (2019) 15606-15618.

[79] M.J. Bos, S. Pietersen, D.W.F. Brilman, Production of high purity CO_2 from air using solid amine sorbents, Chemical Engineering Science: X 2 (2019) 100020.

[80] T. Ji, H. Zhai, C. Wang, C.M. Marin, W.C. Wilfong, Q. Wang, Y. Duan, R. Xia, F. Jiao, Y. Soong, F. Shi, M. Gray, Energy-efficient and water-saving sorbent regeneration at near room temperature for direct air capture, Materials Today Sustainability 21 (2023) 100321.

[81] Q. Shu, M. Haug, M. Tedesco, P. Kuntke, H.V.M. Hamelers, Direct air capture using electrochemically regenerated anion exchange resins, Environ. Sci. Technol. 56 (2022) 11559-11566.

3 Development of a vapor-promoted desorption process for direct air capture

3.1 Introduction

The urgent need to reverse the rising trend of CO_2 concentrations has created a strong demand for large-scale implementation of negative emissions technologies [1-3]. Direct air capture (DAC), involving the direct extraction of CO_2 from the atmosphere, has gained significant attention as a crucial approach for achieving negative emissions [4-6]. Among the various DAC technologies, the adsorption-desorption process using solid adsorbents is particularly promising due to its relatively low regeneration temperature [7-9].

The selection of adsorbents and processes for DAC is constrained by the moisture and extremely low concentration of CO_2 in the air (around 400 ppm) [7]. Among the adsorbents used in DAC, chemisorbents, particularly solid amine sorbents with large heat of adsorption (60-100 kJ/mol) and high CO_2 selectivity, are commonly employed [10, 11]. However, regenerating DAC adsorbents is extremely energy intensive due to the strong affinity of amine groups with CO_2, making DAC highly expensive with a cost of over \$100 /t_{CO2} [10, 12, 13].

Typically, the desorption process in DAC requires elevating the temperature to approximately 100 °C while creating a vacuum to reduce the partial pressure of CO_2, serving as the driving force for adsorbent regeneration [14, 15]. To address this, temperature vacuum swing adsorption (TVSA) processes are commonly used to achieve CO_2 capture from air [2, 10, 16, 17]. Nevertheless, the typical desorption pressure range of 5 to 30 kPa in the TVSA process is insufficient to efficiently release the adsorbed CO_2, leading to a limited CO_2 working capacity of less than 0.5 mmol/g [15, 18, 19]. To promote CO_2 desorption and improve the working capacity, several strategies have been employed, including raising the desorption temperature, reducing the desorption pressure, or implementing steam stripping [19, 20]. However, these approaches increase energy consumption and operating costs, which further compromise the economic viability and hinder large-scale deployment of DAC.

The objective of this chapter is to develop an alternative method to recover the CO_2 adsorbed on solid amine sorbents, aiming to achieve a larger working capacity while minimizing energy consumption. In this chapter, a novel *in situ* vapor-promoted desorption (VPD) process was proposed to efficiently regenerate adsorbents and produce high-purity CO_2 from ambient air without requiring evacuation. This approach substantially reduced CO_2 partial pressure during

regeneration and recovered over 90% of the adsorbed CO_2 at 100 °C by *in situ* vapor purge using water harvested from the atmosphere. The VPD process was demonstrated by constructing a solar-powered DAC prototype that used sunlight as the sole energy source for adsorbent regeneration. This prototype not only showed a significant reduction in energy consumption but also achieved much higher CO_2 working capacities in comparison with prevalent TVSA techniques.

3.2 Experimental

3.2.1 Vapor-promoted desorption process

The entire process is based on temperature-concentration swing adsorption and is composed of four stages (Figure 3.1A) namely, adsorption, preheating, desorption and cooling, employing a double-layered adsorption column. In the adsorption stage, two adsorbents sequentially packed in the column adsorb CO_2 and H_2O from the air. Subsequently, the temperature of the adsorbent bed is elevated through solar or electrical heating. The CO_2 and vapors with increased partial pressures displace the air inside the column, thereby preventing oxidative degradation of the adsorbent at high temperatures. During the desorption stage, the increased vapor partial pressure reduces the carbon dioxide partial pressure and promotes the regeneration of solid amine sorbents. This desorption approach requires only thermal energy obtained from sunlight or waste heat to increase adsorbent temperatures and realize adsorbent regeneration (Figure 3.1B), eliminating the need for an external purge supply or vacuum pumps. The water in the product stream is easily condensed and separated, leaving high-purity CO_2. After collecting the products, fresh air is introduced to lower the adsorbent temperature and initiate the next adsorption cycle.

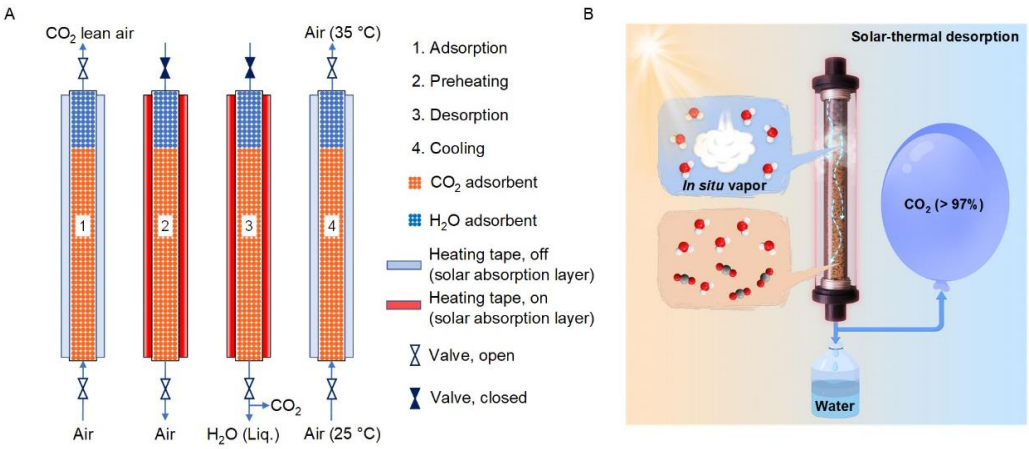

Figure 3.1 Working principle of vapor-promoted desorption for DAC.

3.2.2 Materials and characterizations

In this chapter, direct air capture was performed using Lewatit VP OC 1065 (Lanxess) as the CO_2 adsorbent. The material, which ranges in diameter from 0.3-1.2 mm, is a primary amine functionalized weakly basic anion exchange resin that has been identified as a promising adsorbent for DAC. Type A silica gel (Desicco) with a particle size of 3-5 mm was employed as the water adsorbent. Before usage, the silica gel and resin were pre-treated under vacuum at 110 °C and 80 °C, respectively.

The CO_2 adsorption behavior of VP OC 1065 resin is characterized using a reported Dual-site Langmuir model (Equations 3.1-3.3) [21], with the fitted parameters provided in Table 3.1.

$$q_{CO_2} = \frac{q_1 K_1 P}{1 + K_1 P} + \frac{q_2 K_2 P}{1 + K_2 P} \tag{3.1}$$

$$K_1 = K_{0,1} \exp\left(\frac{-\Delta H_{ads,1}}{RT}\right) \tag{3.2}$$

$$K_2 = K_{0,2} \exp\left(\frac{-\Delta H_{ads,2}}{RT}\right) \tag{3.3}$$

Table 3.1 Dual-site Langmuir model parameters of CO_2 adsorption on Lewatit resin.

Parameter	Value
q_1 (mmol/g)	1.94
q_2 (mmol/g)	1.06
$K_{0,1}$ (1/Pa)	1.11×10^{-15}
$K_{0,2}$ (1/Pa)	1.84×10^{-13}
$-\Delta H_{ads,1}$ (kJ/mol)	75.6
$-\Delta H_{ads,2}$ (kJ/mol)	51.6

The theoretical working capacity (W_c) of Lewatit resin is evaluated by the following equation.

$$W_c = q_{CO_2}\left(T_{ads}, P_{CO_2,ads}\right) - q_{CO_2}\left(T_{des}, P_{CO_2,des}\right) \tag{3.4}$$

$q_{CO_2}\left(T_{ads}, P_{CO_2,ads}\right)$ and $q_{CO_2}\left(T_{des}, P_{CO_2,des}\right)$ represent calculated CO_2 loadings under adsorption and desorption conditions based on the proposed isotherm model. P_{CO_2} and T are the CO_2 partial pressure and adsorbent temperature. In the adsorption process, T_{ads} and

$P_{CO_2,ads}$ are fixed at 25 °C and 40 Pa, respectively.

Fourier-transform infrared spectroscopy (FTIR) spectra were collected using a Nicolet iS50 FTIR Spectrometer. The thermal stability of VP OC 1065 was characterized using thermogravimetric analysis (TGA) with a Mettler Toledo TGA/DSC 1 under the designated atmosphere and conditions. *In situ* FTIR was used to investigate the changes in surface species during the regeneration or deactivation of VP OC 1065 with a Bruker Tensor 27 spectrometer. Before analysis, the sample was exposed to air at 25 °C and 30% RH overnight to adsorb CO_2 and H_2O. Then, the sample was treated with N_2 flow at 100 °C while spectra were recorded every 5 min. The CO_2-induced deactivation mechanism was investigated using *in situ* FTIR under a CO_2 atmosphere at 150 °C. The sample was treated with pure CO_2 at 80 °C for 3 hours and at 150 °C for 15 min before analysis, with spectra collected every 60 min at 150 °C.

3.2.3 Experimental setups for direct air capture

A stainless-steel tube of 8 cm in length and 1 cm in diameter was employed as the adsorption column to analyze the breakthrough curves for CO_2 adsorption (Figure 3.2). The adsorption temperature was controlled by a thermostat oven set to 28 °C. Compressed air with 410 ppm CO_2 was introduced to the adsorption column at a gas-hourly space velocity (GHSV, based on the volume of resin) of 12000 /h. GHSV is a measure of the flow rate of gas through an adsorbent bed per unit volume of adsorbent per hour, making it a representative measure of the volume of air contacted per unit volume of adsorbent. The gas superficial velocity can be calculated based on the size of the adsorption column, the volume of the adsorbent, and the given gas hourly space velocity. The outlet CO_2 concentrations were monitored by an infrared CO_2 sensor (Dynament, 0-1000 ppm), while two humidity sensors (Ningbo Keshun KS-SHT and Vaisala HMT338) continuously recorded the feed and outlet relative humidity. Breakthrough experiments were performed under different humidities to investigate the impact of varying humidities on CO_2 adsorption behavior. A humidifier at 28 °C was used to control the required relative humidity.

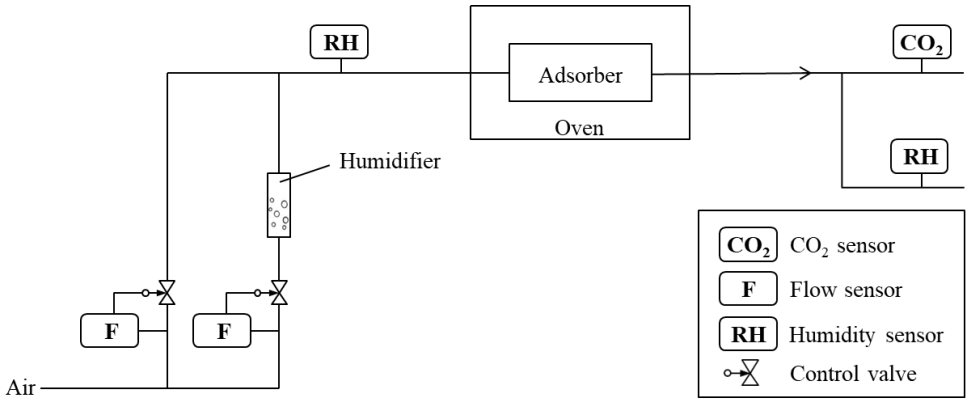

Figure 3.2 Scheme of the setup for breakthrough experiments.

The schematic of the setup used for testing vapor-promoted DAC is illustrated in Figure 3.3. Stainless steel columns, measuring 60 cm in length and 4 cm in diameter, were used as adsorption columns. Silica gel and Lewatit resin were packed sequentially within one adsorption column. Fresh air containing 410-450 ppm CO_2 first flowed over Lewatit resin, and subsequently over silica gel, for CO_2 and H_2O adsorption. GHSV was regulated by flow meters and ranged from 3000 to 10000 /h. The outlet CO_2 concentrations were monitored by an infrared CO_2 sensor (Dynament, 0-1000 ppm), while the feed and outlet relative humidity were continuously recorded by two humidity sensors (Ningbo Keshun KS-SHT and Vaisala HMT338). One of the air streams passed through a 27 °C humidifier to control the humidity of the feed gas.

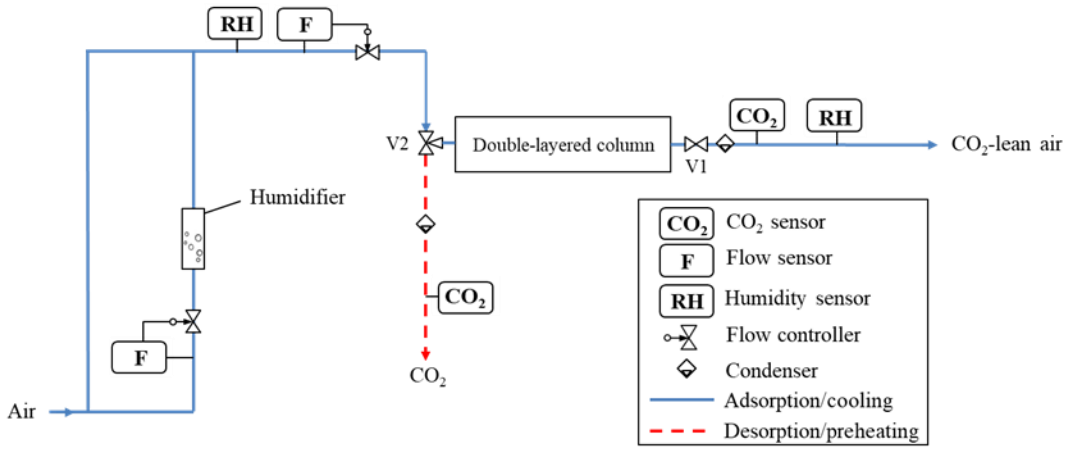

Figure 3.3 Scheme of the setup for testing the cyclic performance of vapor-promoted DAC.

A thermal couple was placed at the center of VP OC 1065 to monitor the temperature profile throughout the adsorption-desorption cycles. The CO_2 uptake ($q_{CO_2}^{ads}$, mmol/g) during the adsorption process was calculated based on the following equation [22].

$$q_{CO_2}^{ads} = \int_0^{t_{ads}} \frac{n_{air}\left(C_{CO_2,in} - C_{CO_2,out}\right)}{m} dt \tag{3.5}$$

where t_{ads} is the adsorption time, n_{air} is the flow rate of the inlet air, $C_{CO_2,in}$ is the atmospheric CO_2 concentration, $C_{CO_2,out}$ is the CO_2 concentration in the outlet gas and m is the mass of VP OC 1065. The water adsorption capacity is determined by the same calculation method.

Thermal energy, either supplied by electrical heating or solar energy, was employed to regenerate the adsorbents and produce high purity CO_2 and water. The adsorption columns used for electrical and solar heating are illustrated in Figure 3.4. The solar-heating column with black coatings could receive solar energy and provide the heat required by adsorbent regeneration. In this study, the electrical heating power applied was 90 W, while the solar flux typically ranged from 400-800 W/m^2 for solar heating in Tianjin, China.

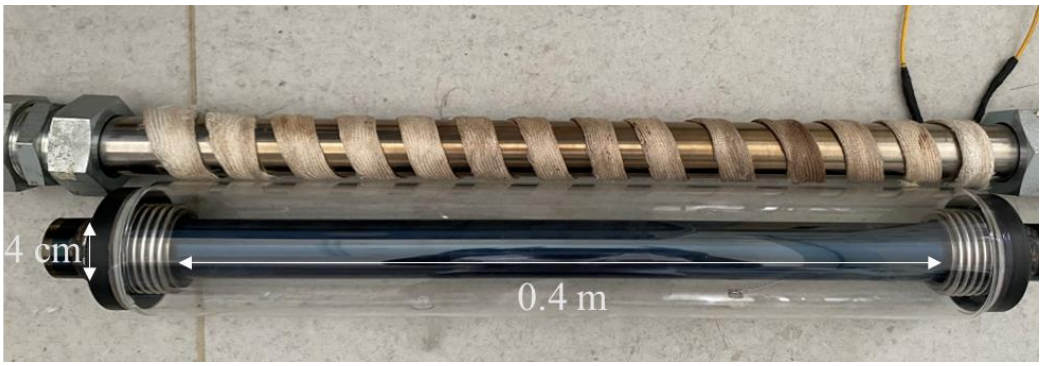

Figure 3.4 Adsorption columns for electrical heating (Top) and solar heating (Bottom).

The solar-powered prototype for DAC is depicted in Figure 3.5. During the preheating and desorption steps, the solar flux was measured by a pyranometer (Renke, RS-RA). As the temperature of the adsorbent increased, the vapors in the product stream were collected as liquid water products by the air-cooled condenser, while the CO_2 product was collected using a syringe to record the product volume profile (Figure 3.5). The collected CO_2 product was then stored in gas sampling bags and analyzed using gas chromatography with a thermal conductivity detector. To monitor the real-time product purity, a CO_2 sensor (Dynament, 0-100%) was directly connected to the condenser and syringe. The volume profile of desorbed CO_2 can be expressed as,

$$V_{CO_2,t_{des}} = \int_0^{t_{des}} C_{CO_2,t} \frac{\partial V_{p,t}}{\partial t} dt \tag{3.6}$$

where $V_{CO_2,t}$ is the desorbed CO_2 volume at a certain desorption time (t), $V_{p,t}$ is the

product volume at t, $C_{CO_2,t}$ is the real-time CO_2 purity of the product at t. Once the volume profile of desorbed CO_2 is obtained, the CO_2 loading of VP OC 1065 during the desorption step can be determined.

The water product collected from the condenser was analyzed using ^1H NMR spectra (Varian VNMRS 600 MHz). To analyze the water vapor pressure inside the column during desorption, a humidity sensor (Vaisala HMT338) was directly inserted into the column to measure the humidity and temperature surrounding VP OC 1065. The water vapor pressure was calculated using the Antoine equation for vapor-pressure data [23]. After the desorption process, the adsorption column was purged with fresh air to rapidly decrease the adsorbent temperature and initiate the next adsorption cycle.

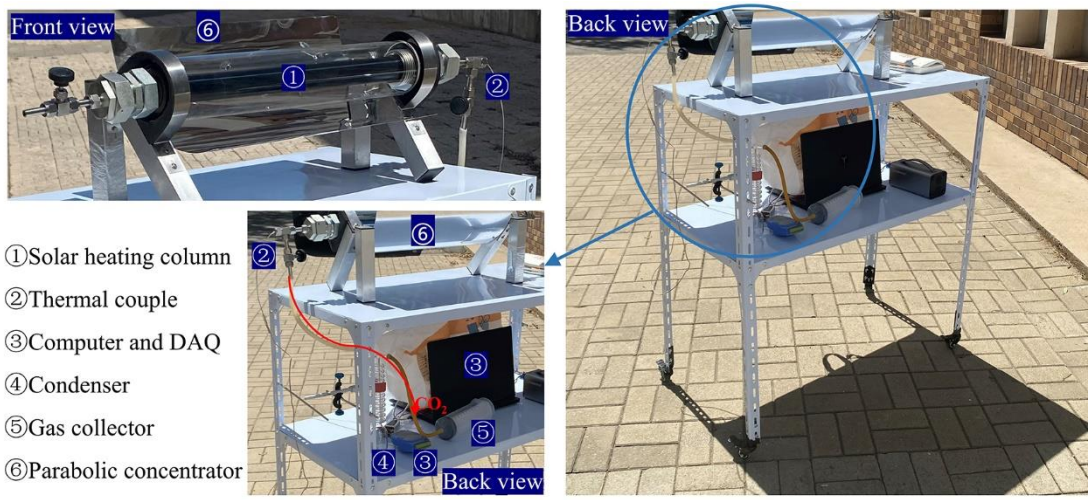

Figure 3.5 Solar-powered DAC prototype for high purity CO_2 and water production from the air.

3.2.4 Energy consumption analysis

To calculate the photothermal conversion efficiency of the solar-powered DAC prototype, temperature increases of an empty solar-heating column were measured under sunlight irradiation. The thermal energy ($Q_{thermal}$) converted from solar energy as well as the photothermal conversion efficiency (α) were calculated using Equations 3.7 and 3.8,

$$Q_{thermal} = \alpha A \int_0^t I_{solar} dt = m_{tube} C_{tube} \Delta T_{tube} \tag{3.7}$$

$$\alpha = \frac{m_{tube} C_{tube} \Delta T_{tube}}{A \int_0^t I_{solar} dt} \tag{3.8}$$

where A is the projected area (0.05 m^2) of the black coating for receiving natural sunlight, I_{solar} is the solar flux, t is the solar irradiation time, m_{tube} refers to the mass of the solar-heating column (1.07 kg), C_{tube} is the heat capacity (500 J/kg·K) of the tube, ΔT_{tube} represents the temperature increase of the adsorption column during solar heating.

A parabolic concentrator was used to enhance the heating power of the photothermal DAC prototype. The optical concentration ratio (σ) of the parabolic concentrator was determined by conducting solar heating experiments under concentrated sunlight and calculated using Equation 3.9.

$$\sigma = \frac{m_{tube} C_{tube} \Delta T_{tube}}{\alpha A \int_0^t I_{solar} dt} \tag{3.9}$$

Subsequently, the heating powers (W) of the photothermal system under various solar intensities were calculated using Equation 3.10.

$$W = \alpha \sigma A I_{solar} \tag{3.10}$$

For the solar-powered DAC system, the thermal energy for adsorbent regeneration (Q_{re}) was calculated based on the following equation,

$$Q_{re} = \sigma \alpha A \frac{\int_o^{t_{des}} I_{solar} dt}{m_{CO_2}} - \frac{m_{tube} C_{tube} \Delta T_{tube}}{m_{CO_2}} \tag{3.11}$$

where t_{des} is the desorption time, and m_{CO_2} is the mass of CO_2 collected under solar irradiation, ΔT_{tube} represents the temperature increase of the adsorption column in the desorption stage. Considering that reported energy consumption analyses typically focus on the energy used for heating the adsorbent and providing latent heat, this study subtracted the heat required for heating the adsorption column, to enable a meaningful comparison.

3.3 Results and discussion

3.3.1 Regeneration efficiency

To evaluate the efficiency of a given desorption technology for DAC, a parameter, termed Regeneration Efficiency (R), is introduced to quantify the percentage of CO_2 that can be recovered from the adsorbents. R is defined by the following equation:

$$R = \frac{W_c}{q_{ad}} \tag{3.12}$$

where W_c is the CO_2 working capacity achieved using the given desorption technology, q_{ad} represents CO_2 loadings on the adsorbent materials after adsorption. A higher regeneration efficiency enhances CO_2 productivity and reduces equipment volume, leading to decreased operating and capital costs for DAC. The regeneration efficiency (R) of the conventional TVSA process was evaluated using CO_2 adsorption isotherm data of a benchmark solid amine sorbent (Lewatit VP OC 1065). The temperature and humidity of ambient air significantly affect the adsorption capacity, thus impacting the calculated working capacity and regeneration efficiency. In this work, a typical temperature of 25 °C was selected to represent the general scenario for DAC. Additionally, a dry condition was employed for adsorption and desorption to estimate the efficiency of a given regeneration process, as the influence of water on CO_2 loading at elevated temperatures was not fully understood.

As shown in Figure 3.6, the TVSA process requires elevated temperatures and reduced pressures for CO_2 desorption. Achieving an R-value over 0.6 requires a desorption temperature of 115 °C and a pressure of 10 kPa. Considering the thermal stability of the material and the desorption pressure achievable by regular vacuum pumps, reaching an R-value > 0.6 is highly challenging.

To address the harsh conditions, vapor-promoted desorption (VPD) is introduced to achieve efficient adsorbent regeneration with an R value exceeding 0.9. This VPD process promotes CO_2 adsorbent regeneration via *in situ* vapor purge using water harvested from the atmosphere. As shown in Figure 3.6B, compared with conventional TVSA, the VPD process can significantly reduce CO_2 partial pressure by vapor purge, providing a tremendous driving force for CO_2 desorption, leading to an increased working capacity and regeneration efficiency.

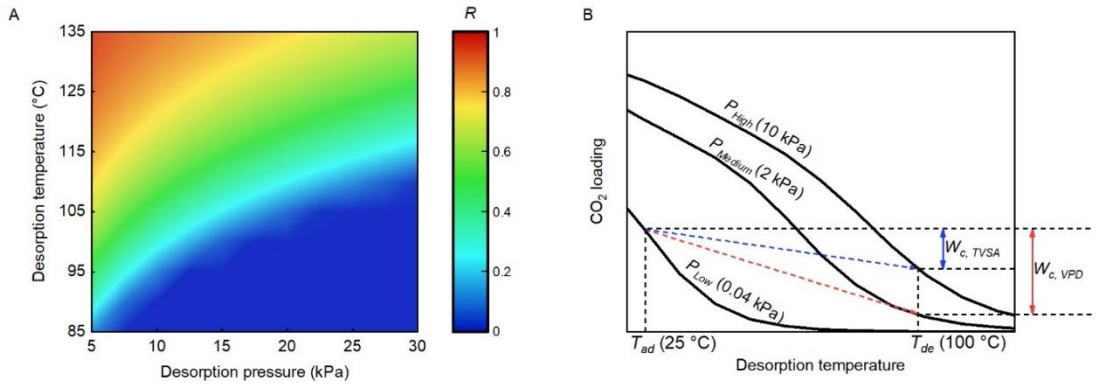

Figure 3.6 Regeneration efficiency and CO_2 working capacities of TVSA and vapor-promoted desorption processes.

(A) Calculated *R* values of conventional TVSA processes at various desorption temperatures and pressures, with fixed adsorption conditions of 25 °C and 400 ppm CO_2. (B) Theoretical working capacities of vapor promoted desorption ($W_{c,VPD}$) and TVSA ($W_{c,TVSA}$) processes calculated from the CO_2 adsorption isobar of Lewatit VP OC 1065 resin. Vapor promoted desorption, conducted without the use of vacuum conditions, results in a significant reduction in CO_2 partial pressure (around 2 kPa) due to the *in situ* purging effect of the generated water vapors.

3.3.2 Adsorption properties

Commercial type A silica gel and Lewatit VP OC 1065 resin were used as the water and CO_2 adsorbents for testing vapor-promoted DAC, respectively. The Lewatit resin exhibited an impressive CO_2 uptake capability of 1.11 mmol/g at 20 °C and 400 ppm (Figure 3.7A). In Figure 3.7B, the hydrophobic styrene-divinylbenzene structure of the Lewatit resin resulted in limited water uptakes at low relative humidities (RH). Silica gel was able to adsorb more than 10 wt% water even under 30% RH conditions, while the VP OC 1065 resin achieved a similar uptake at a relative humidity of nearly 80% (Figure 3.7C). The addition of silica gel could significantly increase the amount of co-adsorbed water, thus providing a solid foundation for vapor-promoted desorption.

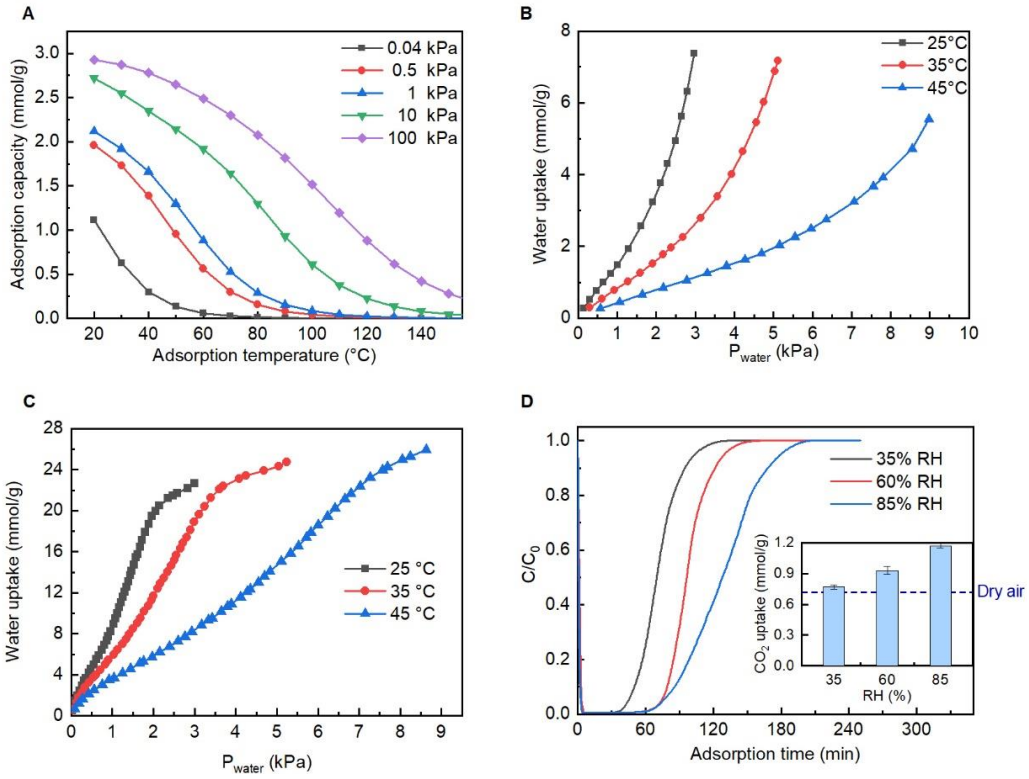

Figure 3.7 Adsorption properties of VP OC 1065 resin and silica gel.

(A) CO_2 adsorption isobar of VP OC 1065. (B) Water adsorption isotherm of VP OC 1065 at 25 °C, 35 °C and 45 °C. (C) Water adsorption isotherms of silica gel at 25 °C, 35 °C, and 45 °C. (D) CO_2 breakthrough curves of VP OC 1065 at 28 °C and 410 ppm, with a gas hourly space velocity of 12000 /h. The inset shows atmospheric CO_2 adsorption capacities under dry and different humidity conditions.

Moisture has been proven to significantly affect the CO_2 adsorption properties of solid amine sorbents [7, 24, 25]. The impact of moisture on the CO_2 adsorption behaviors of the Lewatit resin was studied by conducting breakthrough experiments at varying humidities. Compared with adsorption with dry air, the CO_2 uptakes at 35%, 60%, and 85% RH were observed to increase by 6.9%, 29.2%, and 62.5%, respectively (Figure 3.7D). Specifically, the CO_2 uptake increased from 0.72 to 0.93 mmol/g at 28 °C when dry air was replaced by a humid feed with a relative humidity of 60%. However, higher CO_2 uptakes and slower adsorption kinetics under high humidity conditions led to longer adsorption time for achieving adsorption equilibrium. The reduced adsorption rate might be attributed to the mass transfer restrictions in Lewatit resin with higher water loadings.

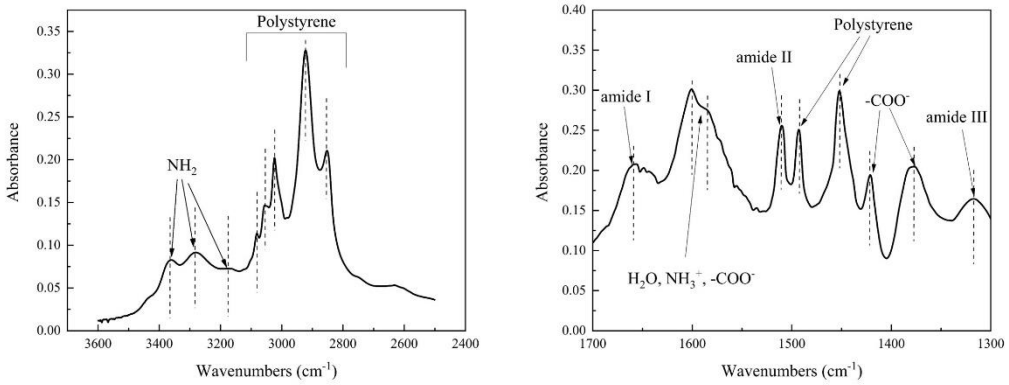

Figure 3.8 Fourier transform infrared spectroscopy spectra of VP OC 1065 pretreated using 25 °C air with 30% relative humidity (RH).

FTIR spectroscopy was used to analyze the surface species of VP OC 1065 after adsorbing atmospheric CO_2. Before the analysis, the sample was pretreated with 25 °C and 30% RH air for 12 hours. The symmetric stretching vibration of $-COO^-$ originating from the carbamate structure was detected at 1380 and 1421 cm^{-1} [26, 27]. The IR band at 1510 cm^{-1} corresponded to the N-H bending vibration and C-N stretching vibration (amide II) of carbamate species [26-28] (Figure 3.8). In addition, the asymmetric stretching vibration of $-COO^-$ and antisymmetric deformation of NH_3^+ at around 1560-1590 cm^{-1} were detected [27,

28]. Generally, carbamic acid, bicarbonate, and ammonium carbamate are regarded as potential species formed on solid amine sorbents during CO_2 adsorption [25, 29, 30], with IR bands in the range of 1700-1300 cm^{-1}. Young et.al proved that the amine efficiency of Lewatit resin was not increased in the presence of moisture when CO_2 adsorption was performed at 1 bar [24]. This indicated that the bicarbonate mechanism is unlikely to occur in Lewatit resin, as the stoichiometric ratio of CO_2/amine would increase from 0.5 to 1 if the bicarbonate was formed. Previous works have also reported that the surface species shifted from carbamic acid to ammonium carbamate for amine-grafted materials in the presence of water [25, 31, 32]. Thus, the resin might adsorb atmospheric CO_2 at 25 °C and 30% RH via a carbamate pathway.

The mechanism of atmospheric CO_2 adsorption on VP OC 1065 was further investigated by recording the *in situ* FTIR spectra during N_2 purge. Upon treatment with a 100 °C N_2 stream, the desorption of CO_2 was reflected in decreases of the absorptance at 1380, 1510 and 1584 cm^{-1} (Figure 3.9), corresponding to the symmetric stretching vibration of -COO-, C-N stretching vibration (amide II) and antisymmetric deformation of NH_3^+ in ammonium carbamate structures, respectively [33, 34]. The results suggested that the formation of ammonium carbamate was the dominant mechanism for atmospheric CO_2 adsorption at 30% RH using VP OC 1065.

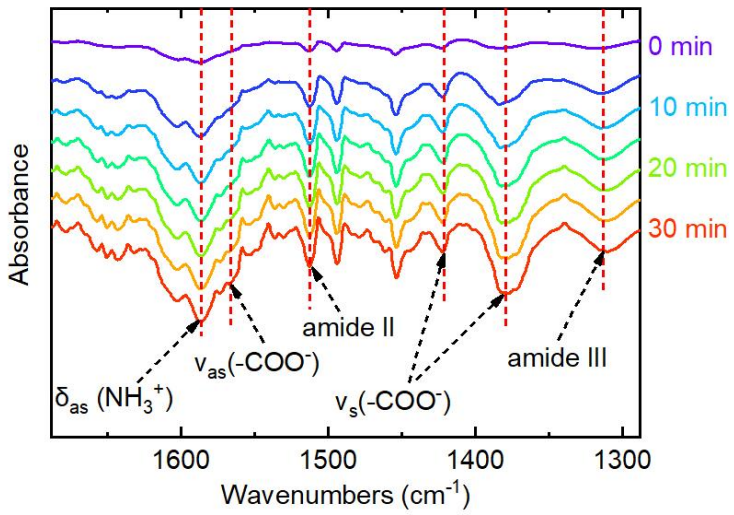

Figure 3.9 *In situ* Fourier transform infrared spectroscopy spectra of VP OC 1065 after 0, 5, 10, 15, 20, 25 and 30 min treatment in flowing N_2 atmosphere at 100 °C. The sample was pretreated with 25 °C and 30% RH air for 12 hours.

Thermal stability can be a major concern for solid amine sorbents during regeneration [35].

Thermogravimetric analysis was conducted at different temperatures and atmospheres to assess the thermal stability of VP OC 1065. The resin kept losing CO_2 sorption capacity after each desorption step at 110 °C in air, totaling more than 20% loss in 6 cycles (Figure 3.10). In contrast, at a desorption temperature of 70 °C, there wasn't any obvious loss of CO_2 sorption capacity, suggesting lower regeneration temperatures are critical to maintaining the performance of the resin for DAC.

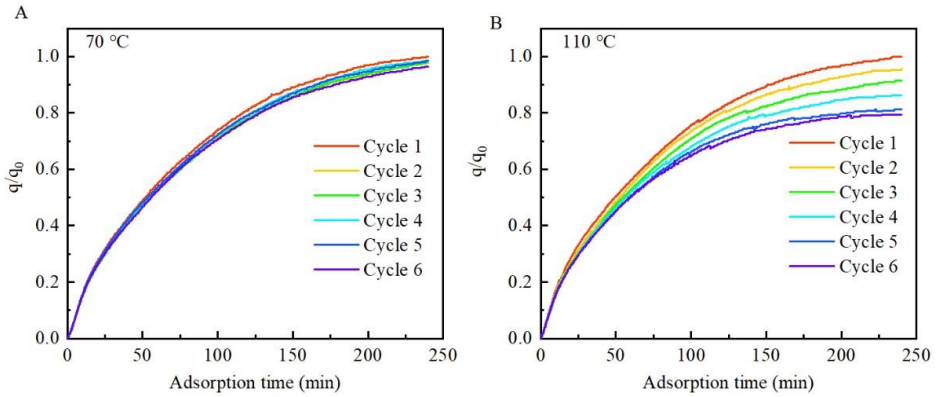

Figure 3.10 Cyclic CO_2 adsorption capacity of VP OC 1065 regenerated under (A) 70 °C and (B) 110 °C air flows. CO_2 adsorption was performed using 30 °C dry air with 400 ppm CO_2. The CO_2 uptake of the first adsorption cycle was denoted as q_0.

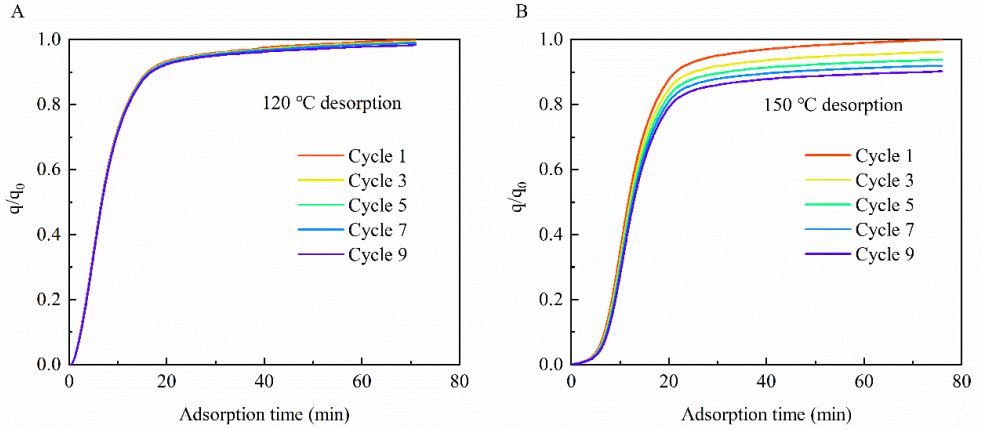

Figure 3.11 Cyclic CO_2 adsorption capacity of VP OC 1065 regenerated under (A) 120 °C and (B) 150 °C CO_2 flows. CO_2 adsorption was performed using CO_2 at 30 °C and 1 bar. The CO_2 uptake of the first adsorption cycle was denoted as q_0.

The stability of the amine under pure CO_2 was also investigated at 120 °C and 150 °C. The sample was pre-treated with carbon dioxide at 30 °C before being exposed to high-temperature CO_2. When pure CO_2 was used for the thermalgravimetric analysis instead

of air, the resin was kept stable at 120 °C after repeated cycles and degradation wasn't seen until the regeneration temperature reached 150 °C (Figure 3.11). In CO_2 atmosphere at 150 °C, the deactivation of amine groups was primarily caused by the formation of cyclic and open-chain ureas, according to the *in situ* FTIR analysis (Figure 3.12). Specifically, using a CO_2 stream to treat the sample at 150 °C, the absorptance of two bands at 1560 and 1654 cm^{-1} associated with open-chain ureas gradually increased. Moreover, a new absorption band at 1702 cm^{-1} was also observed due to the formation of cyclic ureas [36, 37]. Figures 3.12B and 3.12C illustrate the formation mechanisms of open-chain urea and cyclic urea. Specifically, two primary amine groups first react with CO_2 to form the corresponding ammonium carbamate in the CO_2 adsorption process. Subsequently, the ureas are formed through the dehydration of ammonium carbamate at 150 °C [36, 37].

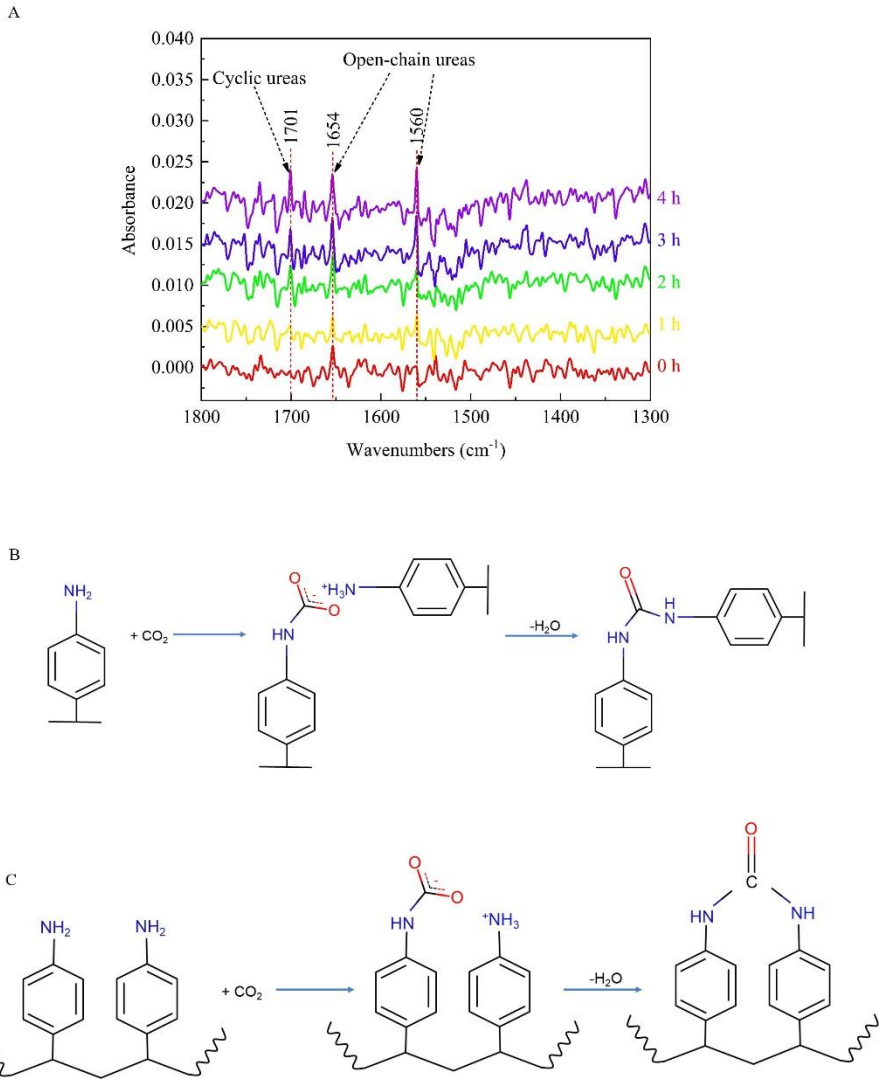

Figure 3.12 CO_2-induced deactivation mechanism analysis. (A) *In situ* FTIR spectra for VP OC 1065 after 0, 1, 2, 3, and 4 hours (bottom to top) treatment using CO_2 stream at

150 °C. (B-C) Proposed mechanism for (B) open-chain ureas formation and (C) cyclic ureas formation.

3.3.3 Cyclic performance of vapor-promoted DAC

To study the cyclic stability of the Lewatit VP OC 1065 under the condition of *in situ* vapor purge, silica gel was packed in the same column for adsorbing moisture from the air and providing the *in situ* vapor, along with the CO_2 capture resin. At a feed gas hourly space velocity (GHSV, based on the volume of resin) of 10000 /h, each adsorption (~3 h) and desorption (~40 min) cycle can produce carbon dioxide at a productivity of 3.7-3.9 kg/(h·m^3_{resin}) (Figures 3.13A and 3.13B). It is noteworthy that the mass productivity is significantly influenced by the air flow rate in the adsorption step or the required adsorption time.

The released CO_2 could reach a maximum purity of over 99% during VPD after 19 min preheating, as shown in Figure 3.13C. The collected products were further analyzed by gas chromatography, showing a CO_2 concentration of 97.7% and an O_2 concentration of 0.5%. The low concentrations of O_2 within the column could reduce the risk of amine oxidation during regeneration. Remarkably, this novel VPD process maintained a stable CO_2 working capacity of 0.9-1.0 mmol/g (Figure 3.13D) over nine cycles, as nearly all the CO_2 products could be collected at temperatures below 105 °C (Figure 3.13E).

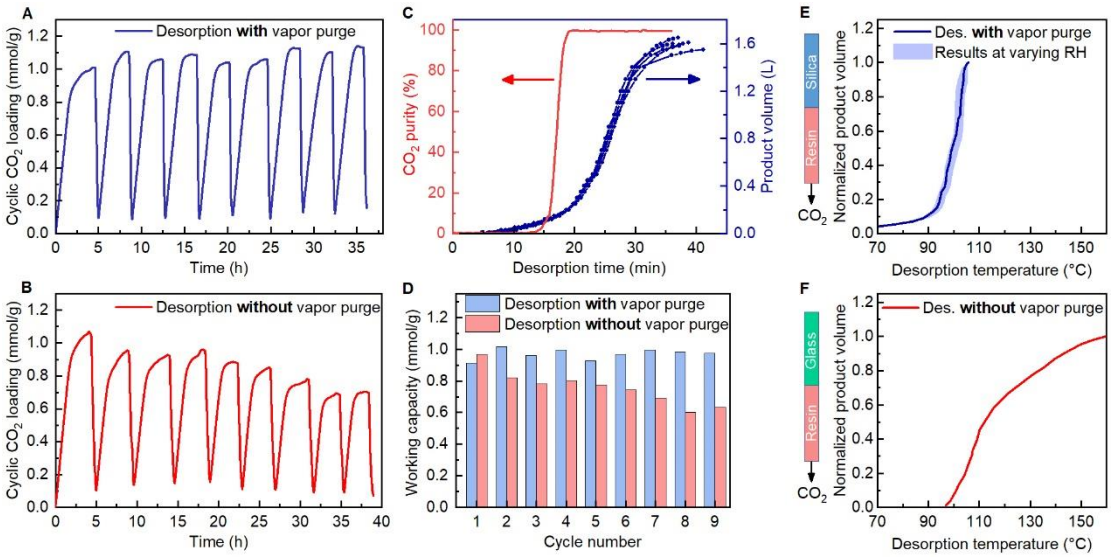

Figure 3.13 Performance of cyclic vapor-promoted DAC in comparison to desorption without *in situ* vapor purge.

Adsorbents: 180 mL VP OC resin and 180 mL silica gel. Fresh air at 27 °C with RH ranging

from 35 to 60% was used as the feed stream with a GHSV of 10000 /h. Desorption without *in situ* vapor purge was performed by replacing silica gel with glass beads. (A and B) Cyclic CO_2 loading profiles for desorption (A) with and (B) without *in situ* vapor purge during nine adsorption-desorption cycles. (C) Real-time CO_2 purity and product volumes of different cycles during VPD. (D) Cyclic working capacities calculated from the CO_2 loading profiles. (E) Normalized product volumes (ratios of collected product volume to final product volume) during desorption with *in situ* vapor purge under different desorption temperatures. The shaded areas illustrate the variations in results obtained under different relative humidities ranging from 35% to 60%. The solid line represents the experiment conducted under a relative humidity of 50%. (F) Normalized product volume during desorption without *in situ* vapor purge, when the adsorption was performed at 35% RH.

By contrast, the DAC without using *in situ* vapor purge, lost 40% of its working capacity at cycle 8, starting from 0.97 mmol/g at cycle 1 (Figures 3.13B and 3.13D). This low stability can be attributed to the significantly higher temperatures required, ranging from 130-150 °C, to achieve a similar product volume compared with VPD (Figure 3.13F). These observations highlight the importance of *in situ* vapor purge in reducing the required regeneration temperatures for CO_2 desorption.

In the above setup using a resin volume fraction of 0.5, the amount of CO_2 desorbed was barely influenced by the feed air humidity, as shown in the shaded area of Figure 3.13E. This suggests the amount of *in situ* vapor could be far more than sufficient for purge. To analyze the necessary amount of co-adsorbed water or silica gel for *in situ* vapor purge, VPD was investigated under various relative humidities and in the meantime the resin volume fraction was increased to 0.8. Figure 3.14 demonstrated stable CO_2 working capacities ranging from 0.85 to 1.00 mmol/g (using 320 mL Lewatit resin and 80 mL silica gel) which is similar to the CO_2 working capacity in the earlier tests using 180 mL resin and 180 mL silica gel (Figure 3.13A).

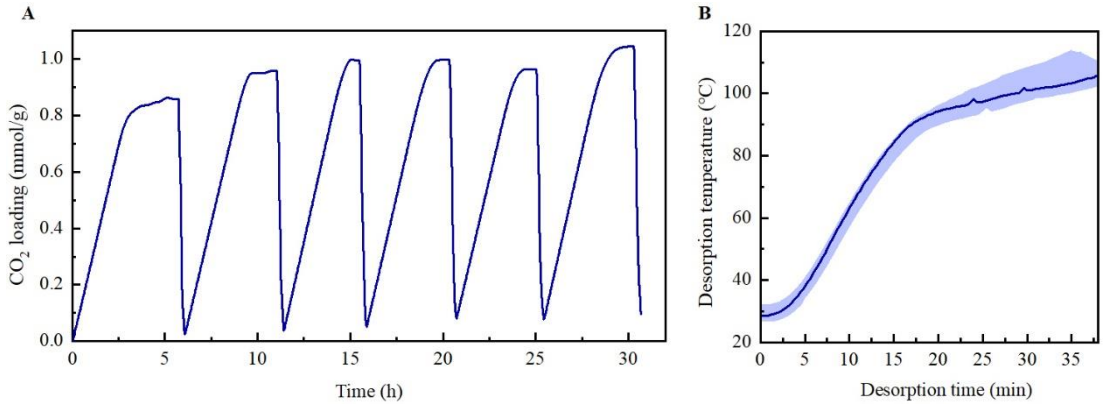

Figure 3.14 Six vapor-promoted DAC cycles using 320 mL VP OC resin and 80 mL silica gel. (A) CO_2 loading and (B) desorption temperature profiles.

Fresh air at around 27 °C with RH ranging from 45 % to 70 % was used as the feed stream which had a gas hourly space velocity (GHSV) of 5600 /h. The shaded areas indicate the variation of temperature results obtained under different relative humidities (45-70%). The solid line represents the experiment conducted under a relative humidity of 60%.

As shown in Figure 3.14B, the desorption temperature profile of VPD exhibited two distinct stages, corresponding to the preheating and desorption steps. Specifically, the temperature initially increased from room temperature to 90 °C, after which it stabilized or gradually increased to around 105 °C. This behavior can be attributed to the consumption of thermal energy by the desorption of CO_2 and H_2O in the desorption step. Wurzbacher et.al also reported a similar temperature evolution in the sorbent bed center during TVSA processes using solid amine materials [16].

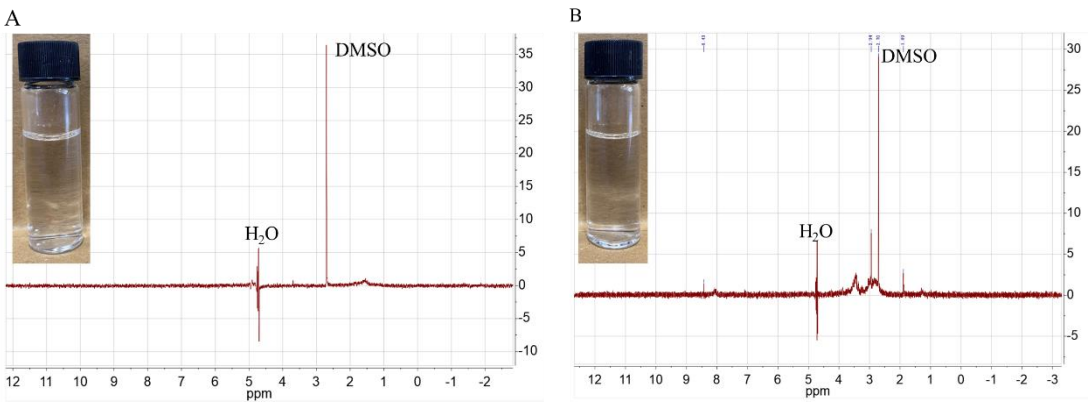

Figure 3.15 ^{1}H NMR spectra for the (A) deionized water and (B) water products. DMSO with 12 ppm concentration was employed as the reference.

At elevated temperatures, the desorbed water first served as the vapor for *in situ* purge of CO_2 within the column. Then the vapor was condensed in the subsequent air-cooled

condenser as high-purity fresh liquid water verified by the ^{1}H NMR results (Figure 3.15).

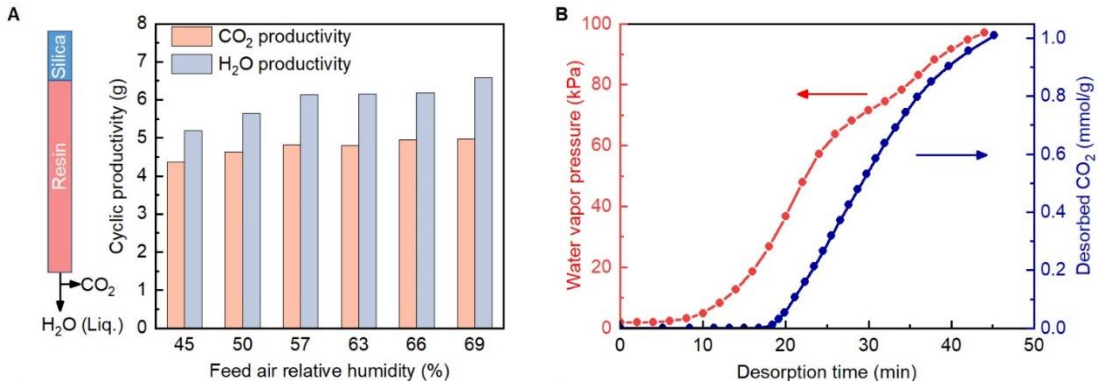

Figure 3.16 Investigation on the impact of feed air humidity and co-adsorbed water in VPD.

Adsorbents: 320 mL VP OC resin and 80 mL silica gel. Fresh air at 27 °C with RH ranging from 45 % to 70 % was used as the feed stream with a GHSV of 5600 /h. (A) Cyclic CO_2 and water productivities under different relative humidities. (B) Amounts of desorbed CO_2 and partial pressures of water vapor inside the column during the regeneration stage.

This gas/liquid separation allowed for the recovery of high-concentration CO_2 products ranging from 4.5 to 5.0 g per cycle. Meanwhile, water productivity ranged from 5.0 to 6.5 g per cycle depending on the atmospheric humidity (Figure 3.16A). Need to be mentioned that only a small fraction of water (~22%) was desorbed, involved as vapors with high partial pressures over 95 kPa within the column (Figure 3.16B), and collected as a liquid product. Whereas the increased vapor pressure could substantially reduce the CO_2 partial pressure, releasing over 90% of the adsorbed CO_2 at temperatures below 110 °C.

The present study only examined the physical mechanism (partial pressure change) for CO_2 desorption. However, considering water's involvement in the reaction between CO_2 and amines, there might be chemical reactions promoting CO_2 desorption. Investigating the binary adsorption equilibrium for CO_2 and water at high temperatures would further elucidate the effects of vapors on CO_2 adsorption/desorption behavior.

3.3.4 Performance estimation for VPD

For this *in situ* vapor purge with a resin volume fraction of 0.8, the required desorption temperatures for achieving different *R* values were determined by the amount of adsorbed water as shown in Figure 3.17. By increasing the molar ratio of equilibrium loading of

adsorbed water to CO_2 (n_{water}/n_{CO2}), the desorption temperature could be lowered due to the increased quality of vapors generated for *in situ* purge.

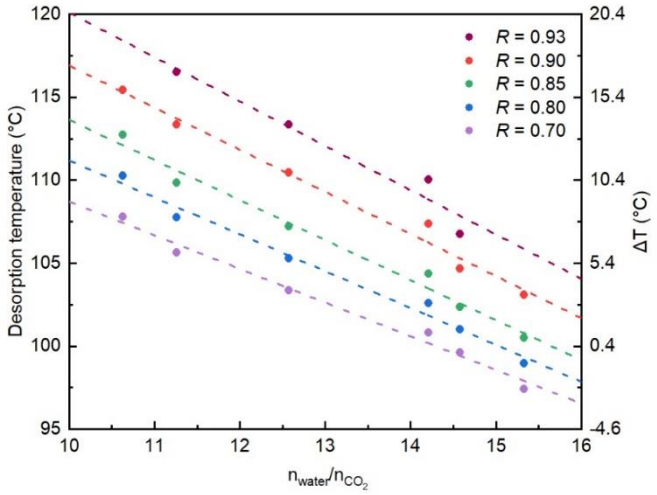

Figure 3.17 To achieve regeneration efficiency *R* ranging from 0.70 to 0.93, the corresponding desorption temperature as a function of the molar ratio of equilibrium loading of adsorbed water to CO_2 (n_{water}/n_{CO2} at the end of the adsorption step).

The dashed lines represent the linear fitting results. The right y-axis shows the required temperature difference (ΔT) between the desorption temperature (T_{de}) and the boiling point of water (T_{bp}) at 1 bar, with ΔT calculated as T_{de} minus T_{bp}.

This linear correlation in Figure 3.17 enables the estimation of the required n_{water}/n_{CO2} for reaching different R values at certain desorption temperatures and 1 bar. Then, the corresponding volume fraction of resin ($V_{f,resin}$) under different atmospheric humidities can be evaluated by Equation 3.13.

$$V_{f,resin} = \frac{q_{water,silica}\rho_{silica}}{\left(q_{CO_2,resin}\rho_{resin}n_{water}/n_{CO_2} - q_{water,resin}\rho_{resin} + q_{water,silica}\rho_{silica}\right)} \quad (3.13)$$

where $q_{water,silica}$ and $q_{water,resin}$ (mmol/g) represent the equilibrium water loadings for silica gel and Lewatit resin at different relative humidities. ρ_{silica} and ρ_{resin} (g/L) are the packing densities of silica gel and Lewatit resin, respectively. To calculate the volume fraction of resin, the adsorption temperature and the equilibrium CO_2 adsorption capacity of Lewatit resin ($q_{CO_2,resin}$) were set at 25 °C and 1 mmol/g, respectively. Then, according to the calculated $V_{f,resin}$, the correlation between regeneration efficiency and given conditions ($V_{f,resin}$, desorption temperature, and relative humidity of feed air) was obtained and depicted in Figure 3.18A.

By adjusting the volume fraction of adsorbents, VPD can be applied in various climate environments, from arid to humid areas. Even in areas with extremely low humidities of around 20-25% typical to average air humidity in deserts [38], VPD can still achieve a regeneration efficiency of 0.9, as demonstrated in the shaded area (Figure 3.18A). In a more humid environment, for example 50% relative humidity air, desorption temperature as low as 103 °C is highly effective in generating abundant vapors for *in situ* purge, releasing over 90% of the adsorbed CO_2. Both of the above examples do not need vacuum pumps for the regeneration of CO_2 adsorbents.

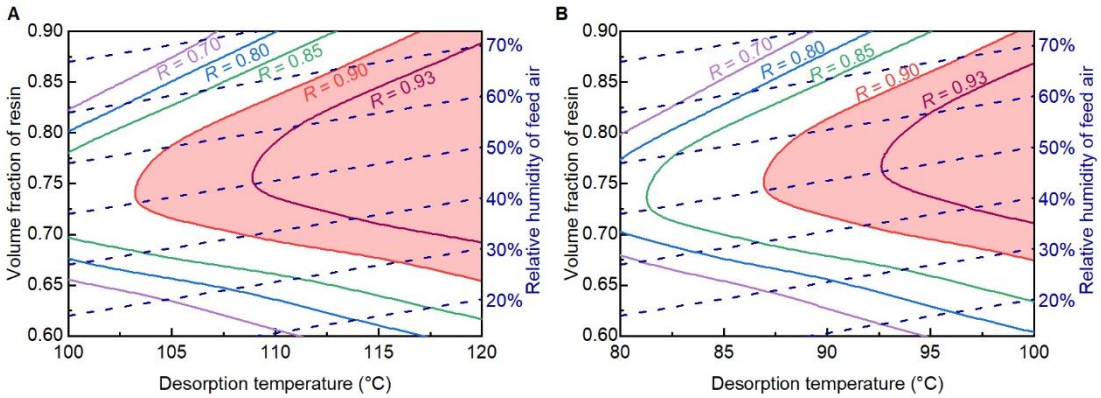

Figure 3.18 Predicting regeneration efficiency *R* of VPD under desorption pressures of (A) 100 kPa and (B) 50 kPa, at given volume fraction of resin, desorption temperature, and relative humidity of feed air.

The calculation was based on an equilibrium CO_2 loading of 1 mmol/g for the chemisorbent in DAC. The shaded red areas represent the recommended operating conditions for vapor promoted DAC with an *R* exceeding 0.9.

When evacuation is applied, the desorption temperature can be further reduced in the VPD process. As shown in Figure 3.17, the temperature difference (ΔT) between the desorption temperature (T_{de}) and the boiling point of water (T_{bp}) was depended on the n_{water}/n_{CO2}. This relationship highlights the potential of operating VPD at lower temperatures by reducing the water boiling point using evacuation, allowing us to predict the corresponding *R* under vacuum conditions. To evaluate the regeneration performance at a moderate desorption pressure of 0.5 bar, three assumptions were considered:

1. The desorption kinetics were assumed to be unchanged compared with vapor-promoted desorption at 1 bar.

2. The increase in equilibrium CO_2 loading with decreasing regeneration temperatures is

expected to be offset by the reduction in CO_2 partial pressure caused by evacuation.

3. Based on the aforementioned two assumptions, it is assumed that the linear correlation observed in Figure 3.17 between ΔT and n_{water}/n_{CO2} at 1 bar remains valid under a moderate desorption pressure of 0.5 bar.

Thus, for achieving different R at 0.5 bar, the required desorption temperature under specific n_{water}/n_{CO2} can be calculated based on Equation 3.14 and Figure 3.17, with $T_{bp,\ 0.5\ bar}$ representing the boiling point of water at 0.5 bar. The performance of vapor-promoted desorption at 0.5 bar can be evaluated using a similar approach as the one employed for predicting regeneration efficiency at 1 bar.

$$T_{de} = \Delta T + T_{bp,0.5bar} \tag{3.14}$$

As shown in Figure 3.18B, by applying a moderate vacuum of 50 kPa, the process only needs a regeneration temperature of 87 °C to recover 90% of the CO_2 from the column; or recover 80% of the CO_2 at 80°C.

In general, for a given air humidity, the resin volume fraction and the desorption temperature can be adjusted to achieve a high CO_2 capture performance using the VPD process (Figure 3.18), while considering the specific environmental conditions, such as weather and the temperature of the heat source available, at the location where DAC is conducted. Besides, since a vacuum condition can reduce the required temperature for *in situ* vapor purge, regeneration conditions such as the desorption pressure can be selected based on the availability of energy sources such as waste heat, solar energy, or renewable electricity around DAC systems.

3.3.5 Solar-powered DAC prototype

As only low-grade heat is required to drive the VPD process, a solar-powered DAC prototype was built to convert solar energy to thermal energy with high efficiencies. As shown in Figure 3.19, the prototype consists of a horizontal adsorption column coated in black and double-glazed with a transparent vacuum isolation and a parabolic solar concentrator with an optical concentration ratio of 1.9 (Figure 3.19C). The photothermal conversion efficiency of the prototype was calculated to be 63.1% by monitoring the temperature changes of the column under solar irradiation. Additionally, a correlation was established between the solar flux and heating power of the prototype. Under a typical solar flux of 500 W/m^2, the prototype

with a projected area of the black coating being 0.05 m^2, is capable of generating thermal energy equivalent to 30 W of electrical heating (Figure 3.19D).

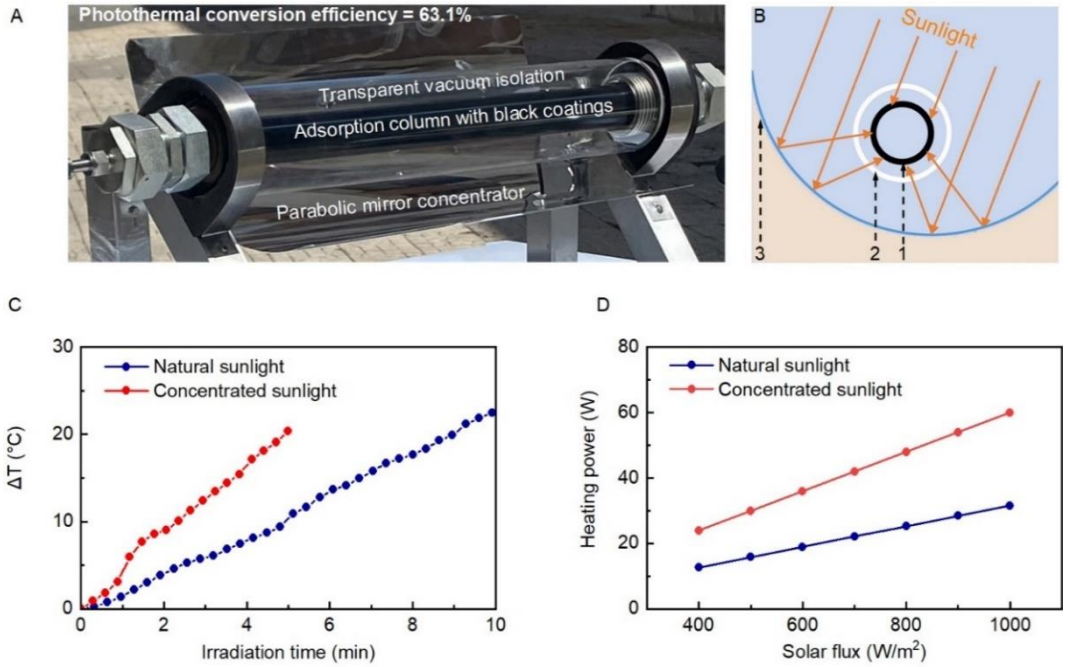

Figure 3.19 Solar heating performance of the photothermal DAC prototype.

(A) Prototype of the photothermal DAC system including an adsorption column with black coatings for photothermal conversion, a transparent vacuum isolation for reducing heat loss, and a parabolic mirror concentrator. (B) Schematic diagram of the photothermal DAC prototype. 1. Adsorption column with black coatings; 2. Transparent vacuum isolation; 3. Parabolic mirror concentrator. (C) Temperature change profiles of the adsorption column under 600 W/m^2 solar irradiation. Concentrated sunlight was generated by the parabolic mirror concentrator. (D) Heating powers of the photothermal system under natural sunlight and concentrated sunlight.

To demonstrate the CO_2 capture performance of this solar-powered DAC prototype, three VPD tests were conducted using varying volumes of adsorbents under different weather conditions (Figures 3.20 and 3.21). After adsorbing atmospheric CO_2 and water, the DAC prototype was directly exposed to sunlight for VPD, generating 2.89, 5.11, and 7.24 g CO_2 per cycle using 200, 320, and 420 mL Lewatit resin, respectively. Under moderate solar intensities ranging from 500-700 W/m^2, nearly all the adsorbed CO_2 was released (R > 0.97) within 50 minutes (Figures 3.20B and 3.21B), driven by *in situ* vapor purge which was powered by solar heating at around 110 °C.

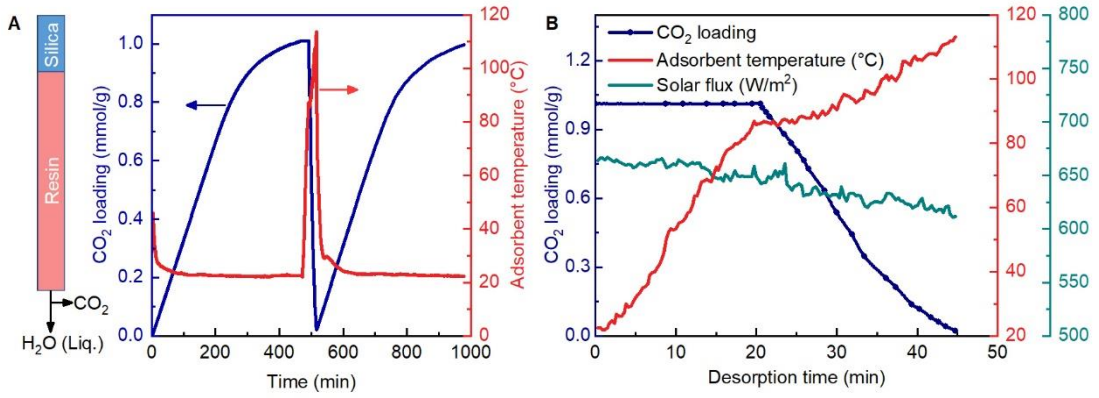

Figure 3.20 Performance of solar-powered DAC prototype with 320 mL resin and 80 mL silica gel (case 1).

Solar-powered DAC was tested at 56% RH and a GHSV of 3750 /h in Tianjin China (39°06'32.9"N 117°10'11.1"E) during May 2022. (A) CO_2 loading and adsorbent temperature profiles during the adsorption-desorption cycles. (B) CO_2 loading, adsorbent temperature, and solar flux profiles during the solar-powered regeneration stage.

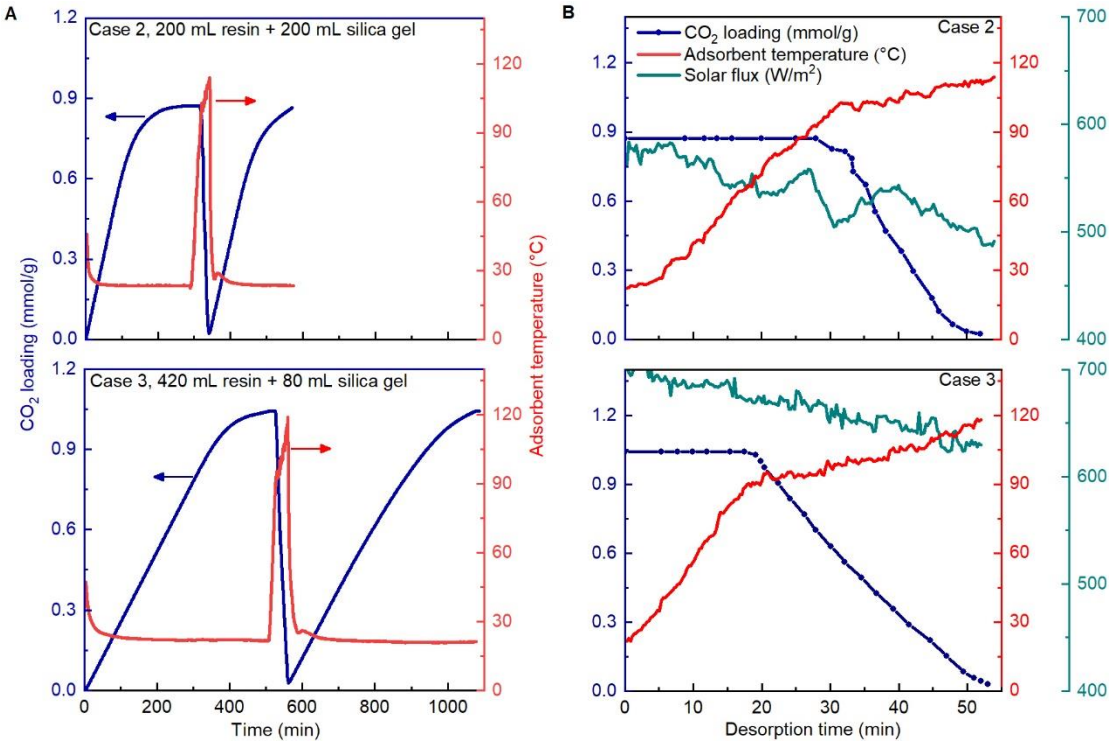

Figure 3.21 Performance of solar-powered DAC prototype with different volume fractions of resin (case 2 and case 3).

(A) CO_2 loading and adsorbent temperature profiles during the adsorption-desorption cycles for Cases 2 and 3. (B) CO_2 loading, adsorbent temperature, and solar flux profiles during the solar-powered regeneration stage for Cases 2 and 3. Case 2: 200 mL resin and 200 mL silica gel, at 40% RH and a gas hourly space velocity GHSV of 6000 /h. Case 3: 420 mL resin and

80 mL silica gel, at 57% RH and a GHSV of 3000 /h.

In temperature swing adsorption processes, the cooling step usually takes the longest time. Shortening the cooling time is critical to improving the overall productivity of the CO_2 capture. In this study, the temperature of the double layered column using both silica gel and resin decreased two times faster than that without silica gel layer. As shown in Figure 3.22, the former decreased from 113 °C to 68 °C within 120 seconds, while the latter only dropped to 92 °C. Such enhanced cooling was caused by the evaporation of water in the double layered column, where the partial pressure of water was significantly reduced by the incoming air. With the aid of heat transfer between incoming air at ambient conditions and the adsorbent, the temperature inside the column during the adsorption step is expected to be low enough to capture atmospheric CO_2. As the column is cooled down to ambient, the equilibrium shifts towards the next cycle of water adsorption.

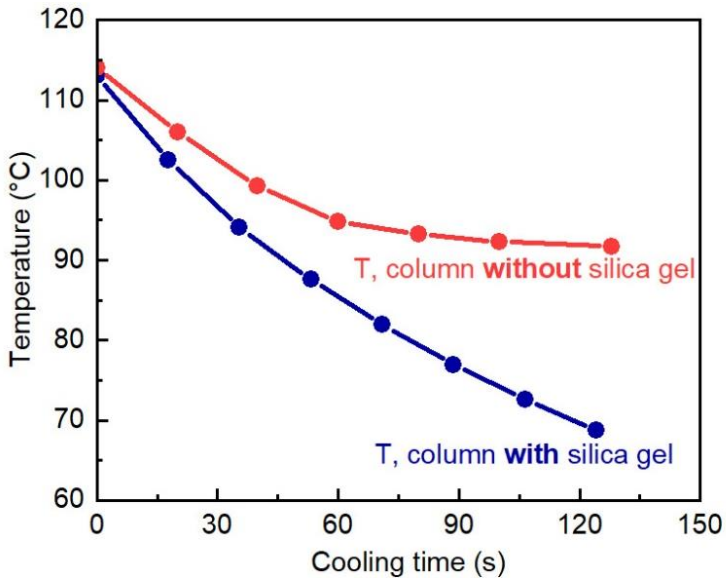

Figure 3.22 Temperature profiles of the resin in the columns with and without silica gel during the cooling process after solar-powered regeneration.

High energy consumption is another concern that compromises the economic feasibility of DAC. The energy consumption of this solar-powered VPD was calculated based on the photothermal conversion efficiency and solar intensities. Figure 3.23 demonstrated that vapor promoted DAC required only 10.4 MJ/kg_{CO2} of thermal energy converted from sunlight for adsorbent regeneration. In comparison, the reported energy consumptions for TVSA and steam-assisted TVSA processes using the same resin as CO_2 adsorbent were in the range of 12-15 MJ/kg_{CO2}, including 1-2 MJ/kg_{CO2} of electrical energy for evacuation [10, 19]. Specifically, the VPD process achieved a regeneration efficiency *R* of 0.98 with 30%

lower energy consumption, in comparison with typical steam-assisted TVSA processes which only have an *R* of around 0.77 [19]. The exceptional performance of vapor-promoted DAC can be attributed to the significant desorption driving force achieved via *in situ* vapor purge.

Compared with steam stripping, a typical regeneration approach for amine-grafted materials, the VPD process does not require an additional water supply and corresponding steam boiler to generate the required purge gases. Gebald et al. analyzed the energy consumption and steam requirement for steam stripping processes [39]. The results indicated that a pure steam process needed 19.6 tons of steam supply to capture 1 ton of CO_2, exhibiting 5 times higher energy and 17 times higher steam demand than the STVSA process. Although the applied steam can be condensed and recycled, the vapors would be adsorbed on the adsorbents during the steam purge and inevitably result in significant losses. Therefore, compared with steam stripping, the VPD process has the additional capability to produce water, making it more suitable for the distributed production of CO_2 and water from the air. When conducting DAC in locations with abundant water sources, using a solar still to generate the necessary steam for conducting an external purge becomes a potential regeneration approach for DAC.

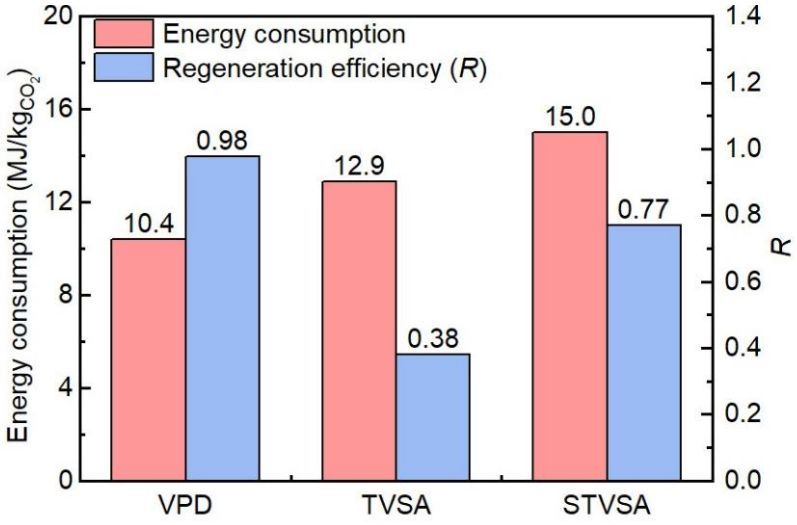

Figure 3.23 Energy consumption and regeneration efficiency *R* of VPD process, compared with reported TVSA and steam-assisted TVSA (STVSA) processes using the same CO_2 adsorbent [19].

3.4 Conclusions

The CO_2 productivity and economic viability of DAC have been compromised by the high

energy consumption for regenerating the adsorbents. In this section, by synergistically harvesting water and carbon dioxide from the atmosphere through a double-layerd adsorption configuration, an amine-grafted CO_2 capture resin could be regenerated using *in situ* vapor purge at low energy and capital cost. The desorption of CO_2 is substantially enhanced in the presence of concentrated water vapors at around 100 °C, concurrently producing 97.7% purity CO_2 and fresh water without the use of vacuum pumps and steam boilers. Moreover, a solar-powered DAC prototype was developed and exhibited the ability to recover 98% of the adsorbed CO_2 under moderate solar intensities of 600 W/m^2. The energy consumption of this vapor-promoted DAC was evaluated to be 10.4 MJ/kg$_{CO2}$, while conventional processes required 12-15 MJ/kg$_{CO2}$. The present DAC process, with the co-production of water, enables sustainable carbon capture from air in a real distributed manner.

3.5 References

[1] M. Erans, E.S. Sanz-Pérez, D.P. Hanak, Z. Clulow, D.M. Reiner, G.A. Mutch, Direct air capture: process technology, techno-economic and socio-political challenges, Energ. Environ. Sci. 15 (2022) 1360-1405.

[2] S. Deutz, A. Bardow, Life-cycle assessment of an industrial direct air capture process based on temperature-vacuum swing adsorption, Nature Energy 6 (2021) 203-213.

[3] D.P. van Vuuren, A.F. Hof, M.A.E. van Sluisveld, K. Riahi, Open discussion of negative emissions is urgently needed, Nature Energy 2 (2017) 902-904.

[4] R. Schäppi, D. Rutz, F. Dähler, A. Muroyama, P. Haueter, J. Lilliestam, A. Patt, P. Furler, A. Steinfeld, Drop-in fuels from sunlight and air, Nature 601 (2022) 63-68.

[5] D.W. Keith, Why capture CO_2 from the atmosphere? Science 325 (2009) 1654-1655.

[6] F.M. Brethomé, N.J. Williams, C.A. Seipp, M.K. Kidder, R. Custelcean, Direct air capture of CO_2 via aqueous-phase absorption and crystalline-phase release using concentrated solar power, Nature Energy 3 (2018) 553-559.

[7] E.S. Sanz-Pérez, C.R. Murdock, S.A. Didas, C.W. Jones, Direct capture of CO_2 from ambient air, Chem. Rev. 116 (2016) 11840-11876.

[8] A. Goeppert, M. Czaun, G.K. Surya Prakash, G.A. Olah, Air as the renewable carbon source of the future: an overview of CO_2 capture from the atmosphere, Energ. Environ. Sci. 5 (2012) 7833-7853.

[9] X. Zhu, W. Xie, J. Wu, Y. Miao, C. Xiang, C. Chen, B. Ge, Z. Gan, F. Yang, M. Zhang, D. O'Hare, J. Li, T. Ge, R. Wang, Recent advances in direct air capture by adsorption, Chem. Soc. Rev. 51 (2022) 6574-6651.

[10] F. Sabatino, A. Grimm, F. Gallucci, M. van Sint Annaland, G.J. Kramer, M. Gazzani, A comparative energy and costs assessment and optimization for direct air capture technologies, Joule 5 (2021) 2047-2076.

[11] M.A. Alkhabbaz, P. Bollini, G.S. Foo, C. Sievers, C.W. Jones, Important roles of

enthalpic and entropic contributions to CO_2 capture from simulated flue gas and ambient air using mesoporous silica grafted amines, J. Am. Chem. Soc. 136 (2014) 13170-13173.

[12] B.R. Sutherland, Pricing CO_2 direct air capture, Joule 3 (2019) 1571-1573.

[13] D.W. Keith, G. Holmes, D. St. Angelo, K. Heidel, A process for capturing CO_2 from the atmosphere, Joule 2 (2018) 1573-1594.

[14] R.P. Wijesiri, G.P. Knowles, H. Yeasmin, A.F.A. Hoadley, A.L. Chaffee, Desorption process for capturing CO_2 from air with supported amine sorbent, Ind. Eng. Chem. Res. 58 (2019) 15606-15618.

[15] J. Elfving, C. Bajamundi, J. Kauppinen, T. Sainio, Modelling of equilibrium working capacity of PSA, TSA and TVSA processes for CO_2 adsorption under direct air capture conditions, Journal of CO2 Utilization 22 (2017) 270-277.

[16] J.A. Wurzbacher, C. Gebald, A. Steinfeld, Separation of CO_2 from air by temperature-vacuum swing adsorption using diamine-functionalized silica gel, Energ. Environ. Sci. 4 (2011) 3584-3592.

[17] W.H. Lee, X. Zhang, S. Banerjee, C.W. Jones, M.J. Realff, R.P. Lively, Sorbent-coated carbon fibers for direct air capture using electrically driven temperature swing adsorption, Joule 7 (2023) 1241-1259.

[18] J. Elfving, J. Kauppinen, M. Jegoroff, V. Ruuskanen, L. Järvinen, T. Sainio, Experimental comparison of regeneration methods for CO_2 concentration from air using amine-based adsorbent, Chem. Eng. J. 404 (2021) 126337.

[19] M.J. Bos, S. Pietersen, D.W.F. Brilman, Production of high purity CO_2 from air using solid amine sorbents, Chemical Engineering Science: X 2 (2019) 100020.

[20] V. Stampi-Bombelli, M. van der Spek, M. Mazzotti, Analysis of direct capture of CO_2 from ambient air via steam-assisted temperature-vacuum swing adsorption, Adsorption 26 (2020) 1183-1197.

[21] W. Buijs, S. de Flart, Direct air capture of CO_2 with an amine resin: A molecular modeling study of the CO_2 capturing process, Ind. Eng. Chem. Res. 56 (2017) 12297-12304.

[22] J.A. Wurzbacher, C. Gebald, N. Piatkowski, A. Steinfeld, Concurrent separation of CO_2 and H_2O from air by a temperature-vacuum swing adsorption/desorption cycle, Environ. Sci. Technol. 46 (2012) 9191-9198.

[23] G.W. Thomson, The antoine equation for vapor-pressure data, Chem. Rev. 38 (1946) 1-39.

[24] J. Young, E. García-Díez, S. Garcia, M. van der Spek, The impact of binary water-CO_2 isotherm models on the optimal performance of sorbent-based direct air capture processes, Energ. Environ. Sci. 14 (2021) 5377-5394.

[25] R.W. Flaig, T.M. Osborn Popp, A.M. Fracaroli, E.A. Kapustin, M.J. Kalmutzki, R.M. Altamimi, F. Fathieh, J.A. Reimer, O.M. Yaghi, The chemistry of CO_2 capture in an amine-functionalized metal-organic framework under dry and humid conditions, J. Am. Chem. Soc. 139 (2017) 12125-12128.

[26] A. Danon, P.C. Stair, E. Weitz, FTIR study of CO_2 adsorption on amine-grafted SBA-15:

Elucidation of adsorbed species, The Journal of Physical Chemistry C 115 (2011) 11540-11549.

[27] Z. Bacsik, N. Ahlsten, A. Ziadi, G. Zhao, A.E. Garcia-Bennett, B. Martín-Matute, N. Hedin, Mechanisms and kinetics for sorption of CO_2 on bicontinuous mesoporous silica modified with n-propylamine, Langmuir 27 (2011) 11118-11128.

[28] Z. Bacsik, R. Atluri, A.E. Garcia-Bennett, N. Hedin, Temperature-induced uptake of CO_2 and formation of carbamates in mesocaged silica modified with n-propylamines, Langmuir 26 (2010) 10013-10024.

[29] W.R. Alesi, J.R. Kitchin, Evaluation of a primary amine-functionalized ion-exchange resin for CO_2 capture, Ind. Eng. Chem. Res. 51 (2012) 6907-6915.

[30] M.W. Hahn, M. Steib, A. Jentys, J.A. Lercher, Mechanism and kinetics of CO_2 adsorption on surface bonded amines, The Journal of Physical Chemistry C 119 (2015) 4126-4135.

[31] A.C. Forse, P.J. Milner, J. Lee, H.N. Redfearn, J. Oktawiec, R.L. Siegelman, J.D. Martell, B. Dinakar, L.B. Zasada, M.I. Gonzalez, J.B. Neaton, J.R. Long, J.A. Reimer, Elucidating CO_2 chemisorption in diamine-appended metal-organic frameworks, J. Am. Chem. Soc. 140 (2018) 18016-18031.

[32] L. Mafra, T. Čendak, S. Schneider, P.V. Wiper, J. Pires, J.R.B. Gomes, M.L. Pinto, Structure of chemisorbed CO_2 species in amine-functionalized mesoporous silicas studied by solid-state NMR and computer modeling, J. Am. Chem. Soc. 139 (2017) 389-408.

[33] H.Y. Huang, R.T. Yang, D. Chinn, C.L. Munson, Amine-grafted MCM-48 and silica xerogel as superior sorbents for acidic gas removal from natural gas, Ind. Eng. Chem. Res. 42 (2003) 2427-2433.

[34] R. Afonso, M. Sardo, L. Mafra, J.R.B. Gomes, Unravelling the structure of chemisorbed CO_2 species in mesoporous aminosilicas: A critical survey, Environ. Sci. Technol. 53 (2019) 2758-2767.

[35] M. Jahandar Lashaki, S. Khiavi, A. Sayari, Stability of amine-functionalized CO_2 adsorbents: a multifaceted puzzle, Chem. Soc. Rev. 48 (2019) 3320-3405.

[36] A. Sayari, Y. Belmabkhout, E. Da Na, CO_2 deactivation of supported amines: Does the nature of amine matter? Langmuir 28 (2012) 4241-4247.

[37] A. Sayari, A. Heydari-Gorji, Y. Yang, CO_2-induced degradation of amine-containing adsorbents: Reaction products and pathways, J. Am. Chem. Soc. 134 (2012) 13834-13842.

[38] H.A. Almassad, R.I. Abaza, L. Siwwan, B. Al-Maythalony, K.E. Cordova, Environmentally adaptive MOF-based device enables continuous self-optimizing atmospheric water harvesting, Nat. Commun. 13 (2022) 4873.

[39] C. Gebald, N. Repond, J.A. Wurzbacher, Steam assisted vacuum desorption process for carbon dioxide capture, US10279306. (2015).

4 Vapor-promoted regeneration of amine-impregnated sorbents

4.1 Introduction

Adsorption based on solid amine sorbents has attracted strong interest as a promising technology for DAC [1-3]. Solid amine sorbents are typically classified into three categories based on their preparation method: physical impregnation, covalent grafting, and *in situ* polymerization [1, 2]. Extensive efforts have been dedicated to the development of amine-impregnated sorbents (AIS) as they are inexpensive, easy to prepare, and have high amine loadings [4-8]. Sorbents impregnated with various amines including polyethylenimine (PEI), tetraethylenepentamine (TEPA) and polyallylamine (PAA) have shown high atmospheric CO_2 uptakes over 3 mmol/g at ambient temperatures [9-13].

Most studies on DAC using AIS have been primarily focused on the design and synthesis of novel materials to enhance the CO_2 adsorption capacity, while the efficient regeneration of AIS is greatly underlooked [14-18]. As the interactions between CO_2 and amine groups are relatively strong compared with physisorption, the recovery of the adsorbed CO_2 from AIS requires high temperatures and is energy-intensive [19-21]. Besides, in large-scale DAC applications, the captured CO_2 products are often required to be sufficiently pure (≥95%) for utilization or storage [22]. Nevertheless, investigations on the regeneration process of AIS to produce high-purity CO_2 are relatively limited. Inert gases such as N_2 have been used to purge and regenerate the adsorbents at elevated temperatures, however, resulting in a diluted mixture product with CO_2 concentrations lower than 7% [23]. Conventional swing technologies, such as temperature vacuum swing adsorption (TVSA), typically exhibit insufficient desorption driving force and limited CO_2 working capacities when applied with AIS [20, 21]. Steam-assisted TVSA or steam stripping shows higher desorption driving forces, however, requires an external water supply and high energy consumption for steam generation [24-26].

In this chapter, the vapor-promoted desorption (VPD) process was employed to regenerate AIS through *in situ* vapor purge using water harvested from the atmosphere. A double-layered adsorption column sequentially packed with AIS and water adsorbents was applied to generate vapors upon heating, *in situ* purging the column to enhance the driving force for CO_2 desorption. This *in situ* vapor purge regenerated polyethylenimine-impregnated sorbents at

temperatures around 105 °C, producing fresh water and 98% purity CO_2 from the air. Compared with existing DAC technologies, the VPD process could recover 95% of the CO_2 adsorbed on AIS while showcasing a reduction in energy consumption.

4.2 Experimental

4.2.1 Materials

Branched polyethylenimine (PEI) with an average molecular weight of 800 g/mol was purchased from Sigma-Aldrich and used for impregnation. HP20 (Diaion, Mitsubishi), HP2MGL (Diaion, Mitsubishi) and fumed silica (S128167, Aladdin) were selected as supporting materials. HP20 is a macroporous resin with a polystyrene/divinylbenzene matrix in beads shape with a diameter of 0.25-0.85 mm. HP2MGL is a macroporous resin with a crosslinked polymethacrylate structure in beads form with a diameter of 0.30-0.85 mm. Fumed silica (FS) is a fine particulate material comprised of spherical microparticles. The supporting materials were dried at 110 °C for 24 hours before amine impregnation. Type A silica gel beads, with a diameter of 3-5 mm were purchased from Desicco and pre-treated under evacuation (<20 kPa) at 110 °C for 3 hours before use.

4.2.2 Preparation of amine-impregnated sorbents

Amine-impregnated sorbents were prepared by physical impregnation [4, 14]. PEI was dissolved in ethanol and then mixed with the pre-dried supporting materials for impregnation, where the loading of PEI on the supporting materials is 33 wt. %. PEI loading significantly influences the adsorption thermodynamics and kinetics due to changes in pore structure after impregnation. A low loading was selected to maintain the excellent pore structure of the resin and facilitate fast diffusion inside the pores. The AIS products are named PEI/HP20, PEI/HP2MGL and PEI/FS, reflecting the respective supporting materials used. The prepared PEI/FS with a particle size of 1.4-2.0 mm was used for the following DAC tests. The activation of the PEI-impregnated sorbents was achieved by purging using pure N_2 at 50 °C, until the outlet CO_2 concentration was below 1 ppm.

4.2.3 Characterizations

The pore structures of the materials prior to and after impregnation were characterized through N_2 adsorption measurement at 77 K with a Micromeritics 3Flex Adsorption Analyzer.

The CO_2 adsorption isotherms of the sorbents were measured at temperatures of 25, 40 and 55 °C with a Belsorp-MAX Analyzer. As the conventional degassing approach employs extremely low pressures (< 10 Pa), the evaporation of the impregnated PEI often occurs. Consequently, a tailored degassing procedure was designed for the PEI-impregnated sorbents, conducted at 60 °C and 10 kPa under N_2 protection. The thermal stability of PEI-impregnated sorbents was assessed by conducting adsorption-desorption cycles using thermogravimetric analysis (TGA) with a Mettler Toledo TGA/DSC 1. The adsorption test was carried out using pure CO_2 at 30 °C with a flow rate of 100 mL/min, while the desorption was conducted at various temperatures using air purge with a flow rate of 100 mL/min.

4.2.4 Vapor-promoted desorption for the regeneration of AIS

Vapor-promoted desorption (VPD) process based on *in situ* vapor purge was used in this study to effectively regenerate AIS. In this process, a double-layered packing configuration was constructed, wherein the adsorption column was sequentially packed with AIS and moisture adsorptive sorbents for the simultaneous capture of atmospheric CO_2 and water. Type A silica gel, with a high atmospheric moisture adsorption capacity exceeding 15 mmol/g at a relative humidity of 50%, was used as the moisture adsorptive sorbent [27]. Upon heating, the water adsorbed on the silica gel was regenerated, namely *in situ* water vapor, which purged the AIS layer, reduced the CO_2 partial pressure and enhanced CO_2 desorption.

The vapor-promoted DAC process comprised four steps: adsorption, preheating, desorption, and cooling, as mentioned in Chapter 3. Using this process, a high-purity CO_2 product can be obtained owing to the exceptional CO_2 adsorption selectivity of AIS over N_2 and O_2 [28].

A stainless-steel column (L×D = 600×40 mm) wrapped with heating tapes and thermal insulation, was employed as the adsorption column. A schematic diagram of the setup is depicted in Figure 4.1. For performing breakthrough experiments, the CO_2 adsorption volume was 200 mL, while the silica gel layer was packed with glass beads. Compressed air containing 390-410 ppm CO_2 and 7% relative humidity was used as the feed gas with a flow rate of 30 L/min. A humidifier placed in a water bath at 25 °C was used to control the relative humidity of the incoming air. The outlet CO_2 concentrations were monitored using an infrared CO_2 sensor (Dynament, 0-1000 ppm) throughout the adsorption process. The humidities of the feed and outlet streams were recorded using humidity sensors (Ningbo Keshun KS-SHT).

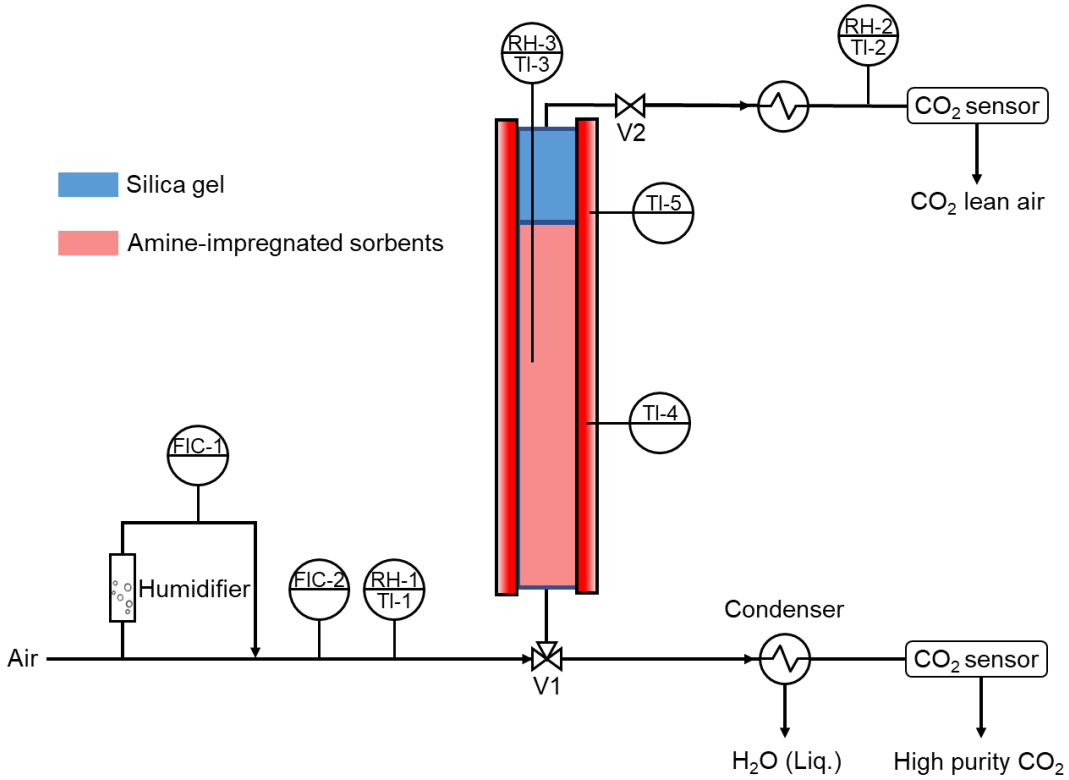

Figure 4.1 Experimental setup for performing breakthrough experiments and DAC cycles.

The experimental procedures for vapor-promoted desorption are similar to those in Chapter 3. As shown in Figure 4.1, for adsorbing atmospheric CO_2 and H_2O, the air first flowed over the AIS, and subsequently over silica gel. The CO_2 uptake (q_{ads}, mmol/g) during the adsorption process was determined using Equation 3.5.

A humidity/temperature transmitter (Vaisala HMT338) was placed within the AIS to monitor the humidity and temperature inside the column. Throughout the regeneration of sorbents, the valve V2 remained closed, while the three-way valve V1 was directly connected to an air-cooled condenser. The heating tapes were employed to achieve the temperature required for sorbent regeneration. The volume of the CO_2 product was measured by connecting a syringe with the outlet of the column. The product purity was monitored using an infrared gas analyzer (Servomex 1440). The accumulated quantity of the desorbed CO_2 can be calculated using Equation 3.6.

4.2.5 Energy consumption analysis

The energy consumption (Q) for sorbent regeneration in the vapor-promoted desorption process includes: the sensible heat (Q_s) required to increase the temperature of sorbents and

adsorbed molecules, as well as the latent heat (Q_d) associated with CO_2 and water desorption, as illustrated by Equation 4.1,

$$Q = \frac{Q_s + Q_d}{m_{CO_2}^{(des)}} \tag{4.1}$$

where $m_{CO_2}^{(des)}$ is the mass of CO_2 collected during desorption. For comparison with other existing processes, the heat loss term was not incorporated since it is influenced by many factors such as column size and thermal insulation strategies. Q_s is computed using the following equation,

$$Q_s = \Delta T(m_{AIS}C_{p,AIS} + m_{SG}C_{SG} + m_{CO_2}^{(ads)}C_{p,CO_2} + m_{H_2O}^{(ads)}C_{p,H_2O}) \tag{4.2}$$

where ΔT signifies the temperature variation during the desorption process; m_{AIS}, m_{SG}, $m_{CO_2}^{(ads)}$ and $m_{H_2O}^{(ads)}$ represent the masses of AIS, silica gel, adsorbed CO_2 and water within the column, respectively; $C_{p,AIS}$, $C_{p,SG}$, C_{p,CO_2} and C_{p,H_2O} denote the specific heat capacities of AIS, silica gel, adsorbed CO_2 and water within the column, respectively.

Table 4.1 Parameters used for evaluating energy consumption in vapor-promoted regeneration.

Parameter	Value
$C_{p,AIS}$ (J/kg·K)	1000 [29]
$C_{p,SG}$ (J/kg·K)	921 [30]
C_{p,CO_2} (J/kg·K)	2000 [31]
C_{p,H_2O} (J/kg·K)	4184
h_{des,CO_2} (kJ/mol)	75
h_{des,H_2O} (kJ/mol)	44 [32]

Equation 4.3 is employed to assess latent heat, where Q_{des,CO_2} and Q_{des,H_2O} represent the heat required for CO_2 and water desorption, respectively; $n_{CO_2}^{(des)}$ and $n_{H_2O}^{(des)}$ represent the moles of collected CO_2 and water products during the desorption process, respectively; h_{des,CO_2} and h_{des,H_2O} are the heat of desorption for CO_2 and water, respectively. The numerical parameters used for evaluating energy consumption are listed in Table 4.1. The heat of desorption for CO_2 on silica gel was not considered in this analysis because silica gel did not have the capability to adsorb atmospheric CO_2, and therefore would not release CO_2 during the regeneration process. When calculating energy consumption for water release, the water desorbed from both silica gel and CO_2 adsorbents was taken into account.

$$Q_d = Q_{des,CO_2} + Q_{des,H_2O} = n_{CO_2}^{(des)} h_{des,CO_2} + n_{H_2O}^{(des)} h_{des,H_2O} \quad (4.3)$$

4.3 Results and discussion

4.3.1 Thermodynamic analysis of AIS regeneration

The adsorption isotherms of CO_2 on the three AIS were analyzed at 25 °C, 40 °C, and 55 °C, as shown in Figure 4.2. All sorbents displayed the ability to adsorb CO_2 at low partial pressures, primarily owing to the strong affinity between amines and CO_2. The CO_2 adsorption capacities under low-pressure conditions are presented in Figure 4.3. For PEI/HP20 and PEI/HP2MGL, the CO_2 adsorption behavior could be described by the Dual-site Langmuir model (Equations 3.1-3.3) [33]. The fitted model parameters were listed in Table 4.2, and the heat of CO_2 adsorption on amines was calculated to be approximately -75 kJ/mol.

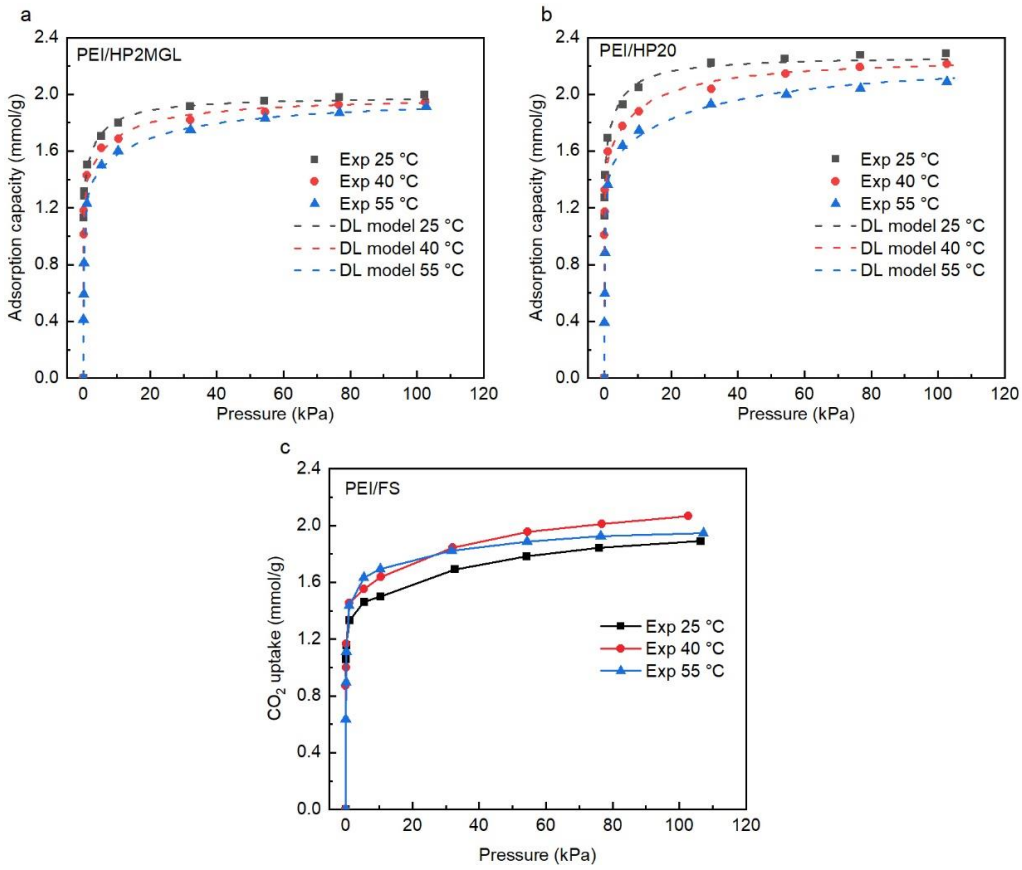

Figure 4.2 CO_2 adsorption isotherms of AIS.

(a-b) Experimental CO_2 adsorption isotherms of (a) PEI/HP2MGL and (b) PEI/HP20 at 25, 40, and 55 °C, fitted to the Dual-site Langmuir model. (c) Experimental CO_2 adsorption isotherms of PEI/FS at 25, 40, and 55 °C.

Table 4.2 Dual-site Langmuir model parameters of CO_2 adsorption on PEI/HP20 and PEI/HP2MGL.

Parameter	PEI/HP20	PEI/HP2MGL
q_1 (mmol/g)	1.508	1.349
q_2 (mmol/g)	0.762	0.639
$K_{0,1}$ (1/kPa)	8.92×10^{-12}	8.45×10^{-12}
$K_{0,2}$ (1/kPa)	3.87×10^{-11}	2.29×10^{-8}
$-\Delta H_{ads,1}$ (kJ/mol)	75.3	75.4
$-\Delta H_{ads,2}$ (kJ/mol)	56.5	40.3

By contrast, as the CO_2 uptake on PEI/FS did not consistently decrease with rising temperatures (Figure 4.2c and Figure 4.3), its adsorption behavior could not be described by regular adsorption models. Although the adsorption of 400 ppm CO_2 on PEI/FS still followed the thermodynamic expectations, the optimal adsorption temperature for 5% CO_2 was around 70 °C. This phenomenon, which has been extensively documented for PEI-impregnated silica, is mainly attributed to the restricted diffusion of CO_2 molecules within pores congested by PEI polymers [9, 34, 35]. Therefore, PEI/HP2MGL was employed as the sorbent to analyze the required regeneration conditions of AIS from a thermodynamic point of view.

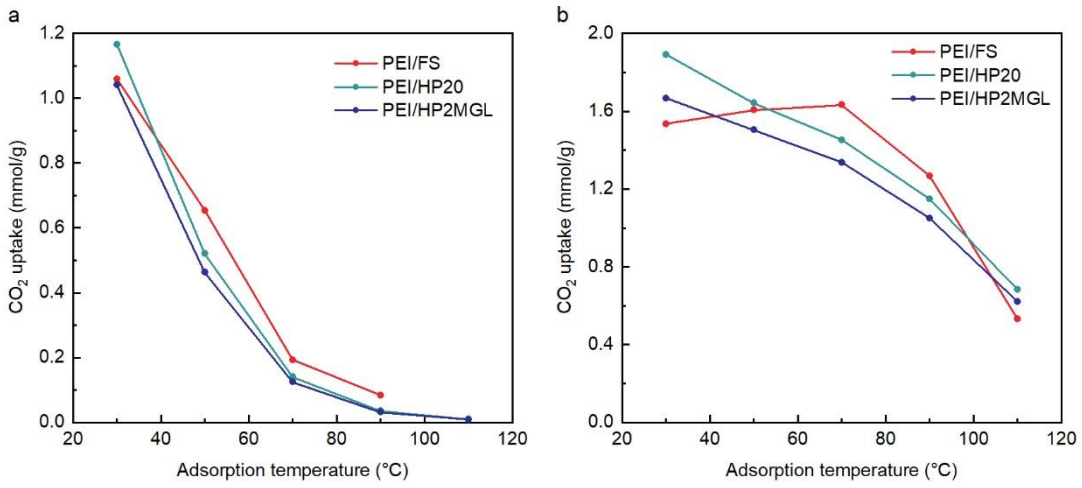

Figure 4.3 Equilibrium adsorption capacities of PEI/HP2MGL, PEI/HP20, and PEI/FS for (a) 400 ppm and (b) 5% CO_2 at different adsorption temperatures, obtained through thermogravimetric analysis.

The regeneration efficiency (R), which quantifies the proportion of recoverable CO_2

adsorbed on solid amine sorbents in a regeneration process, is calculated using Equation 3.12 proposed in Chapter 3. The regeneration efficiencies for PEI/HP2MGL under different temperatures and pressures were shown in Figure 4.4. Results clearly illustrated that elevated temperatures and reduced CO_2 partial pressures were beneficial for the regeneration of CO_2. However, regenerating PEI/HP2MGL at 100 °C and 5 kPa achieved a regeneration efficiency of only 0.3, indicating that 70% of the adsorbed CO_2 remained unrecovered. As the conventional TVSA process relies on vacuum pumps and typically operates at pressures higher than 5 kPa, it does not have the capability to generate a sufficiently high driving force for the desorption of CO_2 from PEI-impregnated sorbents. In the present work, the VPD process with substantial desorption driving force was used to deal with the efficiency limitation of conventional processes.

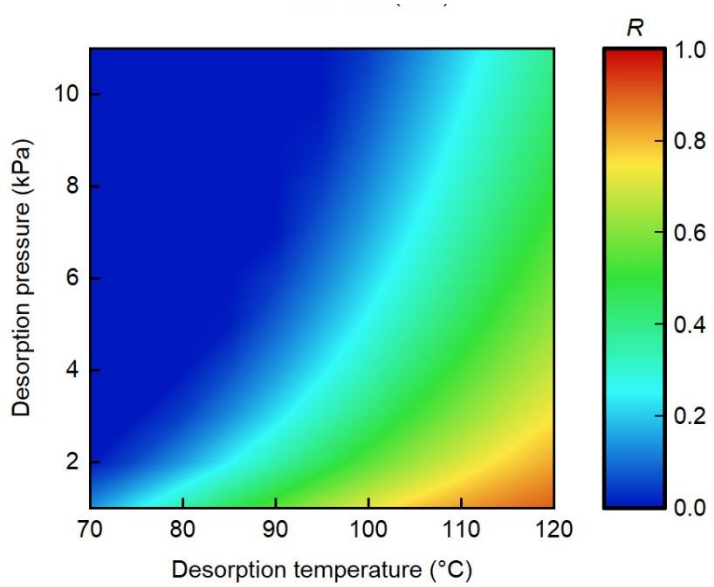

Figure 4.4 Regeneration efficiency (*R*) calculations for PEI/HP2MGL at various desorption temperatures and pressures, with fixed adsorption conditions of 25 °C and 400 ppm CO_2.

4.3.2 Adsorption properties and thermal stability

Before testing VPD, breakthrough experiments were conducted to investigate the adsorption behavior of AIS under practical DAC conditions. As shown in Figure 4.5, the breakthrough curves of CO_2 on all AIS were quite steep and the CO_2 adsorption typically saturated within 6 hours. The adsorption time was long because a large volume of 200 mL adsorbent was used to conduct breakthrough experiments. The CO_2 adsorption kinetics on PEI/FS was the slowest as

its equilibration duration was one hour longer than PEI/HP20 and PEI/HP2MGL. This further confirmed the restricted CO_2 transfer rate as already observed in Figure 4.3b [15].

The dynamic CO_2 adsorption capacities of the sorbents were calculated based on the breakthrough curves (Figure 4.5a). At 25 °C and 60% relative humidity, PEI/HP20, PEI/HP2MGL, and PEI/FS exhibited high CO_2 adsorption capacities of 1.52, 1.63 and 1.71 mmol/g, respectively. When compared with Lewatit VP OC 1065, a commercial sorbent for DAC, the PEI-impregnated sorbents displayed a 60% increase in CO_2 uptake under similar conditions due to the numerous amine sites in PEI molecules. Unlike physisorbents, which favor atmospheric CO_2 adsorption under relatively dry conditions to prevent competitive adsorption between water and CO_2 [10], the presence of moisture in the air could enhance the adsorption of CO_2 on AIS by more than 30%. In this work, the CO_2 uptake on PEI/FS increased by 61%, from 1.06 to 1.71 mmol/g in the presence of moisture (Figure 4.5b). The good sorption performance of the AIS was attributed to the pore structures of the supports used for PEI impregnation. Based on the N_2 adsorption-desorption isotherms (Figures 4.6a-c), the supports were macroporous materials with pore volumes higher than 0.62 cm^3/g. Even after impregnation with a 33% PEI loading, the AIS still maintained large surface areas ranging from 76-128 m^2/g, providing a structural foundation for efficient CO_2 adsorption.

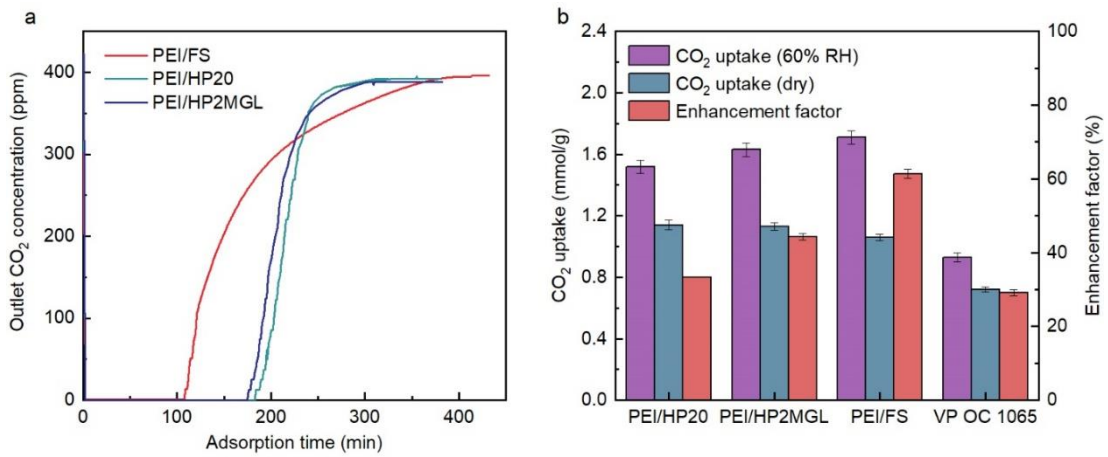

Figure 4.5 CO_2 adsorption properties of PEI/HP20, PEI/HP2MGL, and PEI/FS.

(a) CO_2 breakthrough curves of PEI/HP20, PEI/HP2MGL, and PEI/FS at 25 °C and 60% relative humidity, with an adsorbent volume of 200 mL. The feed gas consisted of air containing 400 ppm CO_2 with a flow rate of 30 L/min. (b) CO_2 adsorption properties of PEI/HP20, PEI/HP2MGL, and PEI/FS under 60% relative humidity and dry conditions. The enhancement factor represents the ratio of adsorption capacity under humid and dry conditions.

Although AIS is effective in capturing atmospheric CO_2, the low thermal stability is one of the major concerns that hinders its long-term operation in practical DAC systems [36]. Adsorption-desorption cycles were conducted to investigate the thermal stability of the prepared AIS using thermogravimetric analysis (TGA). The adsorption step was carried out at 30 °C in CO_2, while the desorption step was performed at different temperatures (70-110 °C) in flowing dry air. Interestingly, despite using the same amine-containing species for impregnation, the sorbents with different support materials exhibited distinct thermal stability. As shown in Figures 4.6d-f, sorbents remained relatively stable throughout twelve adsorption-desorption cycles at a desorption temperature of 70 °C. However, increasing the desorption temperature to 90 °C resulted in 29.1% and 10.4% losses in CO_2 uptake for PEI/HP2MGL and PEI/HP20, respectively, while no noticeable deactivation was observed for PEI/FS (Figure 4.6e). After undergoing twelve adsorption-desorption cycles at 110 °C, PEI/HP20, PEI/FS, and PEI/HP2MGL experienced reductions in CO_2 adsorption capacity by 24.5%, 22.0%, and 52.1%, respectively (Figure 4.6f). The adsorption capacities of each cycle, especially for experiments operated at high temperatures like 110 °C, have laid the foundation for future research on deactivation kinetics.

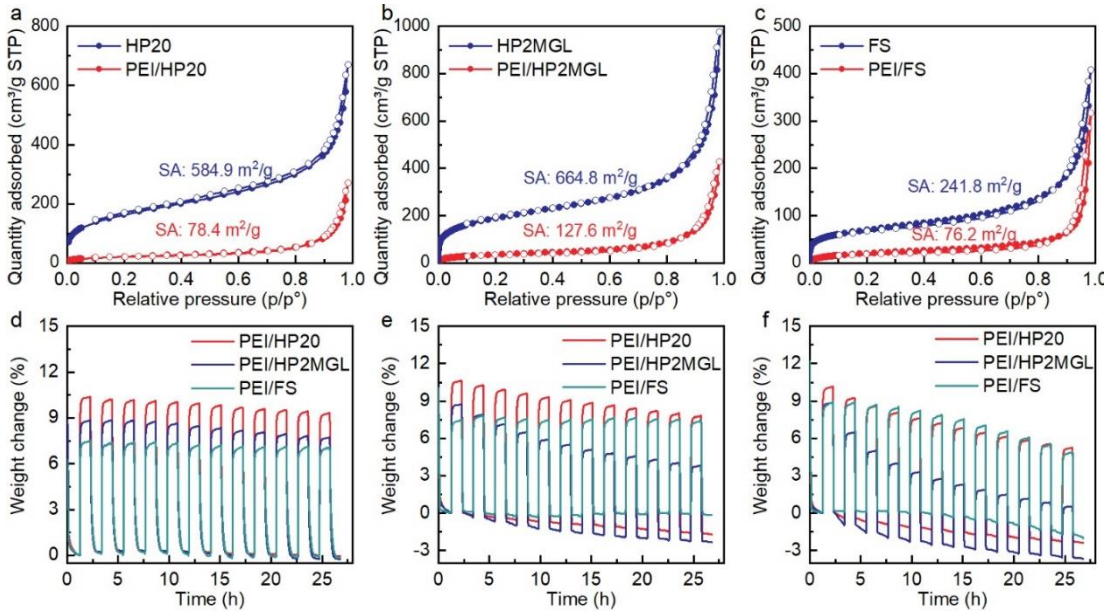

Figure 4.6 Porosity and thermal stability analyses for PEI/HP20, PEI/HP2MGL, and PEI/FS.

(a-c) N_2 adsorption (closed symbols) and desorption (open symbols) isotherms at 77 K for (a) PEI/HP20, (b) PEI/HP2MGL, and (c) PEI/FS. The pore structures of the support material before loading PEI were also characterized. (d-f) Adsorption-desorption profiles of PEI/HP20, PEI/HP2MGL, and PEI/FS during 12 consecutive temperature swing cycles. Adsorption: 100%

CO_2 at 30 °C for 1 h; Desorption: dry air at (d) 70 °C, (e) 90 °C and (f) 110 °C for 1 h.

4.3.3 Performance of the VPD process for regenerating AIS

The VPD process was applied to efficiently recover the substantial amount of CO_2 adsorbed on the prepared AIS. Silica gel and amine-impregnated sorbents, each with a volume of 200 mL, were sequentially packed in the column as water adsorbent layer and CO_2 sorbent layer, respectively. This double-layered configuration allowed for the simultaneous capture of atmospheric water and CO_2 in the adsorption process, and generated *in situ* vapor for providing the primary desorption driving force during the regeneration process. Bead-form sorbents were employed in the column because the present work focused on the regeneration of the sorbents rather than modifying the pressure drop or designing an air contactor. The results obtained using the bead-form sorbents can also be applied to other adsorbents with low pressure drops.

The cyclic results in Figure 4.7a demonstrated that PEI/FS could be efficiently regenerated using the VPD process at temperatures below 105 °C, achieving a regeneration efficiency of 0.95. The desorption process accounted for approximately 10% (40 minutes) of the overall cycle time. Thus, the cyclic time is mainly determined by the adsorption time, which is influenced by kinetics and flow rate. With fast adsorption kinetics and high flow rates, the proportion of desorption time to cyclic time may increase.

The exceptional desorption performance, as indicated by the CO_2 sorption capacity, remained highly stable over six vapor-promoted DAC cycles. The stable performance observed was attributed to the low O_2 concentration inside the column during regeneration, as the air within the column was purged out by the desorbed vapor and CO_2. By contrast, according to the experiments conducted using dry air as the feed stream, no CO_2 product could be collected at 105 °C, indicating the substantial desorption driving force generated by the VPD process.

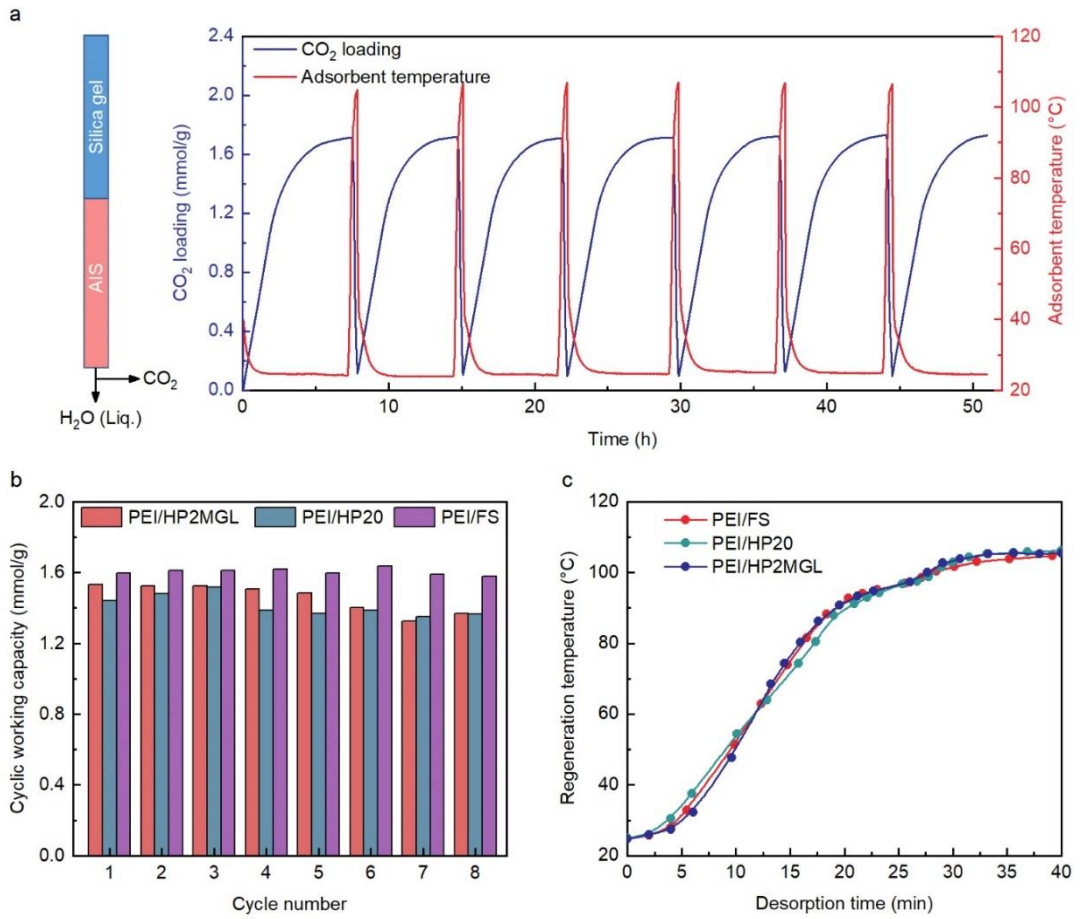

Figure 4.7 Performance of *in situ* vapor purge for the regeneration of AIS.

Adsorbents: 200 mL amine-impregnated sorbents and 200 mL silica gel. Fresh air at 25 °C and 60% RH was used as the feed stream with a flow rate of 30 L/min. (a) CO_2 loading and temperature profiles of PEI/FS during adsorption-desorption cycles. (b) Cyclic CO_2 working capacities of PEI/HP20, PEI/HP2MGL, and PEI/FS regenerated through *in situ* vapor purge. (c) Desorption temperature profiles of PEI/HP20, PEI/HP2MGL, and PEI/FS during the VPD process.

Vapor-promoted desorption was also employed to regenerate PEI/HP20 and PEI/HP2MGL. The calculated cyclic working capacities of the three sorbents were illustrated in Figure 4.7b. With *in situ* vapor purge, approximately 95% of the CO_2 adsorbed on the AIS could be released, resulting in excellent CO_2 working capacities ranging from 1.4-1.6 mmol/g. PEI/FS, which demonstrated the highest thermal stability, also exhibited the highest working capacity and stability in practical DAC experiments. The regeneration temperature profiles of the three AIS during the VPD process were depicted in Figure 4.7c. Following a preheating stage to rapidly increase the temperature to 90 °C, the *in situ* vapor purge for sorbent regeneration was mainly conducted at stabilized temperatures ranging from 90 to 105 °C. All three sorbents

could be efficiently regenerated below 105 °C at atmospheric pressure, without the need for external purge supplies or evacuation. With the increase in desorption temperature, the released water vapor and CO_2 would gradually purge the air out of the column. Thus, degradation of PEI/HP2MGL and PEI/HP20 in the preheating step was expected to be largely avoided. However, the high temperatures during the preheating and cooling stages still posed a risk of slight degradation for the two sorbents. After eight cycles, PEI/HP2MGL and PEI/HP20 lost 10.5% and 5.3% of their working capacities, while PEI/FS remained stable. Further investigating the relationship between support material and stability is important to ensure a long lifetime of amines.

In the VPD process, the key to effectively regenerating PEI-impregnated sorbents is the *in situ* vapor purge using water captured from the air. To gain a deeper understanding of the mechanism, the humidity profiles inside the adsorption column during the regeneration process were analyzed. As shown in Figure 4.8a, as the sorbent temperature increased, the vapors released from the water adsorbent layer created an environment with an RH as high as 100%. Such an extremely humid condition would lead to a significantly high vapor pressure (P_{vapor}) and reduce the CO_2 partial pressure (P_{CO_2}), as described by the following equation:

$$P_{des} = P_{CO_2} + P_{vapor} \tag{4.4}$$

where P_{des} represents the desorption pressure in the regeneration process and is equal to the ambient pressure in the VPD process. In Figure 4.8b, the P_{vapor}, calculated using the Antoine equation, could reach around 100 kPa with *in situ* vapor purge, thereby reducing the P_{CO_2} to below 1 kPa. According to the CO_2 adsorption isotherm of PEI/FS, a reduced P_{CO_2} would decrease the equilibrium adsorption capacity and enhance the desorption of CO_2. As depicted in Figure 4.8b, this vapor-promoted desorption process could recover over 90% of the CO_2 adsorbed on PEI/FS at a vapor pressure of 100 kPa.

It is noteworthy that the desorption process required a long time of 40 minutes due to the insufficient efficiency of heat transfer. As shown in Figure 4.8b, nearly 20 minutes were used to increase the temperature of the adsorbents, and another 20 minutes were employed to release the CO_2. Therefore, modifying the heat transfer in a DAC system is also crucial for reducing the desorption time as well as CO_2 productivity.

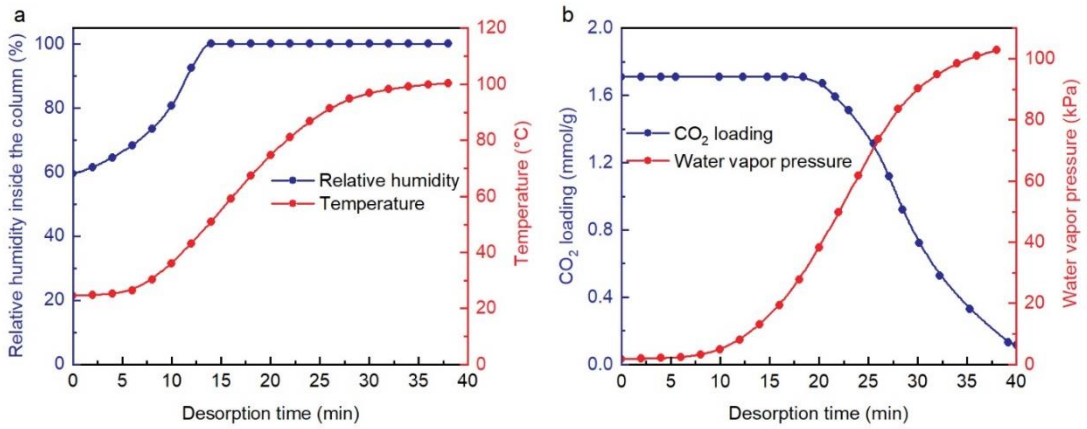

Figure 4.8 Effects of *in situ* vapor for the regeneration of PEI/FS.

Adsorbents: 200 mL PEI/FS and 200 mL silica gel. Fresh air at 25 °C and 60% RH was used as the feed stream. (a) Relative humidity and temperature profiles inside the column during the VPD process. (b) CO_2 loadings of PEI/FS and vapor pressure profile during the VPD process.

In the experiments mentioned above, both the AIS and water adsorbent layers were packed with 200 mL of materials for conducting vapor-promoted DAC. To investigate whether the VPD process can be operated with an increased volume of AIS, the volumes of AIS and silica gel were modified to 320 mL and 80 mL, respectively. As shown in Figure 4.9a, even with a low silica gel volume fraction of 0.2, PEI/FS could still be efficiently regenerated at 104 °C, achieving an extremely high working capacity of 1.61 mmol/g. In contrast, without the promotion of *in situ* vapor purge, only 0.17 mmol/g CO_2 could be desorbed at temperatures lower than 105 °C (Figure 4.9b).

During the VPD process, the co-adsorbed water released as vapors could be condensed as water products. As shown in Figure 4.9c, one vapor-promoted DAC cycle using 80 mL of silica gel and 320 mL of PEI/FS could produce 5.8-7.4 g of fresh water, along with CO_2 production with a cyclic productivity of around 5.3 g. During the desorption process (Figure 4.9d), the purity of the produced CO_2 reached up to 99%, making it suitable for subsequent conversions into valuable chemicals such as methanol [37].

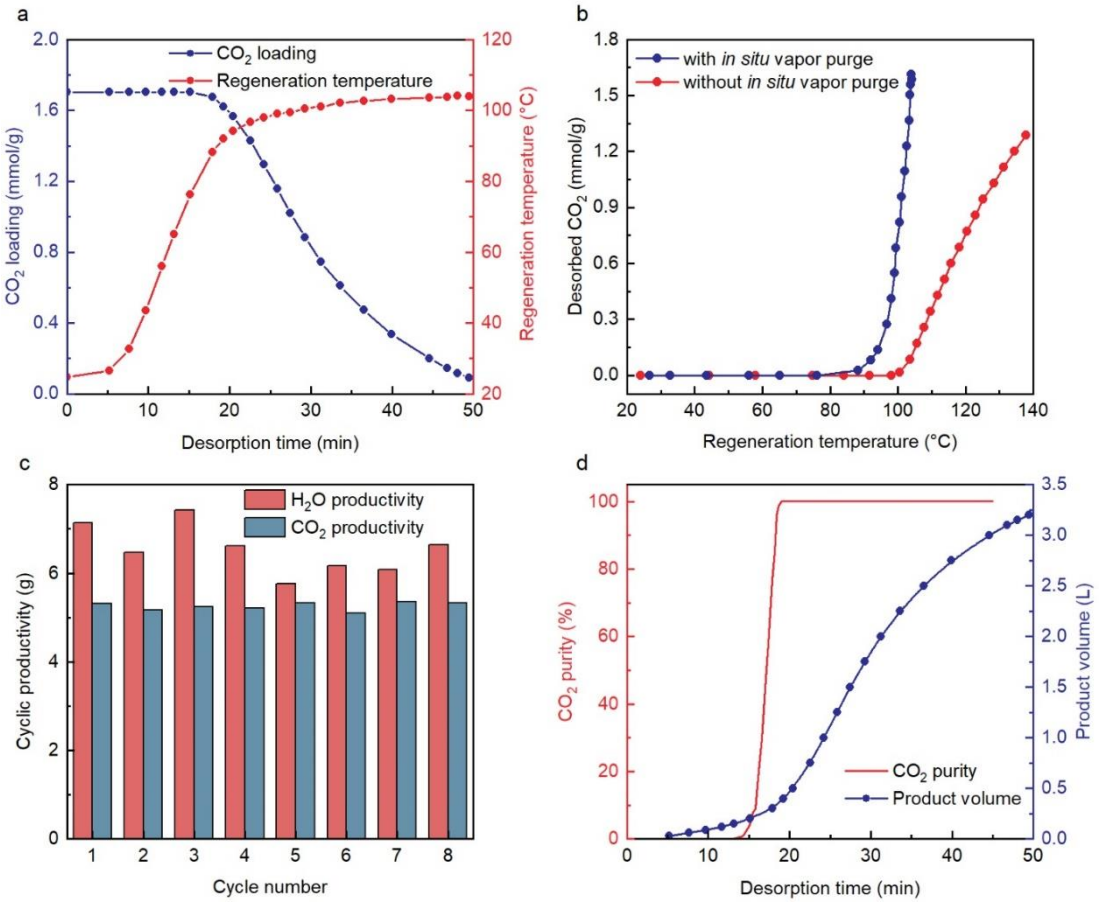

Figure 4.9 Products of cyclic DAC based on vapor-promoted desorption.

Adsorbents: 320 mL PEI/FS and 80 mL silica gel. Fresh air at 25 °C and 60% RH was used as the feed stream with a flow rate of 30 L/min. (a) CO_2 loading and desorption temperature profiles during the regeneration process. (b) CO_2 working capacity achieved under different regeneration temperatures. Desorption without *in situ* vapor purge was performed by replacing silica gel with glass beads. (c) Cyclic CO_2 and water productivity of the vapor-promoted DAC system. (d) Real-time CO_2 purity and product volumes during the regeneration process.

After sorbent regeneration and product collection, the sorbent typically needs to be cooled down for the next cycle, which can take at least 15 min in conventional DAC processes [38, 39]. In the vapor-promoted DAC process, a rapid cooling was achieved by introducing ambient air into the column, thereby reducing the vapor pressure around the water adsorbent layer. This pressure reduction caused the co-adsorbed water in the double-layered column to evaporate rapidly, leading to a sharp temperature decrease of 65 °C in 5 minutes (Figure 4.10). As the temperature dropped and the sorbent's water loading decreased, the equilibrium shifted towards water adsorption, initiating the next cycle for capturing atmospheric CO_2 and moisture.

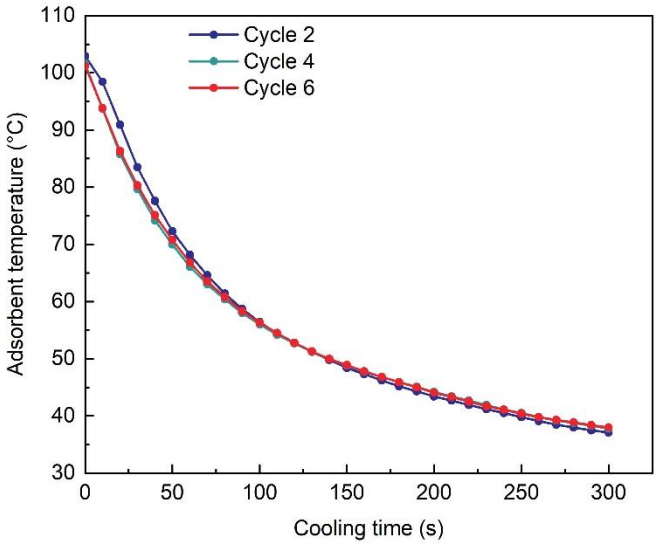

Figure 4.10 The temperature profiles of PEI/FS during the cooling process of various DAC cycles. Fresh air at 25 °C and 60% RH was used as the feed stream, with 320 mL PEI/FS and 80 mL silica gel as adsorbents.

4.3.4 Energy consumption of VPD

A comprehensive analysis was conducted to assess the overall energy requirements for regenerating PEI/FS in the VPD process. Since no electrical energy was used for evacuation, the analysis focused solely on the thermal energy required for regeneration. The energy consumption could be categorized into two components: sensible heat (Q_s) needed to raise the temperatures of sorbents and adsorbed molecules, as well as latent heat (Q_d) associated with CO_2 and water desorption. As shown in Figure 4.11a, the VPD process exhibited a total energy consumption of 8.9 MJ/kg_{CO2} for sorbent regeneration. Among these, approximately 64% of the thermal energy, which included both sensible and latent heat, was attributed to *in situ* vapor purge (Figure 4.11b). Specifically, the sensible heat required to increase the temperatures of co-adsorbed water and silica gel contributed to 22% and 10% of the total energy consumption, respectively, while the latent heat for vapor generation accounted for 32%. The large amount of heat released from vapor condensation could be harnessed through heat management strategies to further reduce the energy consumption for DAC. Importantly, this VPD process based on AIS demonstrated at least 14% lower energy consumption (Figure 4.11a) compared with the work presented in Chapter 3 and other DAC processes like TVSA and steam-assisted TVSA [26]. The low energy penalty could be attributed to the high regeneration efficiency and working capacity of 1.61 mmol/g achieved through the *in situ* vapor purge strategy.

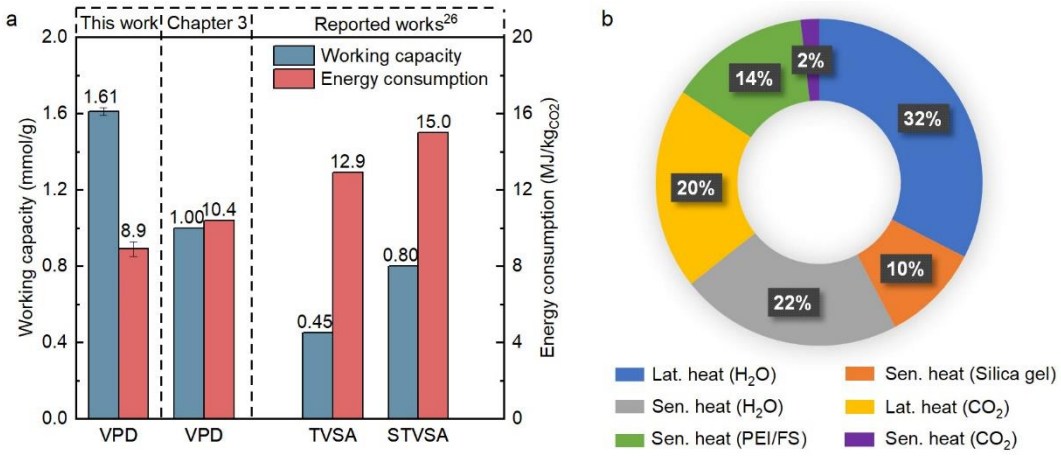

Figure 4.11 Energy consumption for the regeneration of PEI/FS.

(a) Comparative evaluation of energy consumption and working capacity for regenerating solid amine sorbents using different processes, including VPD, TVSA, and steam-assisted TVSA (STVSA). (b) Breakdown of energy consumption for sorbent regeneration in the VPD process. Lat. heat represents the heat associated with the desorption of CO_2 and water. Sen. heat denotes the thermal energy needed to increase the temperature of sorbents and adsorbed molecules.

4.4 Conclusions

Amine-impregnated sorbents (AIS) have been widely reported to capture atmospheric CO_2 with excellent performance, yet little attention has been paid to the recovery of CO_2 adsorbed on the impregnated amines. In this chapter, three PEI-impregnated sorbents with different support materials were prepared, and their regenerability was tested using the developed VPD process with a double-layered configuration. Through *in situ* vapor purge using water harvested from the air, all the prepared AIS could be efficiently regenerated, recovering over 95% of the CO_2 adsorbed on AIS at 105 °C. PEI-impregnated fumed silica, a representative AIS, achieved a stable cyclic CO_2 working capacity of approximately 1.6 mmol/g, with an exceptionally high CO_2 product purity of 99%. The remarkable efficiency of the VPD process could be attributed to the extremely humid environment created by the water desorbed from silica gel, coupled with the significant reduction in CO_2 partial pressure around the AIS. The energy consumption for regenerating PEI/FS was calculated to be 8.9 MJ/kg_{CO2}, which was 14% lower than the VPD process using commercial VP OC 1065 as the CO_2 sorbent. More than half of the thermal energy was consumed for the generation of *in situ* vapors. The VPD process was proven to be an efficient method for recovering adsorbed CO_2 from AIS, providing a foundation for the practical application of these cost-effective chemisorbents.

4.5 References

[1] E.S. Sanz-Pérez, C.R. Murdock, S.A. Didas, C.W. Jones, Direct capture of CO_2 from ambient air, Chem. Rev. 116 (2016) 11840-11876.

[2] A. Goeppert, M. Czaun, G.K. Surya Prakash, G.A. Olah, Air as the renewable carbon source of the future: an overview of CO_2 capture from the atmosphere, Energ. Environ. Sci. 5 (2012) 7833-7853.

[3] X. Zhu, W. Xie, J. Wu, Y. Miao, C. Xiang, C. Chen, B. Ge, Z. Gan, F. Yang, M. Zhang, D. O'Hare, J. Li, T. Ge, R. Wang, Recent advances in direct air capture by adsorption, Chem. Soc. Rev. 51 (2022) 6574-6651.

[4] A. Goeppert, M. Czaun, R.B. May, G.K.S. Prakash, G.A. Olah, S.R. Narayanan, Carbon dioxide capture from the air using a polyamine based regenerable solid adsorbent, J. Am. Chem. Soc. 133 (2011) 20164-20167.

[5] L.A. Darunte, A.D. Oetomo, K.S. Walton, D.S. Sholl, C.W. Jones, Direct air capture of CO_2 using amine functionalized MIL-101(Cr), ACS Sustain. Chem. Eng. 4 (2016) 5761-5768.

[6] A. Goeppert, S. Meth, G.K.S. Prakash, G.A. Olah, Nanostructured silica as a support for regenerable high-capacity organoamine-based CO_2 sorbents, Energ. Environ. Sci. 3 (2010) 1949.

[7] G. Qi, Y. Wang, L. Estevez, X. Duan, N. Anako, A.A. Park, W. Li, C.W. Jones, E.P. Giannelis, High efficiency nanocomposite sorbents for CO_2 capture based on amine-functionalized mesoporous capsules, Energy Environ. Sci. 4 (2011) 444-452.

[8] Y. Miao, Y. Wang, B. Ge, Z. He, X. Zhu, J. Li, S. Liu, L. Yu, Mixed diethanolamine and polyethyleneimine with enhanced CO_2 capture capacity from air, Advanced Science 10 (2023) 1-8.

[9] H.T. Kwon, M.A. Sakwa-Novak, S.H. Pang, A.R. Sujan, E.W. Ping, C.W. Jones, Aminopolymer-impregnated hierarchical silica structures: unexpected equivalent CO_2 uptake under simulated air capture and flue gas capture conditions, Chem. Mater. 31 (2019) 5229-5237.

[10] A. Kumar, D.G. Madden, M. Lusi, K.J. Chen, E.A. Daniels, T. Curtin, J.J. Perry, M.J. Zaworotko, Direct air capture of CO_2 by physisorbent materials, Angewandte Chemie International Edition 54 (2015) 14372-14377.

[11] K. Maresz, A. Ciemięga, J.J. Malinowski, J. Mrowiec-Białoń, Effect of support structure and polyamine type on CO_2 capture in hierarchically structured monolithic sorbents, Chem. Eng. J. 383 (2020) 123175.

[12] Z. Li, H. Chen, C. Chen, Q. Guo, X. Li, Y. He, H. Wang, N. Feng, H. Wan, G. Guan, High dispersion of polyethyleneimine within mesoporous UiO-66s through pore size engineering for selective CO_2 capture, Chem. Eng. J. 375 (2019) 121962.

[13] W. Chaikittisilp, R. Khunsupat, T.T. Chen, C.W. Jones, Poly(allylamine)-mesoporous silica composite materials for CO_2 capture from simulated flue gas or ambient air, Ind. Eng. Chem. Res. 50 (2011) 14203-14210.

[14] Z. Chen, S. Deng, H. Wei, B. Wang, J. Huang, G. Yu, Polyethylenimine-impregnated resin for high CO_2 adsorption: An efficient adsorbent for CO_2 capture from simulated flue gas and ambient air, ACS Appl. Mater. Inter. 5 (2013) 6937-6945.

[15] A. Goeppert, H. Zhang, M. Czaun, R.B. May, G.K.S. Prakash, G.A. Olah, S.R. Narayanan, Easily regenerable solid adsorbents based on polyamines for carbon dioxide capture from the air, ChemSusChem 7 (2014) 1386-1397.

[16] J. Wang, H. Huang, M. Wang, L. Yao, W. Qiao, D. Long, L. Ling, Direct capture of low-concentration CO_2 on mesoporous carbon-supported solid amine adsorbents at ambient temperature, Ind. Eng. Chem. Res. 54 (2015) 5319-5327.

[17] J. Wang, D. Long, H. Zhou, Q. Chen, X. Liu, L. Ling, Surfactant promoted solid amine sorbents for CO_2 capture, Energ. Environ. Sci. 5 (2012) 5742-5749.

[18] W. Choi, K. Min, C. Kim, Y.S. Ko, J.W. Jeon, H. Seo, Y. Park, M. Choi, Epoxide-functionalization of polyethyleneimine for synthesis of stable carbon dioxide adsorbent in temperature swing adsorption, Nat. Commun. 7 (2016)

[19] M.A. Alkhabbaz, P. Bollini, G.S. Foo, C. Sievers, C.W. Jones, Important roles of enthalpic and entropic contributions to CO_2 capture from simulated flue gas and ambient air using mesoporous silica grafted amines, J. Am. Chem. Soc. 136 (2014) 13170-13173.

[20] F. Sabatino, A. Grimm, F. Gallucci, M. van Sint Annaland, G.J. Kramer, M. Gazzani, A comparative energy and costs assessment and optimization for direct air capture technologies, Joule 5 (2021) 2047-2076.

[21] J. Elfving, J. Kauppinen, M. Jegoroff, V. Ruuskanen, L. Järvinen, T. Sainio, Experimental comparison of regeneration methods for CO_2 concentration from air using amine-based adsorbent, Chem. Eng. J. 404 (2021) 126337.

[22] M. Erans, E.S. Sanz-Pérez, D.P. Hanak, Z. Clulow, D.M. Reiner, G.A. Mutch, Direct air capture: process technology, techno-economic and socio-political challenges, Energ. Environ. Sci. 15 (2022) 1360-1405.

[23] W. Zhang, H. Liu, C. Sun, T.C. Drage, C.E. Snape, Capturing CO_2 from ambient air using a polyethyleneimine-silica adsorbent in fluidized beds, Chem. Eng. Sci. 116 (2014) 306-316.

[24] R.P. Wijesiri, G.P. Knowles, H. Yeasmin, A.F.A. Hoadley, A.L. Chaffee, Desorption process for capturing CO_2 from air with supported amine sorbent, Ind. Eng. Chem. Res. 58 (2019) 15606-15618.

[25] A. Sinha, L.A. Darunte, C.W. Jones, M.J. Realff, Y. Kawajiri, Systems design and economic analysis of direct air capture of CO_2 through temperature vacuum swing adsorption using MIL-101(Cr)-PEI-800 and mmen-Mg_2(dobpdc) MOF adsorbents, Ind. Eng. Chem. Res. 56 (2017) 750-764.

[26] M.J. Bos, S. Pietersen, D.W.F. Brilman, Production of high purity CO_2 from air using solid amine sorbents, Chemical Engineering Science: X 2 (2019) 100020.

[27] K.C. Ng, H.T. Chua, C.Y. Chung, C.H. Loke, T. Kashiwagi, A. Akisawa, B.B. Saha, Experimental investigation of the silica gel-water adsorption isotherm characteristics, Appl. Therm. Eng. 21 (2001) 1631-1642.

[28] Y. Belmabkhout, R. Serna-Guerrero, A. Sayari, Amine-bearing mesoporous silica for CO_2 removal from dry and humid air, Chem. Eng. Sci. 65 (2010) 3695-3698.

[29] A.R. Kulkarni, D.S. Sholl, Analysis of equilibrium-based TSA processes for direct capture of CO_2 from air, Ind. Eng. Chem. Res. 51 (2012) 8631-8645.

[30] E. Robens, X. Wang, Investigation on the isotherm of silica gel+water systems, J. Therm. Anal. Calorim. 76 (2004) 659-669.

[31] J.A. Wurzbacher, C. Gebald, S. Brunner, A. Steinfeld, Heat and mass transfer of temperature-vacuum swing desorption for CO_2 capture from air, Chem. Eng. J. 283 (2016) 1329-1338.

[32] H. Demir, M. Mobedi, S. Ülkü, Microcalorimetric investigation of water vapor adsorption on silica gel, J. Therm. Anal. Calorim. 105 (2011) 375-382.

[33] W.R. Lee, S.Y. Hwang, D.W. Ryu, K.S. Lim, S.S. Han, D. Moon, J. Choi, C.S. Hong, Diamine-functionalized metal‑organic framework: exceptionally high CO_2 capacities from ambient air and flue gas, ultrafast CO_2 uptake rate, and adsorption mechanism, Energ. Environ. Sci. 7 (2014) 744-751.

[34] X. Xu, C. Song, J.M. Andresen, B.G. Miller, A.W. Scaroni, Novel polyethylenimine-modified mesoporous molecular sieve of MCM-41 type as high-capacity adsorbent for CO_2 capture, Energ. Fuel. 16 (2002) 1463-1469.

[35] Y. Meng, J. Jiang, A. Aihemaiti, T. Ju, Y. Gao, J. Liu, S. Han, Feasibility of CO_2 capture from O_2-containing flue gas using a poly(ethylenimine)-functionalized sorbent: oxidative stability in long-term operation, ACS Appl. Mater. Inter. 11 (2019) 33781-33791.

[36] M. Jahandar Lashaki, S. Khiavi, A. Sayari, Stability of amine-functionalized CO_2 adsorbents: a multifaceted puzzle, Chem. Soc. Rev. 48 (2019) 3320-3405.

[37] V. Spallina, G. Motamedi, F. Gallucci, M. van Sint Annaland, Techno-economic assessment of an integrated high pressure chemical-looping process with packed-bed reactors in large scale hydrogen and methanol production, Int. J. Greenh. Gas Con. 88 (2019) 71-84.

[38] C.J. E. Bajamundi, J. Koponen, V. Ruuskanen, J. Elfving, A. Kosonen, J. Kauppinen, J. Ahola, Capturing CO_2 from air: Technical performance and process control improvement, Journal of CO2 Utilization 30 (2019) 232-239.

[39] M.M. Sadiq, M.P. Batten, X. Mulet, C. Freeman, K. Konstas, J.I. Mardel, J. Tanner, D. Ng, X. Wang, S. Howard, M.R. Hill, A.W. Thornton, A pilot-scale demonstration of mobile direct air capture using metal-organic frameworks, Advanced Sustainable Systems 4 (2020) 2000101.

5 Enhancing CO_2 desorption by synergistic generation of low-temperature vapors

5.1 Introduction

Amine-impregnated sorbents (AIS), which involve depositing amines onto a solid support, have attracted significant research interest due to their advantages of easy preparation, low cost, and high adsorption capacities [1-5]. However, AIS is usually synthesized using oxidation-prone amines such as branched polyethylenimine (PEI) and tetraethylenepentamine (TEPA), leading to reduced stability at elevated temperatures [6-10]. For instance, in Chapter 4, following eight DAC cycles with a desorption temperature of 105 °C, the PEI-impregnated sorbents exhibited a reduction in their working capacities ranging from 1.0% to 10.5%.

Despite the development of numerous AIS with excellent adsorption performance, researchers prefer using more stable adsorbents bonded with primary amines for DAC [11-13], as the overall capture cost is highly sensitive to the lifetime of the adsorbent [14, 15]. When amine lifespans are lower than one year, the adsorbent cost could even account for half of the total cost, significantly hindering the large-scale deployment of DAC [14, 15]. Therefore, the development of task-specific regeneration processes for AIS is highly demanded to deal with the stability issue and improve their lifetime in practical DAC cycles.

Existing processes, like steam stripping, CO_2 purging, and temperature vacuum swing adsorption (TVSA), typically require elevating the sorbent temperature to above 80 °C, leading to significant deactivation induced by steam, CO_2, or air [15-18]. Simultaneously achieving the long-term operation of impregnated amines and a high regeneration efficiency solely through existing DAC technologies is highly challenging.

In this work, a vapor-promoted temperature vacuum swing adsorption (VPTVSA) process was developed to achieve effective regeneration at temperatures below 60 °C, thus preventing thermal degradation of AIS. This vapor-promoted process generated low-temperature vapors under vacuum using water synergistically harvested from the air, *in situ* purging the AIS to provide a substantial driving force for CO_2 desorption. Such *in situ* vapor purge realized the regeneration of polyethylenimine-impregnated resins at temperatures as low as 60 °C, producing 99% purity CO_2 without noticeable deactivation of amines after 45 DAC cycles. By reducing the temperature needed for releasing CO_2, this alternative regeneration approach enables the long-term use of low-cost chemisorbents for atmospheric CO_2 capture, having

great potential in reducing the overall cost of DAC.

5.2 Experimental

5.2.1 Materials and synthesis

Polyethylenimine (PEI) impregnated materials were prepared by the physical impregnation method using branched PEI (Sigma-Aldrich) with a molecular weight (Mw) of 800. A macroporous adsorption resin, HP20 (Diaion, Mitsubishi), was selected as the support material. The raw resin was dried at 110 °C for 24 hours before conducting PEI impregnation. Two adsorbents were prepared with PEI loadings of 33% and 50% and were denoted as 33PEI/HP20 and 50PEI/HP20, respectively. PEI loading refers to the mass percentage of PEI present in the adsorbent. The required mass of PEI could be calculated based on the PEI loading and the mass of support material. In a typical preparation batch, the desired amount of PEI was dissolved in 600 mL of ethanol under stirring for 10 min, and then mixed with 500 mL of HP20. The mixture was stirred for at least 30 min and then dried under vacuum (<20 kPa) at 60 °C for 24 hours to remove ethanol. Prior to usage, the prepared PEI-impregnated resins were treated by flowing N_2 at 50 °C until the outlet CO_2 concentration was below 1 ppm. To harvest atmospheric water and perform *in situ* vapor purge, a type A silica gel (Desicco) with a particle size of 3-5 mm was employed as the water adsorbent. The as-received silica gel was pretreated under vacuum (<20 kPa) at 110 °C to remove the adsorbed water.

5.2.2 Characterizations

The pore structures of the resins, both before and after impregnation, were characterized by N_2 adsorption at 77 K using the Micromeritics 3Flex Adsorption Analyzer. The CO_2 adsorption isotherms were measured on the BEL Japan Belsorp-MAX at 25 °C, 40 °C, and 55 °C. The conventional degassing approach with extremely low pressures (< 10 Pa) was found to evaporate the impregnated PEI. Thus, a task-specified degassing condition was developed for PEI-impregnated resins, operating at 60 °C and 10 kPa under a N_2 atmosphere. The thermal stability of PEI-impregnated resins was characterized using thermogravimetric analysis (TGA) with a Mettler Toledo TGA/DSC 1 under the designated atmosphere and conditions.

5.2.3 Experimental setup

A stainless-steel tube of 60 cm in length and 4 cm in diameter, wrapped with heating tapes and thermal insulations, was employed as the adsorption column for performing DAC. The schematic of the setup used for analyzing the breakthrough behaviors and testing the VPTVSA process is illustrated in Figure 5.1.

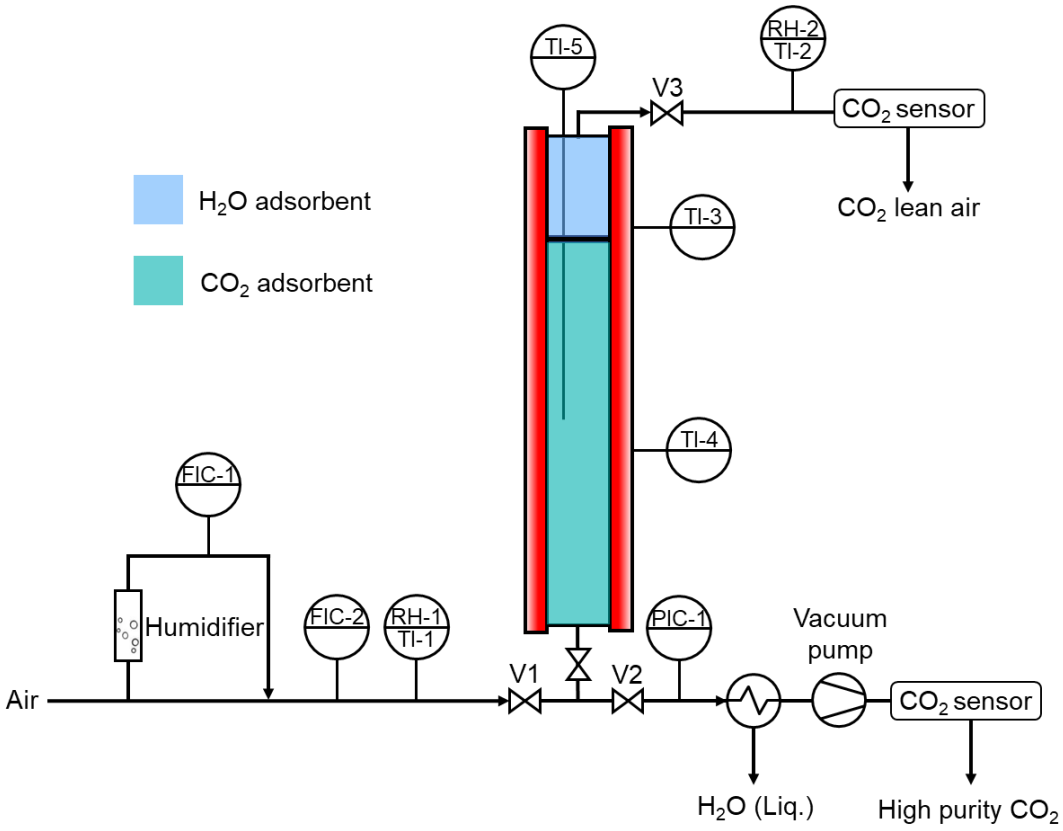

Figure 5.1 Experimental setup for performing breakthrough experiments and DAC cycles.

During the adsorption step, valves V1 and V3 were kept open, while V2 was closed. For performing breakthrough experiments, the CO_2 adsorbent volume was 200 mL, while the silica gel layer was packed with glass beads. Compressed air containing 320-340 ppm CO_2 and 7% relative humidity was used as the feed gas with a flow rate of 30 L/min. The outlet CO_2 concentrations were monitored by an infrared CO_2 sensor (Dynament, 0-1000 ppm). The feed and outlet relative humidity were continuously recorded by two humidity sensors (Ningbo Keshun KS-SHT and Vaisala HMT338). A humidifier at 25 °C controlled the relative humidity of the feed air introduced into the column.

The experimental procedures for conducting VPTVSA are similar to those in Chapters 3 and 4, with the difference being the use of a vacuum pump to reduce the pressure inside the column during regeneration, as shown in Figure 5.1. For conducting DAC cycles based on the VPTVSA process, silica gel and PEI-impregnated resin were packed sequentially within one adsorption column. Fresh air with a flow rate of 30 L/min first flowed over the resin, and subsequently over silica gel, for CO_2 and H_2O adsorption. The CO_2 uptake during the adsorption process was calculated based on Equation 3.5 [19].

During the desorption step, valves V1 and V3 were closed, while valve V2 was directly connected to an air-cooled condenser used for water product collection. Heating tapes with a temperature of 80 °C were employed to provide the thermal energy required by adsorbent regeneration. Before heating the column, the air inside the column was evacuated by a vacuum pump to reach the target desorption pressure. As the temperature of the adsorbent increased, the vapors in the product stream were collected as liquid water products by the air-cooled condenser, while the CO_2 product was collected using a syringe to record the product volume profile. The collected CO_2 product was then stored in gas sampling bags and analyzed using a Servomex 1440 gas analyzer. The real-time analysis of CO_2 product purity follows the procedures outlined in Chapter 3. Once the volume profile of desorbed CO_2 is obtained, the CO_2 loading of PEI impregnated resin during the desorption step can be determined. After the desorption process, the adsorption column was purged with fresh air to rapidly decrease the adsorbent temperature and initiate the next adsorption cycle.

5.2.4 Desorption kinetics model

The CO_2 desorption behavior of PEI-impregnated resins with different PEI loadings was investigated using a flowing N_2 atmosphere at 52-60 °C through thermogravimetric analysis with a Mettler Toledo TGA/DSC 1. Before conducting desorption, the samples were treated with dry air at 30 °C until reaching CO_2 adsorption equilibrium. The linear driving force (LDF) model was used to simulate the CO_2 desorption kinetics of 33PEI/HP20 and 50PEI/HP20, as illustrated by the following equation,

$$\frac{\partial q}{\partial t} = k_{LDF}(q_e - q) \tag{5.1}$$

where q is the CO_2 loading of PEI-impregnated resins, q_e is the equilibrium CO_2 uptake at corresponding desorption conditions, t is the desorption time, k_{LDF} is the mass transfer coefficient of CO_2. As the desorption was performed under N_2 atmosphere, q_e was assumed

to be 0 during the calculation. Then the CO_2 loading could be calculated by Equation 5.2, where q_0 is the CO_2 uptake realized in the adsorption process using dry air at 30 °C.

$$\frac{q}{q_0} = e^{-tk_{LDF}} \tag{5.2}$$

5.2.5 Analysis of energy consumption and exergy demand

The energy consumption (Q) for adsorbent regeneration in the VPTVSA process comprises the sensible heat (Q_s) required to raise the adsorbent temperatures, the latent heat (Q_l) related to CO_2 and water desorption, and the work (W_v) needed to perform evacuation, as illustrated by Equation 5.3, where $m_{CO_2}^{(des)}$ is the mass of CO_2 collected during the desorption process.

$$Q = \frac{Q_s + Q_l + W_v}{m_{CO_2}^{(des)}} \tag{5.3}$$

The required sensible heat is calculated using the following equation,

$$Q_s = \Delta T(m_{resin}C_{p,resin} + m_{silica}C_{p,silica} + m_{CO_2}^{(ads)}C_{p,CO_2} + m_{H_2O}^{(ads)}C_{p,H_2O}) \tag{5.4}$$

where ΔT represents the temperature change during the desorption process. The terms m_{resin}, m_{silica}, $m_{CO_2}^{(ads)}$ and $m_{H_2O}^{(ads)}$ denote the mass of PEI impregnated resin, silica gel, adsorbed CO_2 and adsorbed water within the column, respectively. $C_{p,resin}$, $C_{p,silica}$, C_{p,CO_2} and C_{p,H_2O} indicate the specific heat capacities of PEI impregnated resin, silica gel, adsorbed CO_2 and adsorbed water within the column, respectively.

Latent heat was assessed using Equation 5.5, where Q_{des,CO_2} and Q_{des,H_2O} represent the heat required for CO_2 and water desorption, respectively. $n_{CO_2}^{(des)}$ and $n_{H_2O}^{(des)}$ denote the moles of collected CO_2 and water products during the desorption process. h_{des,CO_2} and h_{des,H_2O} are heat of desorption for CO_2 and water.

$$Q_l = Q_{des,CO_2} + Q_{des,H_2O} = n_{CO_2}^{(des)}h_{des,CO_2} + n_{H_2O}^{(des)}h_{des,H_2O} \tag{5.5}$$

During the pre-evacuation and desorption processes, a vacuum pump was employed to reach the desired desorption pressure (P_{de}, 10 kPa). The work related to evacuation (W_v) is determined using the following equation.

$$W_v = \frac{nRT_{amb}\gamma}{\eta(\gamma - 1)}\left(\frac{P_{amb}}{P_{de}}^{\left(\frac{\gamma-1}{r}\right)} - 1\right) \tag{5.6}$$

where γ represents the specific heat ratio, η is the efficiency for evacuation, T_{amb} is the ambient temperature, P_{amb} is the ambient pressure.

The specific exergy demand (E) is expressed by:

$$E = \frac{1}{m_{CO_2}^{(des)}}[(Q_s + Q_l)\left(1 - \frac{T_{amb}}{T_{hs}}\right) + W_v] \quad (5.7)$$

where T_{hs} represents the temperature of the heat source or the heating tape, and is 80 °C in this chapter.

5.3 Results and discussion

5.3.1 Working principle of vapor-promoted TVSA

In vapor-promoted TVSA process, a double-layered adsorption column, sequentially packed with AIS and water adsorbents, is used to conduct DAC. Along with CO_2 capture in the solid amine layer, a commercial type A silica gel is used in the water adsorbent layer to harvest atmospheric moisture. Compared with the conventional TVSA process, the water adsorbed on silica gel can be released as vapors to provide a driving force for CO_2 desorption, at temperatures ranging from 50-70 °C under a desorption pressure of 10-20 kPa [20].

The DAC cycles based on the vapor-promoted TVSA process are described in Figure 5.2. In the adsorption stage, atmospheric CO_2 and water are concurrently adsorbed in the double-layer column. Then, a vacuum pump is used to pre-evacuate the air inside the column and achieve the desired desorption pressure. During the desorption, by providing thermal energy to raise the adsorbent temperature, low-temperature vapors are released under vacuum and purge the solid amine layer. The combination of vacuum conditions and *in situ* vapor purge substantially reduces the carbon dioxide partial pressure inside the column, promoting the regeneration of AIS by lowering the equilibrium sorption capacity. The vacuum pump removes the generated CO_2 and vapors from the column to maintain the desorption pressure. High-purity CO_2 can be obtained by condensing the vapors in the product stream. After collecting the products, fresh air is introduced to lower the adsorbent temperature and initiate a new adsorption cycle. Compared with the conventional TVSA process, this novel VPTVSA process provides an additional reduction in CO_2 partial pressure by *in situ* vapor purge, showing great potential for prolonging the lifetime of AIS by reducing the regeneration temperature.

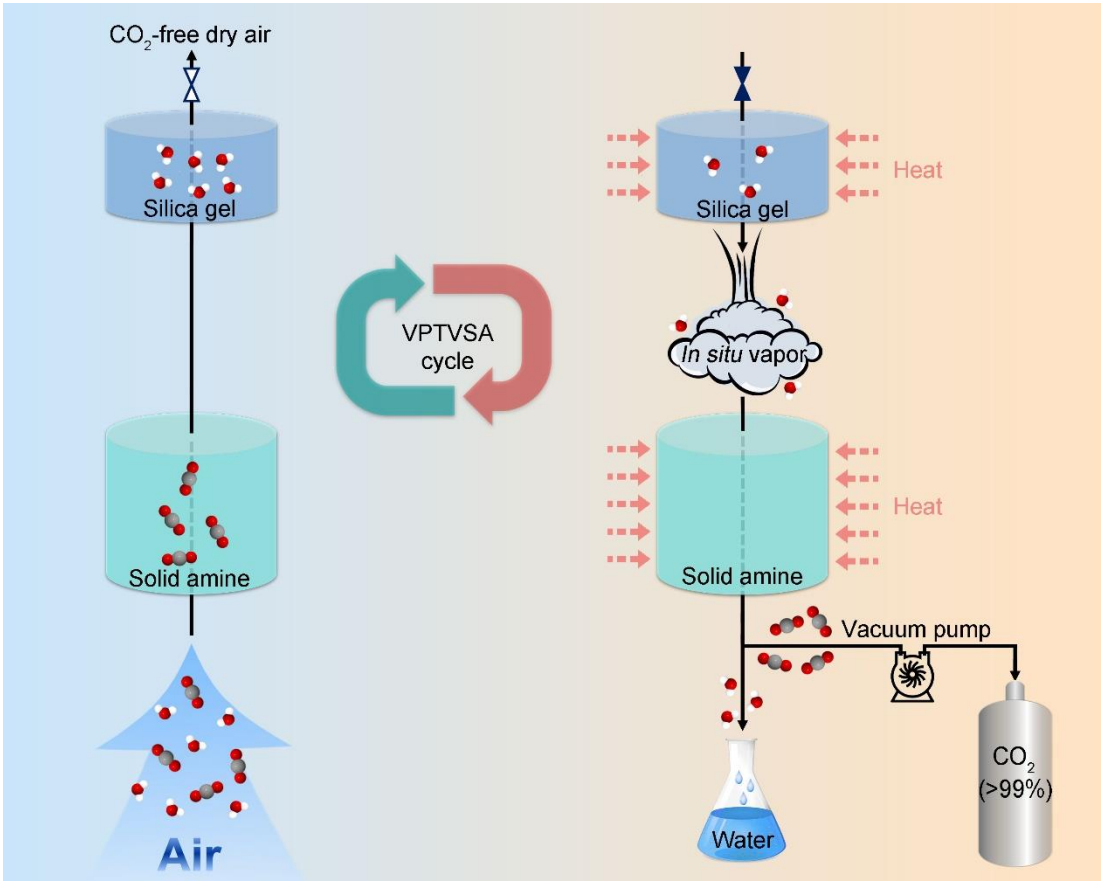

Figure 5.2 Working principle of vapor-promoted temperature-vacuum swing adsorption (VPTVSA) process for DAC.

A double-layered adsorption column, packed with solid anime and silica gel, captures atmospheric CO_2 and H_2O concurrently. During regeneration, the water adsorbent layer generates *in situ* vapor at low temperatures under vacuum to purge the solid amine layer for desorbing CO_2.

5.3.2 Adsorption properties

For preparing amine-impregnated sorbents used in DAC, branched PEI was selected as the amine-containing species for impregnation because of the large amine content and low volatility [21]. HP20 resin with both large pore size and volume was used as the support material [22]. CO_2 adsorbents with PEI loadings of 33 and 50 wt%, namely 33PEI/HP20 and 50PEI/HP20, were prepared by the physical impregnation method. The prepared 33PEI/HP20 is presented in Figure 5.3.

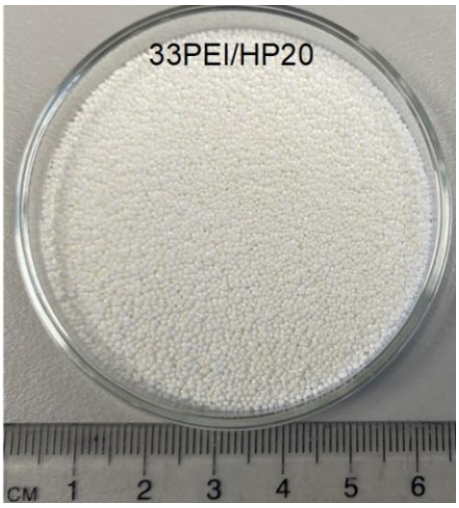

Figure 5.3 Physical appearance of a synthesized PEI-impregnated resin (33PEI/HP20).

Carbon dioxide adsorption isotherms of PEI-impregnated resins were analyzed at different temperatures and fitted by Dual-site Langmuir (DL) adsorption model (Equations 3.1-3.3), as shown in Figure 5.4 [23].

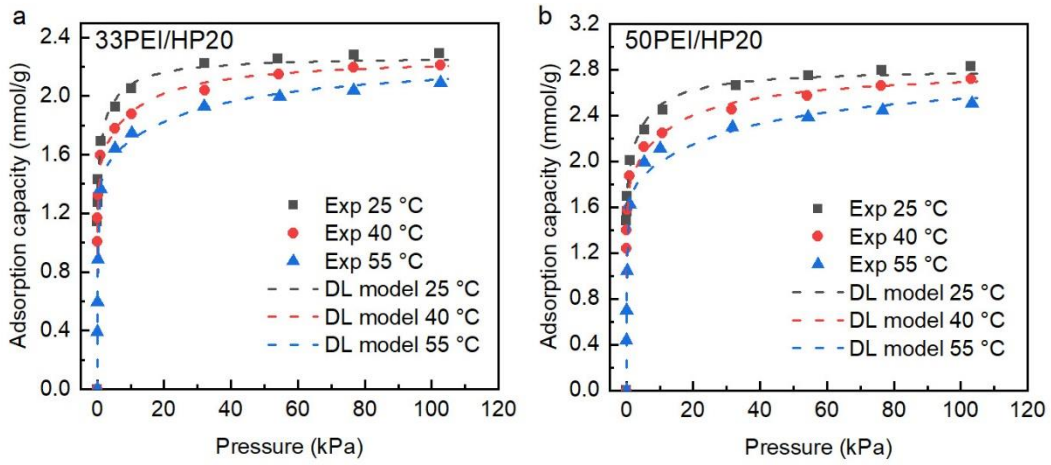

Figure 5.4 Experimental CO_2 adsorption isotherms of (a) 33PEI/HP20 and (b) 50PEI/HP20 at 25, 40 and 55 °C, fitted to the Dual-site Langmuir model.

The strong affinity between PEI and CO_2 (ΔH_{ads}: −75.3 and −85.0 kJ/mol, Table 5.1) enabled the capture of atmospheric CO_2 with uptakes higher than 1 mmol/g.

Table 5.1 Dual-site Langmuir model parameters of CO_2 adsorption on 33PEI/HP20 and 50PEI/HP20.

Parameter	33PEI/HP20	50PEI/HP20
q_1 (mmol/g)	1.508	1.780
q_2 (mmol/g)	0.762	1.030
$K_{0,1}$ (1/kPa)	8.92×10^{-12}	2.60×10^{-13}
$K_{0,2}$ (1/kPa)	3.87×10^{-11}	4.69×10^{-11}
$-\Delta H_{ads,1}$ (kJ/mol)	75.3	85.0
$-\Delta H_{ads,2}$ (kJ/mol)	56.5	55.2

To assess the conditions required for regeneration, the theoretical working capacities (W_c) of PEI-impregnated resins were determined based on the developed Dual-site Langmuir adsorption model and Equation 3.4. According to Figure 5.5, extremely low CO_2 partial pressures below 2 kPa are required to effectively regenerate 33PEI/HP20 and 50PEI/HP20 at temperatures lower than 80 °C. Thus, conventional TVSA processes may not be suitable for regenerating AIS at low temperatures due to the substantial energy consumption and high capital costs associated with reaching low desorption pressures.

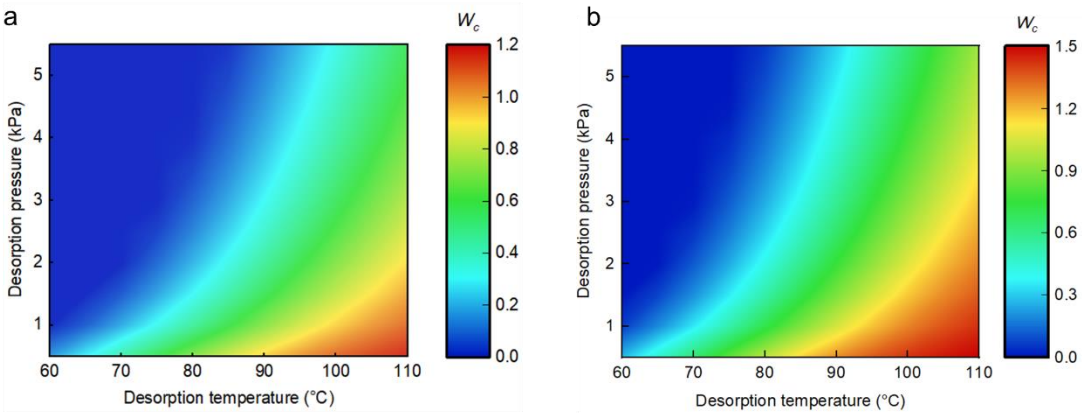

Figure 5.5 Thermodynamic assessment of amine-impregnated sorbent regeneration. (a-b) Calculated CO_2 working capacity (W_c) of (a) 33PEI/HP20 and (b) 50PEI/HP20 in conventional TVSA process at various desorption temperatures and pressures, with fixed adsorption conditions of 25 °C and 400 ppm CO_2.

Before investigating the regeneration of AIS, breakthrough experiments were conducted using fresh air with varying relative humidities to understand the adsorption behaviors of PEI-impregnated sorbents. In Figure 5.6a, 33PEI/HP20 demonstrated excellent CO_2 adsorption kinetics, as evidenced by the steep breakthrough curves with short periods of 5

hours required to achieve adsorption equilibrium. In contrast, 50PEI/HP20 exhibited a significantly longer equilibrium time of 15 hours for CO_2 adsorption (Figure 5.6b). The slower adsorption rate in 50PEI/HP20 can be attributed to mass transfer limitations caused by the pore blockage after PEI impregnation [24-26]. As shown in Figure 5.6c, pore structure analyses revealed a remarkably low surface area of 20.8 m^2/g in 50PEI/HP20, while the support material had excellent porosity with a surface area of 584.6 m^2/g.

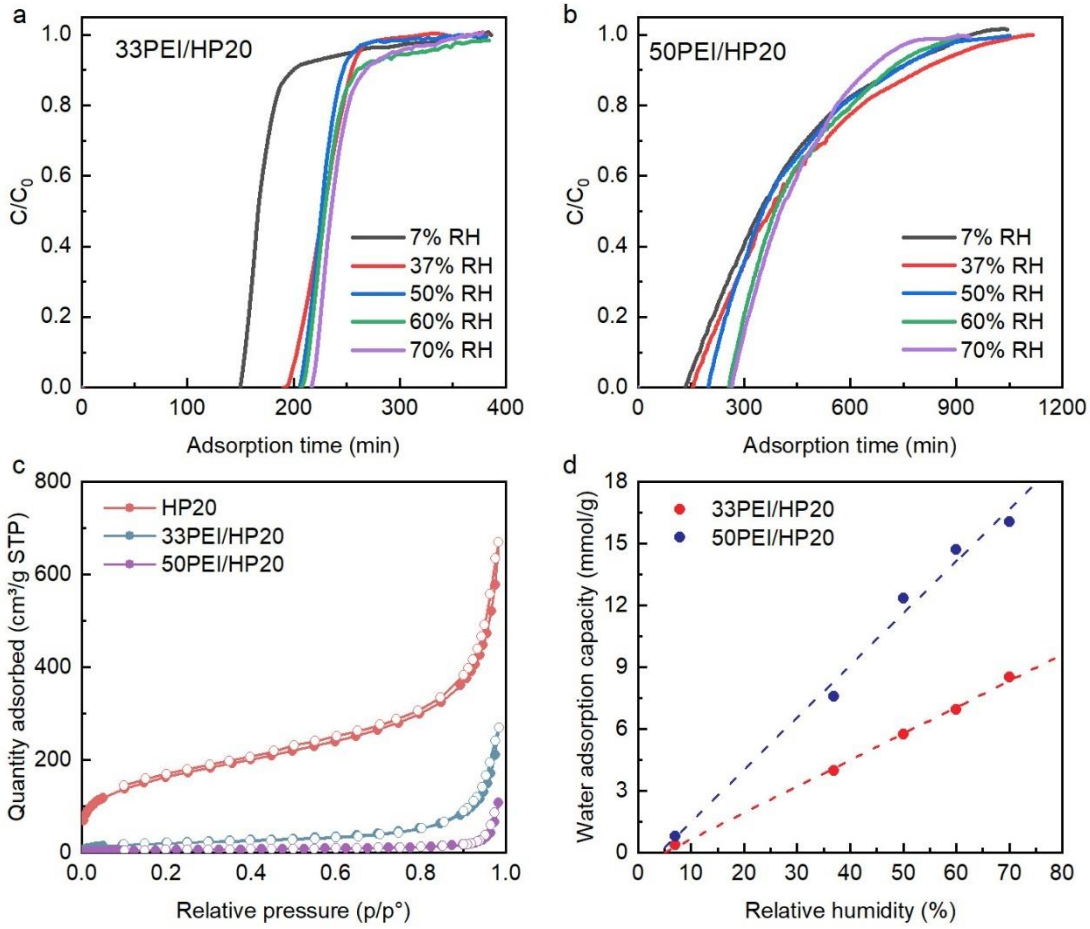

Figure 5.6 Adsorption properties and pore structures of 33PEI/HP20 and 50PEI/HP20. (a-b) CO_2 breakthrough curves of (a) 33PEI/HP20 and (b) 50PEI/HP20 at 25 °C and 330 ppm, with an airflow rate of 30 L/min and an adsorbent volume of 200 mL. (c) N_2 adsorption (closed symbols) and desorption (open symbols) isotherms at 77 K for non-modified HP20 support, 33PEI/HP20, and 50PEI/HP20. (d) Water adsorption capacities of 33PEI/HP20 and 50PEI/HP20 at 25 °C under various relative humidities of the feed air, as determined from the breakthrough experiments.

Notably, conducting adsorption at higher humidities within the relative humidity range of 7-70% could improve the adsorption kinetics of 50PEI/HP20 (Figure 5.6b). Under higher

humidities, the hydrophilic PEI in the sorbents would adsorb more water and reduce the viscosity of amines (Figure 5.6d), promoting the rate of CO_2 diffusion within the PEI phase, particularly for sorbents with high PEI loadings and suffering from pore blockage.

In addition to kinetics, the presence of moisture also showed a positive influence on the water and CO_2 adsorption capacity. Both PEI-impregnated sorbents exhibited linear isotherms for water adsorption due to the introduction of a hydrophilic layer through PEI impregnation, with a higher PEI loading adsorbed more atmospheric water (Figure 5.6d). For CO_2 adsorption, when the RH changed from 7% to 37%, the equilibrium sorption capacity of 33PEI/HP20 and 50PEI/HP20 increased by 25.0% and 11.3%, respectively (Figure 5.7). This moisture-promoted sorption of CO_2 only presented in the low humidity range, while surpassing an RH of 37% did not further noticeably enhance the CO_2 adsorption capacity. Under moderate atmospheric relative humidities of 40-70% at 25 °C, the resins with 33% and 50% PEI loading exhibited impressive CO_2 uptakes of approximately 1.36 and 1.88 mmol/g, respectively.

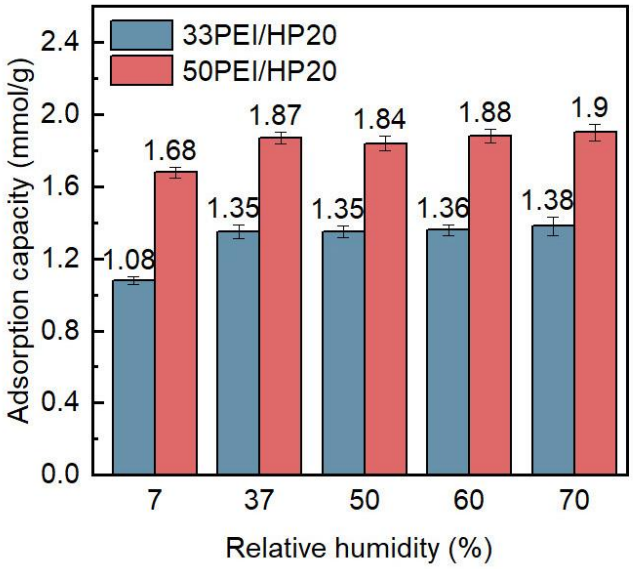

Figure 5.7 CO_2 adsorption capacities of PEI-impregnated resins under different feed air relative humidities at 25 °C and 330 ppm.

Thermal stability studies were carried out on the prepared PEI-impregnated sorbents to provide guidance for choosing regeneration temperatures in practical DAC cycles. Adsorption-desorption cycles were performed using thermogravimetric analysis (TGA), with desorption conducted at different temperatures (70-110 °C) in flowing air. When the regeneration was performed at 70 °C, the adsorption capacities of 33PEI/HP20 remained stable throughout the cyclic experiments (Figure 5.8a). However, 33PEI/HP20 and

50PEI/HP20 experienced reductions of 9.8% and 47.8% in CO_2 adsorption capacity after 12 cycles at 90 °C (Figure 5.8b). Notably, an increased PEI loading compromised the thermal stability of CO_2 adsorbents and led to significant deactivation of amine groups at high temperatures around 90-110 °C, as shown in Figures 5.8b and 5.8c. Therefore, to preserve the adsorption ability of PEI for a long period, it is crucial to employ a regeneration temperature around or even below 70 °C.

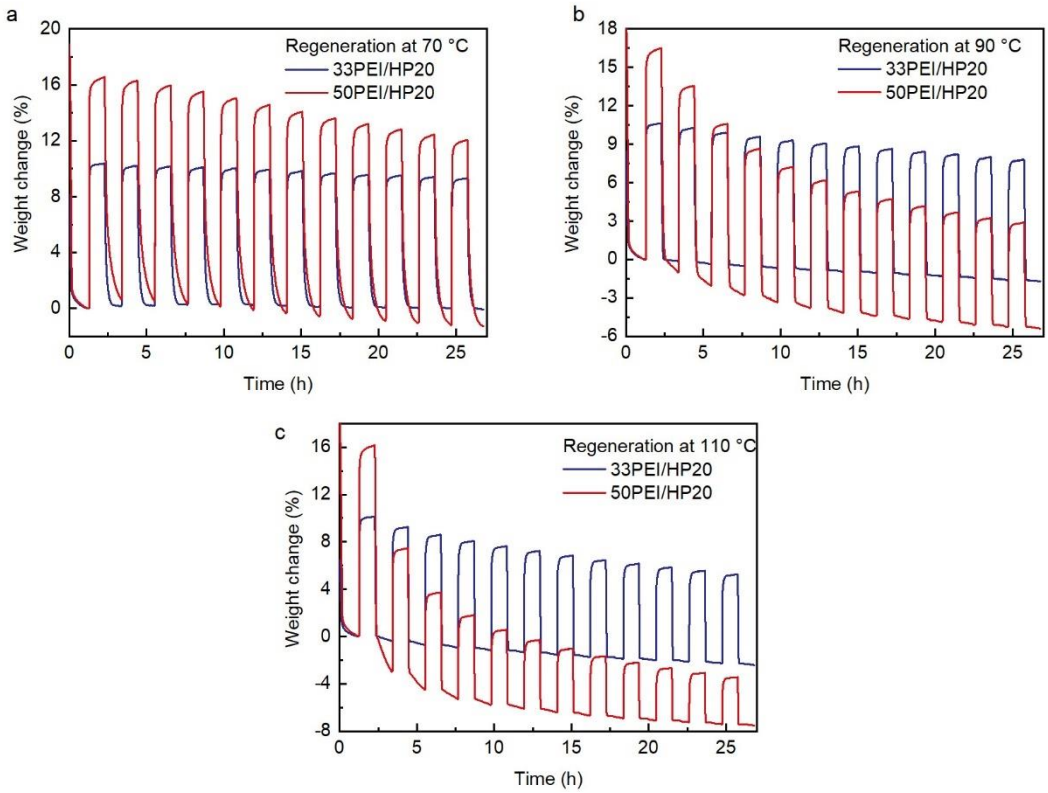

Figure 5.8 Adsorption-desorption profiles of 33PEI/HP20 and 50PEI/HP20 during 12 consecutive temperature swing cycles. Adsorption: 100% CO_2 at 30 °C; Desorption: dry air at (a) 70 °C, (b) 90 °C and (c) 110 °C.

5.3.3 VPTVSA cycles for direct air capture

For realizing the regeneration of PEI-impregnated sorbents at temperatures lower than 70 °C, the VPTVSA process was applied to conduct DAC, with *in situ* vapor purge as an additional driving force for CO_2 desorption. Silica gel and 33PEI/HP20, each with a volume of 200 mL, were packed in one single column to capture atmospheric water and CO_2. Figure 5.9a illustrates the experimental setup used for conducting DAC cycles. In the desorption stage, the pressure inside the column was regulated using a vacuum pump, while the temperature of the

adsorbent bed was raised by a heating tape wrapped around the column wall. The cyclic results in Figure 5.9b illustrated that 33PEI/HP20 could be efficiently regenerated at 10 kPa, with an excellent CO_2 working capacity of 1.12 mmol/g at temperatures around 60 °C. Nearly 80% of the adsorbed CO_2 could be released at such low temperatures, with the combination of evacuation and *in situ* vapor purge for reducing the CO_2 partial pressure. During each adsorption (~ 300 min) and desorption cycle (~ 90 min), approximately 3.5 g of CO_2 could be generated from the air (Figure 5.9d). The produced CO_2 exhibited extremely high purity of over 98%, with water as the main impurity (Figure 5.9c). After purifying with 3A molecular sieve, CO_2 purity could be higher than 99%. The desorbed vapors which served as the purge gas for promoting CO_2 desorption, could also be collected by condensation after leaving the column, with a cyclic water productivity of around 9.5 g (Figure 5.9d).

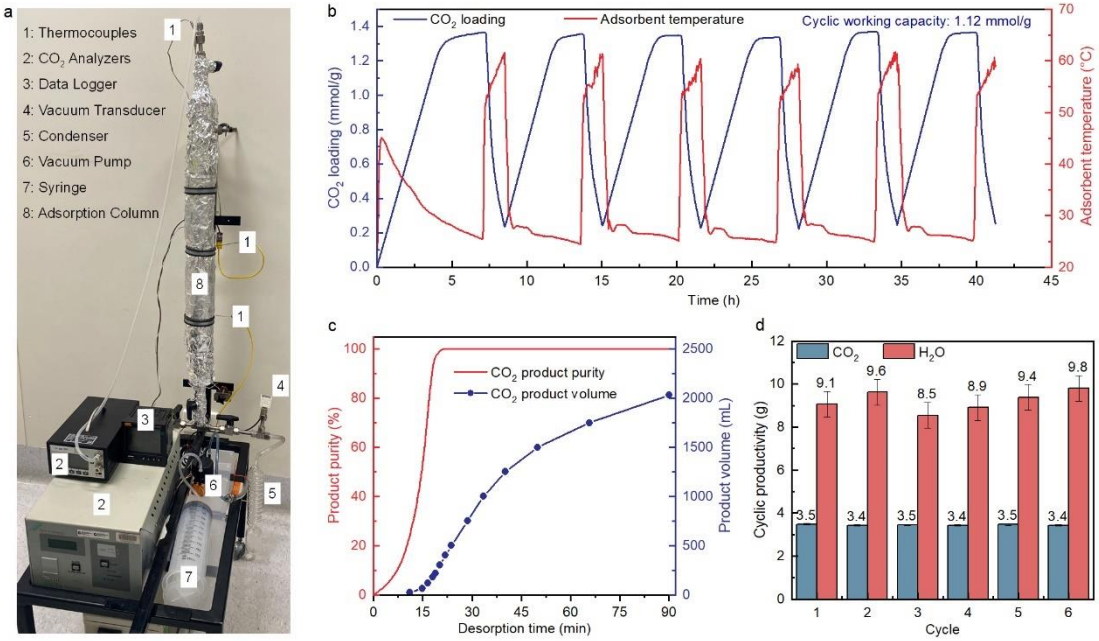

Figure 5.9 Performance of cyclic DAC based on vapor-promoted TVSA.

(a) Experimental setup for the vapor-promoted TVSA process during the regeneration step. (b) CO_2 loading and temperature profiles of 33PEI/HP20 during six adsorption-desorption cycles. Adsorbents: 200 mL 33PEI/HP20 and 200 mL silica gel. Fresh air at 25 °C and 50% RH was used as the feed stream with a flow rate of 30 L/min. The desorption was conducted under a 10 kPa vacuum condition. (c) Real-time CO_2 purity and product volumes during the regeneration step. (d) Cyclic CO_2 and water productivity of the VPTVSA process.

To investigate if this excellent CO_2 productivity can be maintained for a prolonged period, the VPTVSA process was conducted for 45 cycles, lasting 300 hours. As shown in Figure 5.10, the cyclic CO_2 working capacity exhibited stable fluctuations between 1.10 and 1.13 mmol/g

during 45 adsorption-desorption cycles. By contrast, existing regeneration processes, such as steam stripping operated at around 100 °C, led to significant degradations of PEI-impregnated sorbents by 9% over 20 cycles and TEPA-impregnated sorbents by 46% in 30 cycles [27, 28]. The stable DAC performance of VPTVSA could be attributed to the moderate regeneration temperatures (around 60 °C) realized by *in situ* vapor purge.

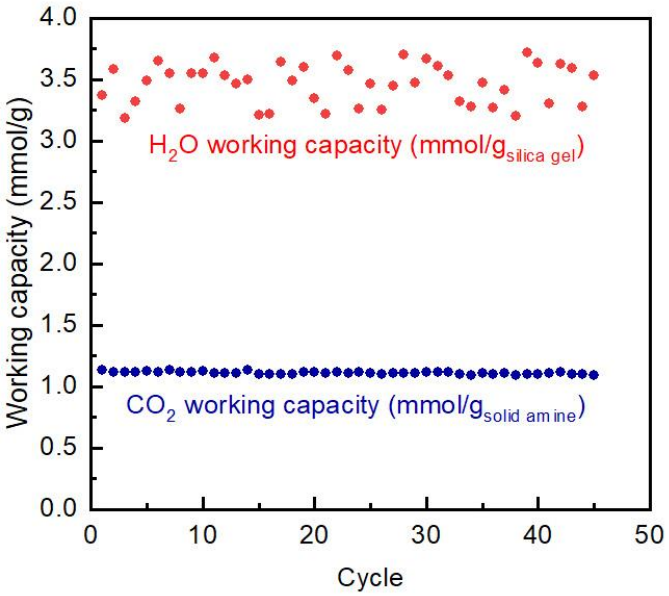

Figure 5.10 Cyclic CO_2 and water working capacities during 45 DAC cycles.

In VPTVSA, the key to the low-temperature regeneration of PEI-impregnated sorbents is the *in situ* vapor purge using water captured from the air. The influence of co-adsorbed water on the regeneration performance was analyzed by performing DAC using 33PEI/HP20 under varying atmospheric relative humidities. As shown in Figure 5.11, using a feed air with 7% RH, nearly no CO_2 could be released even when the adsorbent temperature was elevated to 80 °C. By contrast, the adsorbent could be efficiently regenerated at 62 °C with a high CO_2 working capacity of 1.17 mmol/g when the RH increased to 37%, highlighting the significance of vapors and co-adsorbed water in desorbing CO_2. Increasing the feed air relative humidity to 65% would decrease the regeneration temperature to around 55 °C, as more thermal energy would be allocated to provide latent heat for water desorption. Although this temperature decrease led to a slight reduction in working capacity, it has the potential to extend the lifetime of amines by enabling *in situ* vapor purge at lower temperatures.

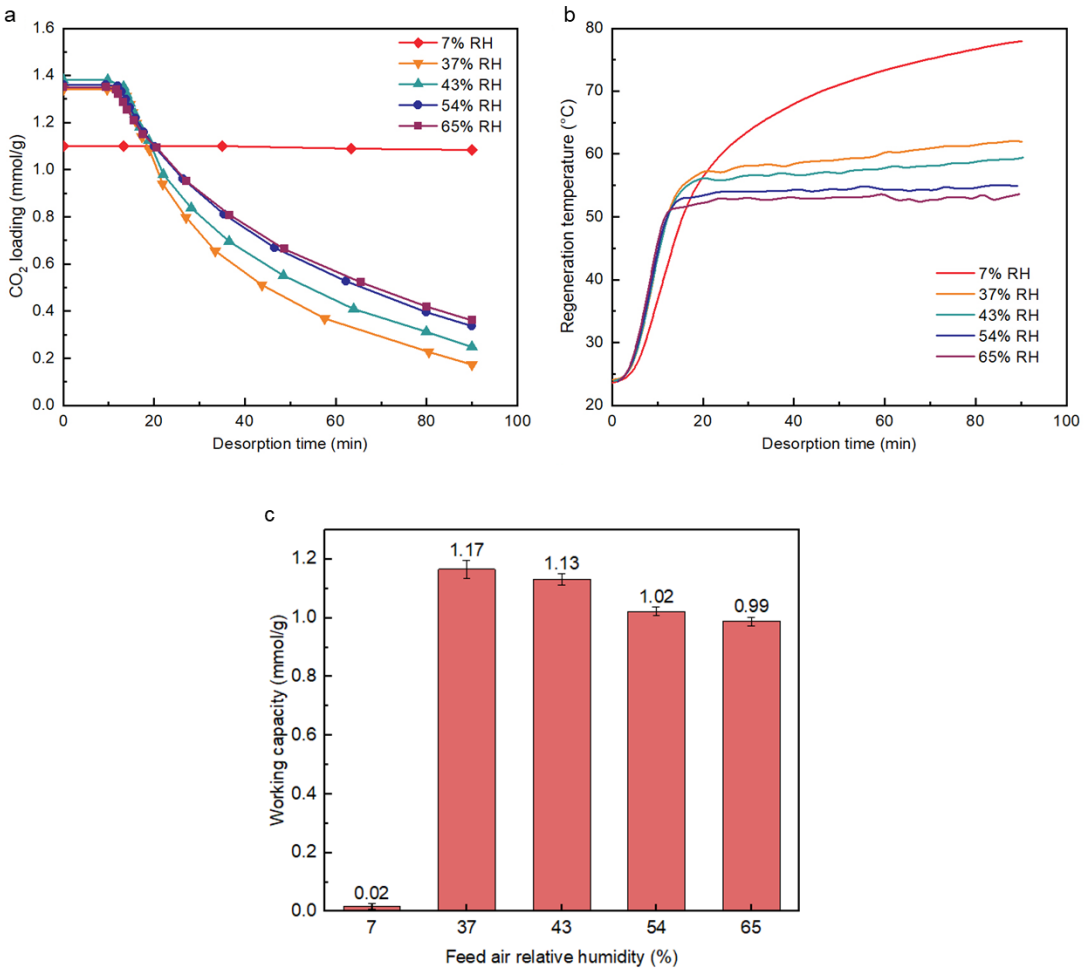

Figure 5.11 The influence of feed air relative humidity on the VPTVSA process.

(a) CO_2 loading profiles and (b) Adsorbent temperature profiles during regeneration under different feed air relative humidities. (c) The influence of feed air relative humidity on the CO_2 working capacity of 33PEI/HP20. Adsorbents: 200 mL 33PEI/HP20 and 200 mL silica gel. Fresh air at 25 °C with RH ranging from 7%-70% was used as the feed stream with a flow rate of 30 L/min. The regeneration was performed at 10 kPa.

As the generation of low-temperature vapors heavily relies on vacuum conditions, the required vacuum levels to perform *in situ* vapor purge and regenerate 33PEI/HP20 were investigated. As shown in Figure 5.12, with the desorption pressure increased from 10 to 18 kPa, a higher temperature of 70.8 °C was required to release co-adsorbed water as vapors to conduct *in situ* purge. Consequently, the reduced vapor quantity weakened the driving force for CO_2 desorption, leading to a significant decrease in the working capacity from 1.15 to 0.59 mmol/g (Figure 5.12c). Therefore, in the VPTVSA process, a desorption pressure below 18 kPa is required to ensure an adequate supply of low-temperature vapors and maintain a desorption temperature below 70 °C.

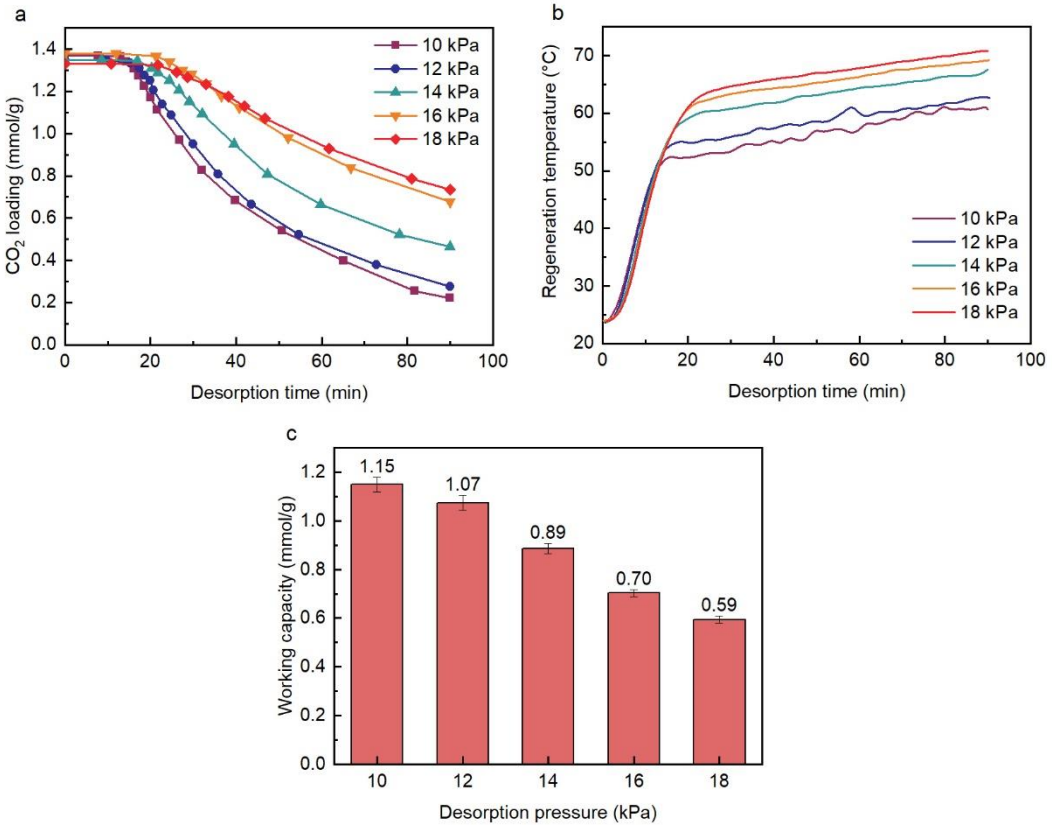

Figure 5.12 (a) CO_2 loading profiles, (b) regeneration temperature profiles and (c) CO_2 working capacity of 33PEI/HP20 during regeneration under different desorption pressures.

Adsorbents: 200 mL 33PEI/HP20 and 200 mL silica gel. Fresh air at 25 °C and 50% RH was used as the feed stream with a flow rate of 30 L/min.

In the above process, a sorbent with 33% PEI loading was primarily used for DAC. Although the optimum PEI loading is determined by the pore volume and pore diameter distribution, PEI loadings were always higher than 33%, sometimes reaching 50% in published reports. Thus, the feasibility of employing 50PEI/HP20 in the VPTVSA process was also assessed in this section (Figure 5.13). The regeneration was performed at low temperatures ranging from 56 to 66 °C, depending on the desorption pressure. At 10 kPa, the sorbent exhibited a working capacity of 0.84 mmol/g, indicating that 45.6% of the adsorbed CO_2 was released with *in situ* vapor purge. Increasing the desorption pressure significantly reduced the amount of CO_2 desorbed, resulting in a working capacity of 0.58 mmol/g at 18 kPa. Compared with 33PEI/HP20, the regeneration of 50PEI/HP20 was more challenging, leading to a 27% lower working capacity at 10 kPa.

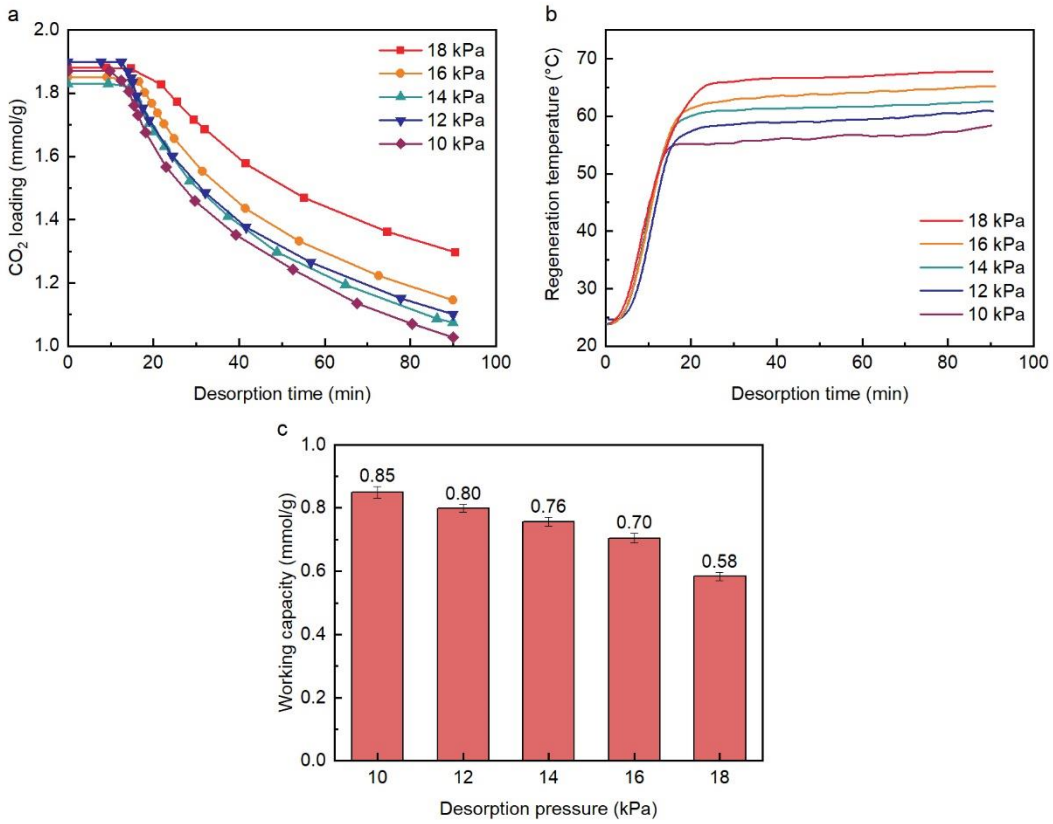

Figure 5.13 (a) CO_2 loading profiles, (b) regeneration temperature profiles and (c) CO_2 working capacity of 50PEI/HP20 during regeneration under different desorption pressures.

Adsorbents: 200 mL 50PEI/HP20 and 200 mL silica gel. Fresh air at 25 °C and 50% RH was used as the feed stream with a flow rate of 30 L/min.

Thermogravimetric analysis was conducted under flowing N_2 to understand the regeneration behavior and desorption kinetics of sorbents with different PEI loadings. A linear driving force (LDF) model was used to simulate the CO_2 loading profiles during the desorption process at different regeneration temperatures (Figures 5.14a and 5.14b). For both sorbents, elevating the regeneration temperature improved desorption kinetics and the mass transfer coefficient of CO_2 (Figure 5.14c). At 60 °C, increasing the PEI loading from 33% to 50% resulted in a substantial decrease in the mass transfer coefficient from 0.054 to 0.019 /min due to the reduced porosity, significantly hindering the release of adsorbed CO_2. Thus, when developing new types of amine-impregnated sorbents, it is important to control the amine loading, considering not only the thermodynamic adsorption capacity but also the kinetic behavior of the sorbent. Using HP20 as the support for PEI impregnation, a PEI loading of 33% is more suitable for the VPTVSA process compared with a 50% loading due to the better kinetics and higher working capacity achieved under the same desorption conditions.

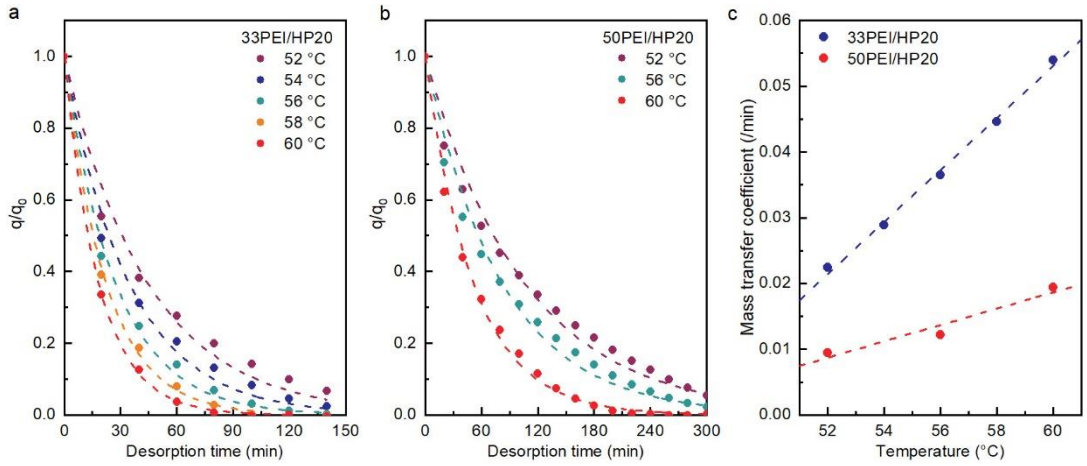

Figure 5.14 CO_2 desorption kinetics analysis for PEI-impregnated resins with different PEI loadings.

(a-b) Regeneration of 33PEI/HP20 and 50PEI/HP20 using N_2 at temperatures ranging from 52 to 60 °C, after treating in air atmosphere with 400 ppm CO_2 at 30 °C. Dashed lines are results simulated from the linear driving force (LDF) model. q represents the CO_2 loading on PEI-impregnated resins, while q_0 is the initial CO_2 loading prior to the desorption process. (c) The mass transfer coefficients for CO_2 desorption in the LDF model at various regeneration temperatures.

5.3.4 VPTVSA with different adsorbent volume fractions

To further optimize the regeneration of 33PEI/HP20, the effect of adsorbent volume fraction on the VPTVSA process was analyzed. Different amounts of silica gel and resin were used with a fixed bed volume of 400 mL, with the DAC test without silica gel representing the conventional TVSA process without *in situ* vapor purge (Figure 5.15).

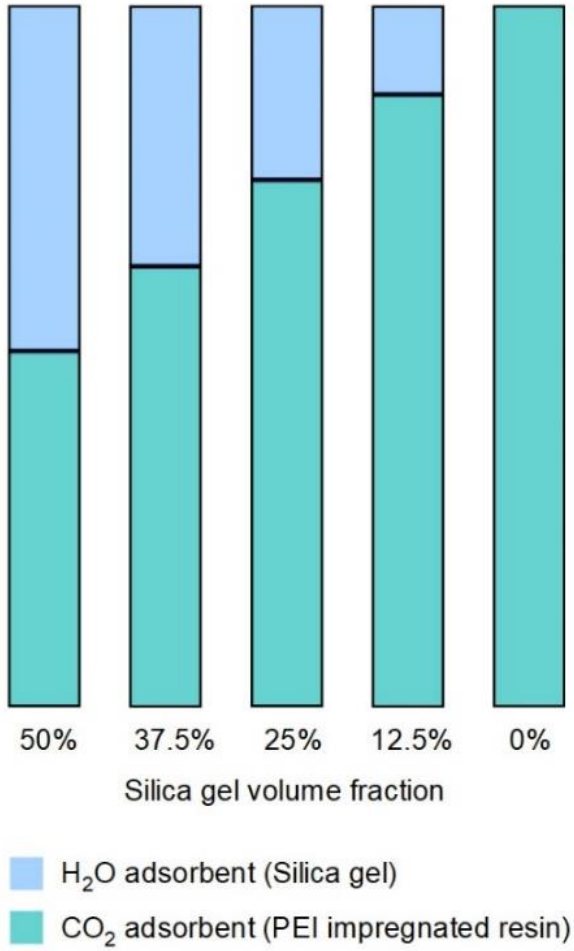

Figure 5.15 Schematic diagram illustrating different adsorbent volume fractions applied in VPTVSA.

As shown in Figure 5.16, at a silica gel volume fraction of 37.5%, the cyclic working capacity reached a peak value of 1.19 mmol/g, releasing 88% of the adsorbed CO_2 from 33PEI/HP20 at 61 °C. By contrast, conventional TVSA (without silica gel) achieved a significantly lower working capacity of 0.29 mmol/g (Figures 5.16a and 5.16c), releasing only 22% of the adsorbed CO_2 due to insufficient vapors for reducing carbon dioxide partial pressure. Additionally, the application of silica gel also increased water productivity, with a single VPTVSA cycle capable of producing 10.5 g of water using 200 mL of silica gel (Figure 5.16d). It is noteworthy that only a small portion (< 33%) of the co-adsorbed water is released as vapors and condensed as water products during the *in situ* purge.

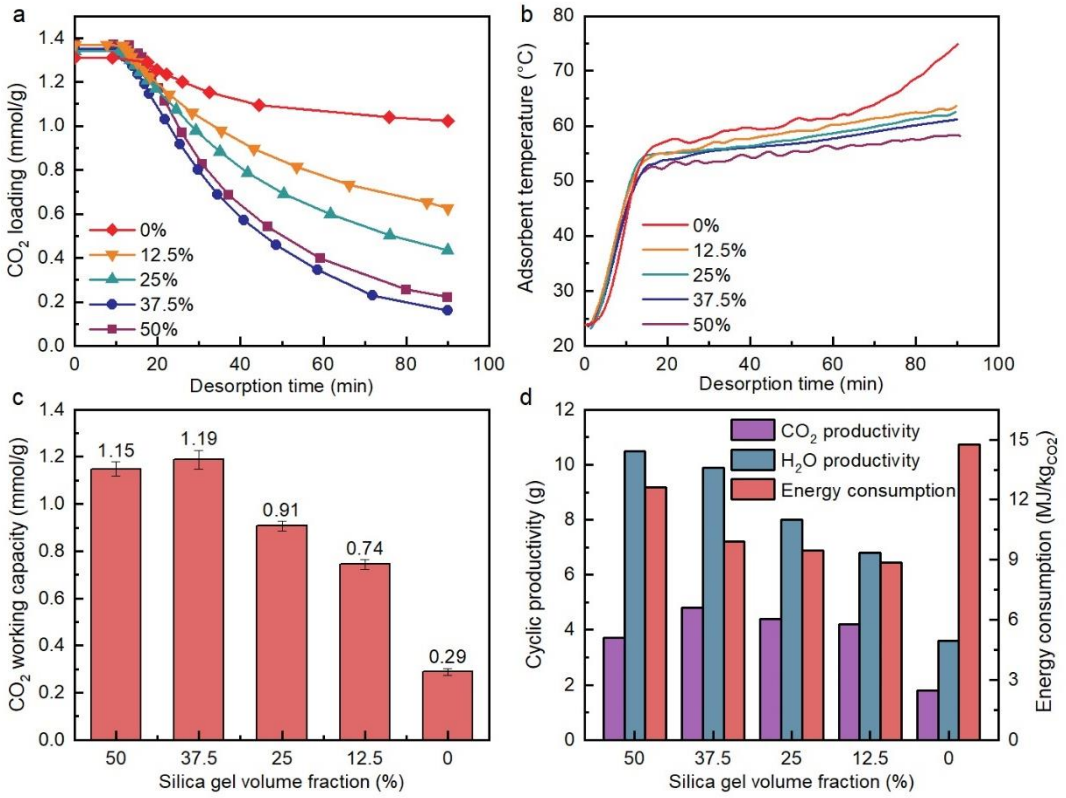

Figure 5.16 Performance of the VPTVSA process with different silica gel volume fractions.

Fresh air at 25 °C and 40% RH was used as the feed stream with a flow rate of 30 L/min. The desorption was conducted at 10 kPa. The double-layered bed volume was fixed at 400 mL. When the silica gel volume fraction is 0, the process is equivalent to the conventional TVSA. (a) CO_2 loading profiles during desorption at various silica gel volume fractions. (b) Temperature profiles of 33PEI/HP20 during regeneration at different silica gel volume fractions. (c) CO_2 working capacity of 33PEI/HP20 with different silica gel volume fractions. (d) Cyclic CO_2 and water productivity, along with the energy consumption in the desorption process.

To assess whether the generation of low-temperature vapors introduces an additional energy penalty, the energy consumption for adsorbent regeneration in the VPTVSA process was analyzed (Figures 5.16d and 5.17). The parameters used for evaluating energy consumption were listed in Table 5.2.

Table 5.2 Parameters used for evaluating energy consumption and exergy demand of VPTVSA process.

Parameter	Value
T_{amb} (°C)	25
T_{hs} (°C)	80
η	0.75
P_{amb} (kPa)	100
P_{de} (kPa)	10
$C_{p,resin}$ (J/kg·K)	1500 [29, 30]
$C_{p,silica}$ (J/kg·K)	921 [31]
C_{p,CO_2} (J/kg·K)	2000 [32]
C_{p,H_2O} (J/kg·K)	4184
h_{des,CO_2} (kJ/mol)	75.3
h_{des,H_2O} (kJ/mol)	44.0 [33]

The energy demand was categorized into sensible heat (Q_s) required to raise the temperatures, the latent heat (Q_l) associated with CO_2 and water desorption, and the work (W_v) needed for evacuation (Figure 5.17). This VPTVSA process demonstrated a total energy consumption of 8.8-12.6 MJ/kg_{CO2} for adsorbent regeneration, while the system with 12.5% silica gel volume fraction exhibited the lowest energy consumption. Thus, the driving force for CO_2 desorption can be significantly improved by incorporating a small volume fraction of silica gel inside the column. In the VPTVSA process, the majority of the energy (approximately 65%) was used to provide the latent heat required for the desorption of carbon dioxide and water, with only a small amount of electrical energy (0.3-0.4 MJ/kg_{CO2}) being used for evacuation (Figure 5.17). Despite the additional energy needed for vapor generation, the energy consumption of the VPTVSA process remained considerably lower than that of TVSA processes (14.7 MJ/kg_{CO2}) due to the much higher CO_2 working capacities realized by *in situ* vapor purge.

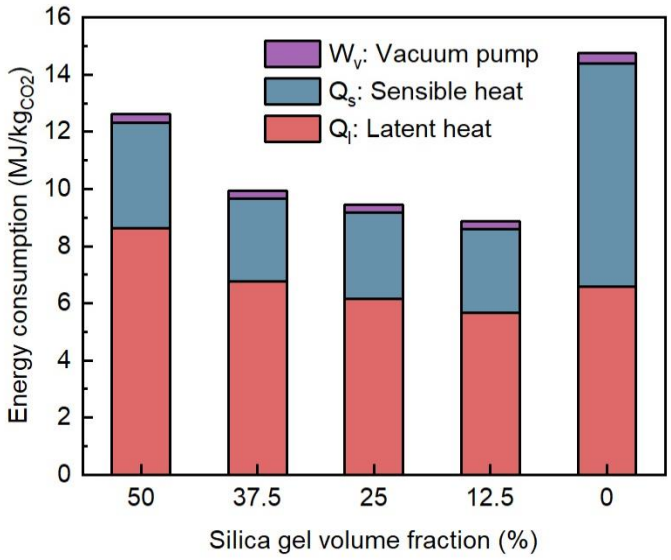

Figure 5.17 The breakdown of energy consumption for providing sensible heat (Q_s), latent heat (Q_l), and evacuation (W_v) in the desorption stage of the VPTVSA process. The process without silica gel is equivalent to the conventional TVSA.

As the VPTVSA process significantly decreased the required temperatures for releasing CO2, the minimum work (exergy) requirement for adsorbent regeneration is expected to be reduced. While the theoretical minimum work required to produce 99% CO_2 from the atmosphere is approximately 0.45 MJ/kg$_{CO2}$ [34], the VPTVSA process realized an exergy demand for adsorbent regeneration as low as 1.62 MJ/kg$_{CO2}$ (Figures 5.18a and 5.18b) with a silica gel volume fraction of 12.5%. Around 54% of the work was used to provide the thermal energy required by the desorption of CO_2 and water (Figure 5.18c). Reported DAC processes such as TVSA and steam-assisted TVSA (STVSA) typically necessitate a heat source above 100 °C to supply the thermal energy for desorption, resulting in significantly higher minimum work requirements ranging from 2.0 to 3.2 MJ/kg$_{CO2}$ (Figure 5.18b) [13, 15, 35]. In addition, compared with STVSA with an external steam purge, the present VPTVSA process has the ability to produce water as a byproduct, without the requirement of an additional water supply and a corresponding steam boiler to provide the purge gases. The low exergy demand of the VPTVSA process is attributed to the exceptional working capacity (0.7-1.2 mmol/g) at low desorption temperatures. Therefore, the VPTVSA process not only improves the adsorbent lifespan by reducing the desorption temperature but also lowers the exergy demand for adsorbent regeneration.

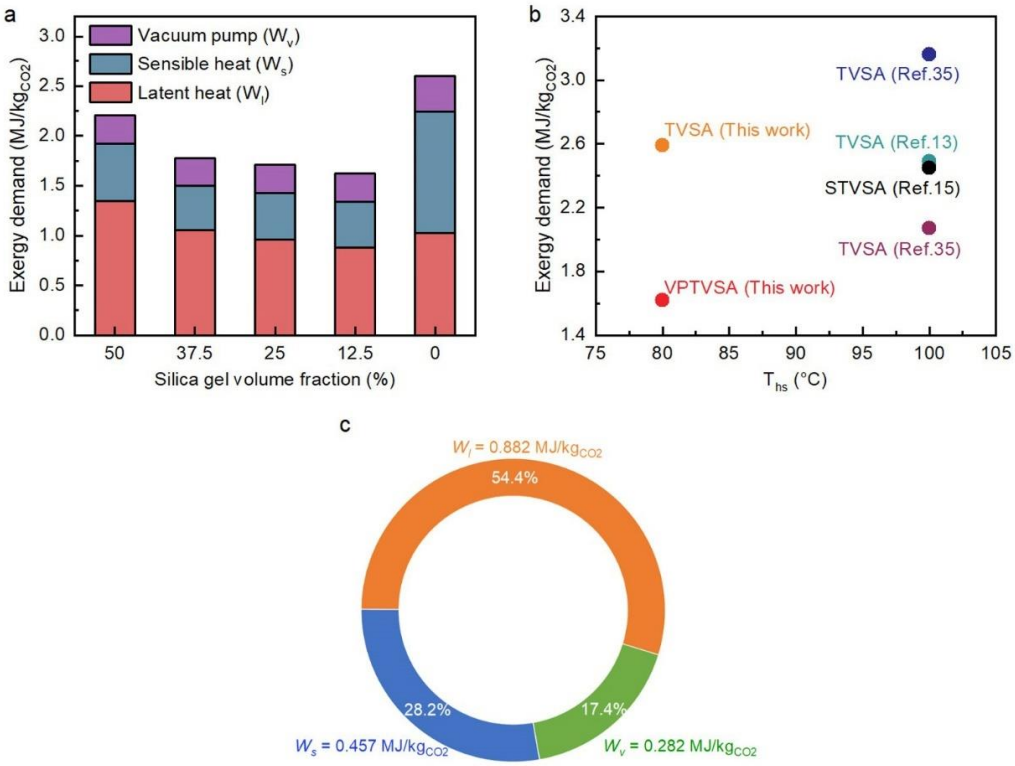

Figure 5.18 Analysis of minimum work requirements for regenerating 33PEI/HP20 in the VPTVSA process.

(a) Breakdown of exergy demand for adsorbent regeneration in the VPTVSA process with different silica gel volume fractions. (b) Comparative analysis of exergy demand for the regeneration of solid amine sorbents using various processes. T_{hs} represents the temperature of the heat source used for providing thermal energy. (c) Exergy breakdown illustrating the work requirements for providing sensible heat (W_s), latent heat (W_l), and evacuation (W_v) during the regeneration step with a silica gel volume fraction of 12.5%.

5.4 Conclusions

Although the VPD process has demonstrated remarkable efficiency in regenerating amine-based sorbents for CO_2 capture, its reliance on high temperatures exceeding 100 °C poses challenges, leading to the deactivation of impregnated amines. To address this issue, a vapor-promoted temperature-vacuum swing adsorption (VPTVSA) process was developed in this section. This approach involved *in situ* generation of low-temperature vapors under vacuum conditions using water harvested from the air. PEI-impregnated HP20 resins with varying amine loadings were employed as CO_2 capture materials. Under vacuum conditions of 10 kPa, the temperature required for *in situ* vapor generation was significantly reduced to

60 °C, resulting in the release of over 80% of the absorbed CO_2 from the 33PEI/HP20 sorbent. Throughout 45 cycles, the process maintained a consistently stable CO_2 working capacity of approximately 1.13 mmol/g. The influence of PEI loading on both adsorption thermodynamics and kinetics was found to be significant. Although the sorbent 50PEI/HP20 with a higher PEI loading of 50% exhibited greater CO_2 adsorption capacity, its working capacity achieved through VPTVSA was lower than that of 33PEI/HP20 due to limited desorption kinetics. The conventional TVSA process, conducted without the use of silica gel, was also employed for DAC and compared with the VPTVSA process. By incorporating silica gel at a volume fraction of only 12.5%, an increase in CO_2 working capacity from 0.29 to 0.74 mmol/g was observed, leading to a 40% reduction in overall energy required for regeneration. Furthermore, owing to the lower regeneration temperature in the VPTVSA process, the sorbent regeneration required only a low exergy demand of 1.62 MJ/kg_{CO2}, significantly lower than reported processes. This low-temperature regeneration approach offers a promising means to maintain amine adsorption performance during DAC cycles, potentially enhancing economic feasibility by reducing energy penalties and extending amine lifetimes.

5.5 References

[1] A. Goeppert, M. Czaun, R.B. May, G.K.S. Prakash, G.A. Olah, S.R. Narayanan, Carbon dioxide capture from the air using a polyamine based regenerable solid adsorbent, J. Am. Chem. Soc. 133 (2011) 20164-20167.

[2] L.A. Darunte, A.D. Oetomo, K.S. Walton, D.S. Sholl, C.W. Jones, Direct air capture of CO_2 using amine functionalized MIL-101(Cr), ACS Sustain. Chem. Eng. 4 (2016) 5761-5768.

[3] A. Goeppert, S. Meth, G.K.S. Prakash, G.A. Olah, Nanostructured silica as a support for regenerable high-capacity organoamine-based CO_2 sorbents, Energ. Environ. Sci. 3 (2010) 1949.

[4] G. Qi, Y. Wang, L. Estevez, X. Duan, N. Anako, A.A. Park, W. Li, C.W. Jones, E.P. Giannelis, High efficiency nanocomposite sorbents for CO_2 capture based on amine-functionalized mesoporous capsules, Energy Environ. Sci. 4 (2011) 444-452.

[5] Y. Miao, Y. Wang, B. Ge, Z. He, X. Zhu, J. Li, S. Liu, L. Yu, Mixed diethanolamine and polyethyleneimine with enhanced CO_2 capture capacity from air, Advanced Science 10 (2023) 1-8.

[6] Y. Miao, Y. Wang, X. Zhu, W. Chen, Z. He, L. Yu, J. Li, Minimizing the effect of oxygen on supported polyamine for direct air capture, Sep. Purif. Technol. 298 (2022) 121583.

[7] Y. Meng, J. Jiang, A. Aihemaiti, T. Ju, Y. Gao, J. Liu, S. Han, Feasibility of CO_2 capture from O_2-containing flue gas using a Poly(ethylenimine)-functionalized sorbent:

Oxidative stability in long-term operation, ACS Appl. Mater. Inter. 11 (2019) 33781-33791.

[8] M. Jahandar Lashaki, S. Khiavi, A. Sayari, Stability of amine-functionalized CO_2 adsorbents: a multifaceted puzzle, Chem. Soc. Rev. 48 (2019) 3320-3405.

[9] K. Min, W. Choi, C. Kim, M. Choi, Oxidation-stable amine-containing adsorbents for carbon dioxide capture, Nat. Commun. 9 (2018) 1-7.

[10] A. Goeppert, H. Zhang, R. Sen, H. Dang, G.K.S. Prakash, Oxidation‐resistant, cost‐effective epoxide‐modified polyamine adsorbents for CO_2 capture from various sources including air, ChemSusChem 12 (2019) 1712-1723.

[11] Q. Yu, J.D.L.P. Delgado, R. Veneman, D.W.F. Brilman, Stability of a benzyl amine based CO_2 capture adsorbent in view of regeneration strategies, Ind. Eng. Chem. Res. 56 (2017) 3259-3269.

[12] J.A. Wurzbacher, C. Gebald, A. Steinfeld, Separation of CO_2 from air by temperature-vacuum swing adsorption using diamine-functionalized silica gel, Energ. Environ. Sci. 4 (2011) 3584-3592.

[13] J. Young, E. García-Díez, S. Garcia, M. van der Spek, The impact of binary water-CO_2 isotherm models on the optimal performance of sorbent-based direct air capture processes, Energ. Environ. Sci. 14 (2021) 5377-5394.

[14] H. Azarabadi, K.S. Lackner, A sorbent-focused techno-economic analysis of direct air capture, Appl. Energ. 250 (2019) 959-975.

[15] A. Sinha, L.A. Darunte, C.W. Jones, M.J. Realff, Y. Kawajiri, Systems design and economic analysis of direct air capture of CO_2 through temperature vacuum swing adsorption using MIL-101(Cr)-PEI-800 and mmen-Mg_2(dobpdc) MOF adsorbents, Ind. Eng. Chem. Res. 56 (2017) 750-764.

[16] M.A. Sakwa-Novak, C.W. Jones, Steam induced structural changes of a poly(ethylenimine) impregnated γ-Alumina sorbent for CO_2 extraction from ambient air, ACS Appl. Mater. Inter. 6 (2014) 9245-9255.

[17] S. Hammache, J.S. Hoffman, M.L. Gray, D.J. Fauth, B.H. Howard, H.W. Pennline, Comprehensive study of the impact of steam on polyethyleneimine on silica for CO_2 capture, Energ. Fuel. 27 (2013) 6899-6905.

[18] T.C. Drage, A. Arenillas, K.M. Smith, C.E. Snape, Thermal stability of polyethylenimine based carbon dioxide adsorbents and its influence on selection of regeneration strategies, Micropor. Mesopor. Mat. 116 (2008) 504-512.

[19] J.A. Wurzbacher, C. Gebald, N. Piatkowski, A. Steinfeld, Concurrent separation of CO_2 and H_2O from air by a temperature-vacuum swing adsorption/desorption cycle, Environ. Sci. Technol. 46 (2012) 9191-9198.

[20] M. Hamdy, A.A. Askalany, K. Harby, N. Kora, An overview on adsorption cooling systems powered by waste heat from internal combustion engine, Renewable and Sustainable Energy Reviews 51 (2015) 1223-1234.

[21] E.S. Sanz-Pérez, C.R. Murdock, S.A. Didas, C.W. Jones, Direct capture of CO_2 from ambient air, Chem. Rev. 116 (2016) 11840-11876.

[22] Z. Chen, S. Deng, H. Wei, B. Wang, J. Huang, G. Yu, Polyethylenimine-impregnated resin for high CO_2 adsorption: An efficient adsorbent for CO_2 capture from simulated flue gas and ambient air, ACS Appl. Mater. Inter. 5 (2013) 6937-6945.

[23] W.R. Lee, S.Y. Hwang, D.W. Ryu, K.S. Lim, S.S. Han, D. Moon, J. Choi, C.S. Hong, Diamine-functionalized metal‐organic framework: exceptionally high CO_2 capacities from ambient air and flue gas, ultrafast CO_2 uptake rate, and adsorption mechanism, Energ. Environ. Sci. 7 (2014) 744-751.

[24] S. Choi, J.H. Drese, P.M. Eisenberger, C.W. Jones, Application of amine-tethered solid sorbents for direct CO_2 capture from the ambient air, Environ. Sci. Technol. 45 (2011) 2420-2427.

[25] H.T. Kwon, M.A. Sakwa-Novak, S.H. Pang, A.R. Sujan, E.W. Ping, C.W. Jones, Aminopolymer-impregnated hierarchical silica structures: unexpected equivalent CO_2 uptake under simulated air capture and flue gas capture conditions, Chem. Mater. 31 (2019) 5229-5237.

[26] J.A.A. Gibson, A.V. Gromov, S. Brandani, E.E.B. Campbell, The effect of pore structure on the CO_2 adsorption efficiency of polyamine impregnated porous carbons, Micropor. Mesopor. Mat. 208 (2015) 129-139.

[27] M. Isenberg, S.S.C. Chuang, The nature of adsorbed CO_2 and amine sites on the immobilized amine sorbents regenerated by industrial boiler steam, Ind. Eng. Chem. Res. 52 (2013) 12530-12539.

[28] N.K. Sandhu, D. Pudasainee, P. Sarkar, R. Gupta, Steam regeneration of polyethylenimine-impregnated silica sorbent for postcombustion CO_2 capture: A multicyclic study, Ind. Eng. Chem. Res. 55 (2016) 2210-2220.

[29] W.R. Alesi, J.R. Kitchin, Evaluation of a primary amine-functionalized ion-exchange resin for CO_2 capture, Ind. Eng. Chem. Res. 51 (2012) 6907-6915.

[30] R.R. Veneman, T.T. Hilbers, D.W.F.W. Brilman, S.R.A.S. Kersten, CO_2 capture in a continuous gas-solid trickle flow reactor, Chem. Eng. J. 289 (2016) 191-202.

[31] E. Robens, X. Wang, Investigation on the isotherm of silica gel+water systems, J. Therm. Anal. Calorim. 76 (2004) 659-669.

[32] J.A. Wurzbacher, C. Gebald, S. Brunner, A. Steinfeld, Heat and mass transfer of temperature-vacuum swing desorption for CO_2 capture from air, Chem. Eng. J. 283 (2016) 1329-1338.

[33] H. Demir, M. Mobedi, S. Ülkü, Microcalorimetric investigation of water vapor adsorption on silica gel, J. Therm. Anal. Calorim. 105 (2011) 375-382.

[34] K.Z. House, A.C. Baclig, M. Ranjan, E.A. van Nierop, J. Wilcox, H.J. Herzog, Economic and energetic analysis of capturing CO_2 from ambient air, Proceedings of the National Academy of Sciences 108 (2011) 20428-20433.

[35] F. Sabatino, A. Grimm, F. Gallucci, M. van Sint Annaland, G.J. Kramer, M. Gazzani, A comparative energy and costs assessment and optimization for direct air capture technologies, Joule 5 (2021) 2047-2076.

6 Summary and future work

6.1 Summary

The rising atmospheric CO_2 concentration necessitates the urgent development and deployment of negative emission technologies to limit global warming to below 1.5 °C. Direct air capture (DAC), which extracts CO_2 directly from ambient air, has gained significant attention as an essential approach for reversing the increasing trend of CO_2 concentrations. Among the existing DAC techniques, the adsorption processes, using solid amine sorbents with high atmospheric CO_2 adsorption capacities, are particularly promising. However, due to the strong affinity of amine groups with CO_2, regenerating solid amine sorbents typically demands raising the temperature to around 100 ℃ and simultaneously creating a vacuum to enhance the desorption driving force, resulting in high costs for DAC.

A vapor-promoted desorption (VPD) process was developed in this research to achieve high CO_2 working capacity with a low energy penalty through *in situ* purge of vapor synergistically harvested from the air. The process used double-layered Lewatit VP OC 1065 resin and silica gel for adsorbing atmospheric CO_2 and water. During regeneration, water vapors desorbed from silica gel significantly reduced CO_2 partial pressures, promoting the desorption of carbon dioxide. The stable CO_2 working capacity, maintained at approximately 1.0 mmol/g after nine cycles, was achieved by *in situ* vapor purge at moderate regeneration temperatures of around 105 °C. In this VPD process, the temperature required to achieve a regeneration efficiency *R* was found to be determined by the molar ratio of equilibrium loading of adsorbed water to CO_2 (n_{water}/n_{CO2}). This correlation was further used to predict the VPD performance under varying adsorbent volume fractions and feed air humidities. The vapor-promoted DAC demonstrated operational flexibility across a broad range of atmospheric humidities in both arid and humid environments, effectively releasing over 90% of the adsorbed CO_2 from the chemisorbent at 103-120 °C. By applying a moderate vacuum of 50 kPa, the regeneration temperature can be efficiently reduced to about 85 °C.

To minimize the carbon footprint associated with raising the adsorbent temperature and generating vapors, solar energy was used to power VPD with a photothermal conversion efficiency of 63.1%. Even under low solar intensities of 600 W/m^2, around 98% of the adsorbed CO_2 could be released within 50 minutes. The energy consumption for solar-powered VPD was calculated to be 10.4 MJ/kg_{CO2}, significantly lower than reported

TVSA and steam-assisted TVSA processes using the same CO_2 adsorbent. The work described in Chapter 3 provides an alternative process for efficiently regenerating chemisorbents through *in situ* vapor purge without relying on external purge gas or evacuation, demonstrating the potential techno-economic viability in DAC.

Amine-impregnated sorbents (AIS) have been extensively investigated for direct air capture due to their high CO_2 adsorption capacity and selectivity. Although AIS has demonstrated exceptional atmospheric carbon dioxide uptake, limited research has focused on the recovery of CO_2 adsorbed on the impregnated amines. The developed VPD process was applied to efficiently regenerate AIS through *in situ* vapor purge using water harvested from the air. A double-layered adsorption column, packed with AIS and water adsorbents, was used to capture atmospheric CO_2 and moisture simultaneously. During the regeneration process, this double-layered configuration generated water vapor to provide an extremely high desorption driving force, recovering over 95% of the CO_2 adsorbed on AIS at 105 °C. PEI/FS, a representative AIS, achieved a stable cyclic CO_2 working capacity of approximately 1.6 mmol/g, with an exceptionally high CO_2 product purity of 99%. The mechanism behind achieving this high CO_2 working capacity was the substantial increase in vapor pressure inside the column. The energy consumption for regenerating PEI/FS was calculated to be 8.9 MJ/kg_{CO2}, which is 14% lower than the VPD process using commercial VP OC 1065 as the CO_2 sorbent. This research in Chapter 4 successfully achieved the efficient regeneration of AIS through *in situ* vapor purge, opening up pathways for the practical applications of low-cost impregnated amines in DAC systems.

A primary challenge in widely implementing AIS for DAC is the high temperatures required by regeneration processes and the consequent deactivation of amines. A vapor-promoted temperature-vacuum swing adsorption (VPTVSA) process was developed to effectively address this issue by *in situ* generating low-temperature vapors under vacuum using water harvested from the air. Silica gel and PEI-impregnated HP20 resins were sequentially packed within one adsorption column, for harvesting atmospheric water and CO_2. This configuration substantially increased the CO_2 desorption driving force through the combination of evacuation and *in situ* vapor purge, releasing over 80% of the CO_2 absorbed on 33PEI/HP20 at 60 °C and 10 kPa. A consistently stable cyclic CO_2 working capacity of approximately 1.13 mmol/g during 45 adsorption-desorption cycles was achieved by the VPTVSA process. Under relatively dry conditions (7% RH), no CO_2 product could be collected, highlighting the importance of co-adsorbed water in enhancing the desorption of CO_2. In addition, amine

loading significantly affects the regeneration process, and increasing the PEI loading from 33% to 50% led to a reduction of approximately two-thirds in the desorption kinetics.

Compared with the conventional TVSA process, this vapor-promoted process with a silica gel volume fraction of only 12.5% increased the CO_2 working capacity from 0.29 to 0.74 mmol/g, achieving a 40% decrease in energy consumption. The VPTVSA process also demonstrated a lower exergy demand of 1.62 MJ/kg_{CO2} compared with other DAC processes, attributable to the reduced temperatures required for releasing CO_2. This work in Chapter 5 presents one alternative DAC process to regenerate AIS through *in situ* purge with low-temperature vapors, showcasing the great potential for improving the economic feasibility of DAC by reducing the energy penalty and extending the lifetime of amines.

6.2 Future work

Moisture in the air has been proven to enhance the carbon dioxide adsorption capacity of solid amine sorbents. This unique adsorption behavior poses significant challenges in precisely modelling the performance of DAC processes using solid amines as CO_2 adsorbents. There is currently a lack of sufficient equilibrium adsorption data to analyze the adsorption behavior of water and carbon dioxide on amine groups. Therefore, it is necessary to investigate the binary adsorption isotherm of CO_2 and water on solid amine sorbents. Based on these isotherms, adsorption models should be developed to simulate the adsorption behavior of carbon dioxide and water, enabling the calculation of equilibrium CO_2 loading under different conditions.

Although a regeneration process was developed to promote the desorption of CO_2, the stability issue of amine-based adsorbents remains unsolved. The current processes operate at elevated temperatures ranging from 60 to 110 °C, which may still lead to degradation of the adsorbent. Further lowering the desorption temperature or developing chemisorbents with excellent stability is crucial for reducing the cost associated with adsorbent replacement.

The VPD process, employing a double-layered adsorption column, has shown promise in effectively regenerating solid amine sorbents. However, in the present study, the process has not been fully optimized. There is a critical need for a mathematical model to simulate the double-layered configuration and predict the optimal operating conditions for the VPD process, aiming to maximize CO_2 productivity or minimize energy consumption. This model can also be used to predict the performance of CO_2 sorbents with varying adsorption

capacities and regenerabilities, providing valuable insights for the design of solid amine sorbents. In addition, using mathematical modeling to develop heat management approaches for harnessing the adsorption heat of water and the heat released from water condensation is a potential method for reducing the overall energy consumption for DAC.

The pressure drop in the DAC contactor significantly influences the cost of air blowing, although it was not specifically addressed in this study. Optimizing the packing of adsorbents in the column, for instance, through the use of honeycomb structures, represents a potential strategy to mitigate pressure drops. Research into the configuration of adsorbents and its effect on pressure drop is essential for further enhancing the economic feasibility of DAC.

In the present work, only commercial silica gel was tested as the water adsorbent for performing VPD. The application of a water adsorbent with higher water uptake and improved regenerability is expected to reduce the required water adsorbent volume fraction and increase the overall performance of the VPD process. In recent years, with the development of atmospheric water harvesting (AWH) technologies, numerous sorbent materials have been developed to capture free water molecules in the air through adsorption or absorption. Different regeneration technologies, such as solar heating, have been used to effectively release the captured water with high energy efficiency. Sorbents designed for AWH, such as hygroscopic salts and metal-organic frameworks, usually exhibit high water adsorption capacities and are easily regenerated, making them potential candidates as water adsorbents in the VPD process. It is worth trying to apply the research outcomes in the field of AWH to the VPD process, further enhancing the performance of direct air capture.